Prediction of Wetting Front Instability in Homogeneous Soils - Empirical Approach and Mathematical Modeling

by

Tzung-Mow, Mike, Yao

Dissertation

Submitted in partial fulfillment of the requirements
for the degree of
Doctor of Philosophy
in Hydrology

New Mexico Institute of Mining and Technology

1998

Abstract

Application of vertical one-dimensional models using averaged transport parameters is common in studies of contaminant leaching to groundwater. However, significant pollution of the groundwater has occurred in cases where these models predicted none. The cause for these cases of groundwater contamination is presumably the occurrence of preferential flow paths in the vadose zone which cannot be addressed by the employed models.

In homogeneous soils, instability of wetting fronts causes preferential flow in fingers. Systematic laboratory experiments revealed that soil hydraulic properties, initial soil water content, and infiltration rate exert an important control on instability. Coarser soil textures will enhance instability, increased initial soil water contents will dampen instability, and low infiltration rates will stabilize the wetting front. Based on these experimental results an empirical approach for the evaluation of wetting front instability in dry soils has been developed. It was found that the instability in a field soil depends on both soil type and the intensity of precipitation. Stability criteria were derived for three different classes of infiltration rates. At high infiltration rates where viscous forces dominate, wetting fronts are stable. At intermediate infiltration rates where gravity forces dominate, gravity-driven fingers can occur if the total amount of applied water exceeds the amount needed to wet a distribution layer near the surface. At low infiltration rates where capillary forces dominate, wetting fronts become stable again.

We performed a perturbation analysis on the unsaturated water flow equation and derived an analytical stability solution that can be applied to sharp and gradual wetting fronts

at all times. This solution, which requires standard soil hydraulic properties and infiltration rates as input, can be applied to all homogeneous field soils under all circumstances. Verification with our experimental data shows that it accurately predicts wetting front instabilities in different soil types for a wide range of infiltration rates. Predictions from the empirical and mathematical models were compared with laboratory and field observations in two field soils: New Mexico and Dutch dune sands. The phenomenon that fingers are frequently found in Dutch dune sands but rarely in New Mexico dune sands was well predicted by both our empirical and mathematical models. Predictions of finger characteristics with our mathematical model are close to the ones observed in the field. Previous models for stability prediction only performed well in so-called delta function soils that have very sharp wetting fronts. In contrast, our models are capable of accurate instability predictions in all homogeneous soils under a wide range of precipitation rates using standard soil hydraulic properties and rainfall intensities.

Acknowledgments

Special thanks are due to my family: my wife, Yueh-hua Dai, for her non-stop support and tolerance for the long journey of my study; my parents who gave their endless care, support, and encouragement all the time; and my two sons, Andrew and Stephen, who came to the world and became part of my spirit to make the best part of our lives happen. I could not have accomplished this achievement without the effort and support of my whole family.

I am in debt to my research advisor, Dr. Jan Hendrickx, for his enthusiastic involvement with my research and generous support; Dr. William Stone for his help with mathematical modeling; Dr. John Wilson, Dr. Rob Bowman, Dr. Chia Chen, Dr. Fred Philip, and Dr. Robert Glass for their brilliant teaching and instructions that gave me the necessary background to finish my research; and Dr. J.-Y. Parlange for his help with instability modeling.

I am grateful to my former colleague, Xiao-Hong Du, for solving our most difficult mathematical problem of the stability analysis of the unsaturated flow equation; Jun Lin, for his help with coding and discussion with modeling problems; and Jelle Beekma, for his suggestions and corrections to my earlier versions of texts. Finally, I thank the main members of my laboratory and field crew for their effort to make this research complete: Steve Bower, Jay Cabrales, Kelly Krier, Jeff Long, Alexander Pirandelo, and Tim House.

Table of contents

List of tables

List of figures

1. Introduction

Modeling has been widely applied in hydrology for predictions and to solve complicated hydrological problems. The validity of predictions depends on the correct conceptualization of the problem which is not always possible because of a hiatus in our knowledge. For example, the application of one dimensional models for the prediction of groundwater contamination by transport of contaminants through the vadose zone indicated negligible risk of groundwater contamination due to sufficient residence time in the vadose zone. However, significant pollution of the groundwater has occurred where these models predicted none. The cause for these cases of groundwater contamination is presumably the occurrence of preferential flow paths in the vadose zone. Such preferential flow paths can be caused by macropores such as cracks in swelling soils or old root channels, spatial variability of hydraulic conductivity, presence of water repellent soils, or by the occurrence of unstable wetting fronts.

A stable wetting front is a horizontal wetting front which moves downward without breaking into fingers. The behavior of such a front can be simulated with one-dimensional computer models. Unstable wetting fronts start out as horizontal wetting fronts which under certain conditions break into 'fingers' or 'preferential flow paths' as the front moves downward, much like rain running off a sheet of glass breaking into streams. These fingers facilitate the transport of contaminants to the groundwater at velocities many times those calculated if a stable horizontal front is assumed.

Infiltration is the process that denotes the entry of water into the soil through its surface. To describe this infiltration process, the generally accepted model that depicts a sharp stable wetting front was formulated by Green and Ampt in the year 1911. Forty six years later, a theoretical study of one-dimensional infiltration by Philip (1957) confirmed again the basic features of Green and Ampt's infiltration model. Philip (1969) in a review article concluded that 'the exact solutions for one-dimensional infiltration are in excellent agreement with the relevant experimental data'. Most of these experimental data were obtained in ideal laboratory columns and field data that did not fit the infiltration model with the sharp stable wetting front, were discarded as anomalies caused by 'the very variable nature of soil profiles ..... in the field' (Marshall and Holmes 1979). The one dimensional model was still the widely accepted and trusted one to represent the infiltration process, while unstable wetting phenomena were treated as anomalies.

The stability of an interface between two fluids in a porous medium has received attention from the petroleum field due to its importance in the extraction of oil from oil-bearing porous media. Viscous fingering has been studied by Hill (1952), Chuoke et al. (1959), and Saffman and Taylor (1959). It was not until early 70's that Hill and Parlange (1972) started research on layered soils and found fingering phenomena in soils. The following year, Raats (1973) proposed criteria for the stability of infiltration flows in uniform and nonuniform soils. This paper has served as an important and useful stimulus to soil-physical studies of the stability of infiltration flows, in spite of some corrections by Philip (1975a) to this paper. Successive theoretical (Diment et al. 1982; Glass et al. 1989a; Hillel

and Baker 1988; Parlange and Hill 1976; Philip 1975a,b) and experimental work (Baker and Hillel 1990; Glass et al. 1988, 1989b; Hendrickx and Dekker, 1991; Hendrickx et al. 1988a, b, 1993; Selker et al. 1992; Van Ommen et al.1989; White et al. 1976) yielded convincing evidence that unstable wetting fronts do indeed occur in soils.

Unstable flows were studied intensively in other areas of the hydrodynamics of porous media (Chuoke et al. 1959; Heller 1966; Homsy 1987; Kueper and Frind 1988; Perrine 1961; Rachford 1964; Saffman 1986; Saffman and Taylor 1958; Tanveer 1987a,b; Van Meurs 1957). However, our understanding of the conditions under which unstable wetting manifests itself in field soils is still very limited. Consequently, we cannot predict when and where unstable wetting will occur in field soils. One reason is that the mathematical analysis of instability is difficult due to the highly nonlinear behavior of the Richards' equation for unsaturated water flow through the soil. Therefore, Raats (1973) and Philip (1975a,b) use the Green and Ampt (1911) model for infiltration to study wetting front instability with a linear hydrodynamic stability analysis. This model linearizes the infiltration process by the use of a special diffusivity function which -unfortunately- is only representative for a limited number of soils and soil conditions. Subsequent studies by Parlange and Hill (1976) and Glass et al. (1991) still treat the wetting front as a discontinuity. This type of model performs well for sandy soils due to their sharp wetting front nature but is of limited use in soils with gradual wetting fronts. Gradual wetting fronts were used by Diment et al. (1982) for their hydrodynamic stability analysis using numerical simulation (Diment and Watson, 1983). They found no evidence of unstable wetting under conditions

where it was expected: moisture redistribution, and heterogeneous and layered systems. This may have been due to poor performance of their model at initial water contents around 0.05 cm^3/cm^3. They concluded that additional work is required to develop stability analysis for non-sharp gradual fronts that can handle very low initial water content conditions.

Recapitulating, there is a great need for a stability model that can handle instabilities in real field soils under the full range of initial and boundary conditions. Therefore, we conducted a stability analysis that considers a gradual wetting front, which can represent all types of soil. In order to verify existing models and the model we are developing, we performed a series of experiments. This was necessary to fill the data gap since systematic investigations of unstable wetting fronts in soils have been rare. The objectives of this study are: 1) to conduct series of laboratory and field experiments to verify existing models and to enable development of our model; 2) to build an instability model that can deal with real homogeneous field soils under a wide range of infiltration rates; and 3) to validate this model with experimental laboratory and field data.

Organization

This dissertation is composed of nine chapters. Excluding the introduction and last chapter with general conclusions, each chapter is presented in the format of a journal article. Chapters 2 and 4 were published, respectively, in Soil Science Society of America Journal and Geoderma. Chapter 5 was resubmitted to Soil Science Society of America Journal.

Chapters 3, 6, and 7 have been submitted to Water Resources Research. Chapter 8 will be submitted shortly.

The works and subjects covered in this thesis can be divided into two stages. The first stage includes the experimental studies of wetting front instabilities. In spite of the numerous research mentioned in the introduction, the conditions under which unstable wetting fronts form in the field are not yet fully understood. This is due to the small amount of systematic investigations of unstable wetting fronts in soils. In chapter 2, we describe a systematic laboratory lysimeter study to investigate the major factors that control wetting front instability for different grades of coarse sand within the range of natural precipitation rates. The experimental data verify the validity of a previous model by Parlange et al. (1991) that was adopted to be used by practitioners (chapter 3). We propose a scheme that can take those hard to measure parameters in the model by Parlange et al. (1991) and replace them with easily measured parameters using an approximate formula. Based on the laboratory data we develope an empirical approach and scheme to predict instability (chapter 4). This scheme uses a number of readily available data which can be easily used for the prediction of instability in field. The empirical method accurately predicts wetting front stability in dry field soils using soil and precipitation data.

The second stage includes the derivation of instability theory and the comparisons of experimental results to the model's predictions. We develop a model that can handle real field soils with a gradual wetting front. To achieve this we first derive a new infiltration

solution to represent the gradual wetting front for all times. The one-dimensional model we developed is introduced in chapter 5. It represents the wetting front profile at any time and is not restricted to only small or large times as the solutions by Philip (1969).

In chapter 6 we use this model to conduct a rigorous stability analysis for gradual wetting fronts. We derive analytical instability criteria and finger characteristics which can be solved numerically. In chapter 7, the procedures of the numerical scheme are described. Predictions with the numerical scheme were compared to experimental results and a sensitivity analysis was performed for different soil properties. We conclude that our mathematical model allows an analysis of instability of the nonlinear Richards' equation for all soils under a wide range of infiltration rates..

Finally, in chapter 8 we take the empirical model from chapter 4 and the mathematical model from chapters 6 and 7 to predict instability criteria and finger characteristics for field soils in New Mexico and the Netherlands. The models give accurate predictions when compared with field and laboratory measurements of the same soils.

References

Baker, R.S., and D. Hillel. 1990. Laboratory tests of a theory of fingering during infiltration into layered soils. Soil Sci. Soc. Am. J. 54:20-30.

Chuoke, R.L., P. van Meurs, and C. van der Poel. 1959. The insatbility of slow, immiscible,

viscous liquid and liliquid displacements in permeable media. Trans. AIME 216: 188-194.

Diment, G.A., and K.K. Watson. 1983. Stability analysis of water movement in unsaturated porous materials: 2. Numerical studies. Water Resour. Res. 19:1002-1010.

Diment, G.A., K.K. Watson, and P.J. Blennerhassett. 1982. Stability analysis of water movement in unsaturated porous materials: 1. Theoretical considerations. Water Resour. Res. 18: 1248-1254.

Glass, R.J., T.S. Steenhuis, and J.-Y. Parlange. 1988. Wetting front instability as a rapid and far-reaching hydrologic process in the vadose zone. J. of Cont. Hydrology 3:207-226.

Glass, R.J., J.-Y. Parlange., and T.S. Steenhuis, 1991. Immiscible displacement in porous media: Stability analysis of three-dimensional, axisymmetric disturbances with application to gravity-driven wetting front instability. Water Resour. Res. 27:1947-1956.

Glass, R.J., T.S. Steenhuis, and J.-Y. Parlange. 1989a. Wetting front instability: 1. Theoretical discussion and dimensional analysis. Water Resour. Res. 25:1187-1194.

Glass, R.J., T.S. Steenhuis, and J.-Y. Parlange. 1989b. Wetting front instability: 2.

Heller, J.P. 1966. Onset of instability patterns between immiscible fluids in porous media. J. Apply. Phys. 37:1566-1579.

Green, W.H. and G.A. Ampt. 1911. Studies on soil physics: I. The flow of air and water through soils. J. Agric. Sci. 4:1-24.

Hendrickx, J.M.H., and L.W. Dekker. 1991. Experimental evidence of unstable wetting fronts in non-layered soils. p. 22-31. *In* Proc. Natl. Symp. Preferential Flow,

Chicago, IL. 16-17 Dec. 1991. Am. Soc. Agric. Eng., St. Joseph, MI.

Hendrickx, J.M.H., L.W. Dekker, and O.H. Boersma. 1993. Unstable wetting fronts in water repellent field soils. J. of Environmental Quality. 22:109-118.

Hendrickx, J.M.H., L.W. Dekker, and P.A.C. Raats. 1988a. Formation of sand columns caused by unstable wetting fronts. Grondboor en Hamer. 6:173-175. (in Dutch).

Hendrickx, J.M.H., L.W. Dekker, E.J. Van Zuilen, and O.H. Boersma. 1988b. Water and solute movement through a water repellent sand soil with grass cover. pp. 131-146. *In* Wierenga, P.J. and D. Bachelet. Validation of flow and transport models for the unsaturated zone: Conference Proceedings; May 23-26, 1988 Ruidoso, New Mexico. Research Report 88-SS-04 Dept. of Agronomy and Horticulture, New Mexico State University, Las Cruces, N.M. 545 p.

Homsy, G.M. 1987. Viscous fingering in porous media. Annu. Rev. Fluid Mech. 19:271-311.

Hill, D.E., and J.-Y. Parlange. 1972. Wetting front instability in layered soils. Soil Sci. Soc. Am. Proc. 36:697-702.

Hillel, D., and R.S. Baker. 1988. A descriptive theory of fingering during infiltration into layered soils. Soil Sci. 146:51-56.

Kueper, B.H., and E.O. Frind. 1988. An overview of immiscible fingering in porous media. Journal of Contaminant Hydrology 2:95-110.

Marshall, T.J, and J.W. Holmes. 1979. Soil physics. Cambridge Univ. Press. pp. 345.

Parlange, J.-Y., R.J. Glass, and T.S. Steenhuis. 1991. Application of scaling to the analysis to unstable flow phenomena. *In* D. Hillel et. al. (ed.) Scaling in soil physics:

Principles and applications. SSSA Spec. Publ. 25. SSSA, Madison, WI.

Parlange, J.-Y., and D.E. Hill. 1976. Theoretical analysis of wetting front instability in soils. Soil Sci. 122:236-239.

Philip, J.R., The theory of infiltration: 4. Sorptivity and algebraic infiltration equations, *Soil Sci. 84*, 257-264, 1957.

Philip, J.R., Theory of infiltration, *Advance.* Hydroscience, *5*, 215-296, 1969.

Philip, J.R. 1975a. Stability analysis of infiltration. Soil Sci. Soc. Am. Proc. 39:1042-1049.

Philip, J.R. 1975b. The growth of disturbances in unstable infiltration flows. Soil Sci. Soc. Am. Proc. 39 :1049-1053.

Perrine, R.L. 1961. Development of stability theory for miscible liquid-liquid displacements. Soc. Pet. Eng. J. 1:17-25.

Raats, P.A.C. 1973. Unstable wetting fronts in uniform and nonuniform soils. Soil Sci. Soc. Am. Proc. 37:681-685.

Rachford, H.H. 1964. Instability in waterflooding oil from water-wet porous media containing connate water. Soc. Pet. Eng. J. 4:133-148.

Saffman, P.G. 1986. Viscous fingering in Hele Shaw cells. J. Fluid Mech. 173:73.

Saffman, P.G., and G. Taylor. 1958. The penetration of a fluid into a porous medium or Hele Shaw cell containing a more viscous liquid. Proc. R. Soc. London Ser. A. 245:312-331.

Selker, J.S., T.S. Steenhuis, and J.-Y. Parlange. 1992. Wetting front instability in homogeneous sandy soils under continuous infiltration. Soil Sci. Soc. Am. J. 56:1346-1350.

Tanveer, S. 1987a. Analytic theory for the selection of a symmetric Saffman-Taylor finger in a Hele Shaw cell. Phys. Fluids 30:1589-1605.

Van Ommen, H.C., R. Dijksma, J.M.H. Hendrickx, L.W. Dekker, J. Hulshof, and M. van den Heuvel. 1989. Experimental assessment of preferential flow paths in a field soil. J. of Hydrology 105:253-262.

Van Meurs, P. 1957. The use of three-dimensional models for studying the mechanisms of flow processes in oil reservoirs. Trans. Am. Inst. Min. Metall. Pet. Eng. 210, 295.

White, I., P.M. Colombera, and J.R. Philip. 1976. Experimental study of wetting front instability induced by sudden change of pressure gradient. Soil Sci. Soc. Am. J. 40:824-829.

2. Stability of Wetting Fronts in Dry Homogeneous Soils Under Low Infiltration Rates

Tzung-mow Yao and Jan M.H. Hendrickx

Hydrology Program, Department of Earth and Environmental Sciences,

New Mexico Tech, Socorro, NM 87801

Abstract

Our understanding of unstable wetting phenomena in soils is limited. Therefore, lysimeter experiments were conducted in the laboratory to validate current wetting front instability theories. Four different grades of sieved and air-dried perlite and quartz sand were used as the experimental material. Water was applied by a sprinkler system at rates within the range of natural precipitation rates in New Mexico. Experiments were conducted in small lysimeters (diameter 30 cm, height 50 cm) as well as a large one (diameter 100 cm, height 150 cm). The experimental results show that wetting front instability will cause fingering phenomena in a homogeneous soil system. This observation confirms experimental and

theoretical results of other workers. The diameter of fingers was observed to be a function of the grain size of the sand. Small fingers (3-4 cm diameter) were found in coarse sand (grain size 1.41-0.84 mm); large diameter fingers (12 cm diameter) were observed in fine sand (grain size 0.42-0.25 mm). Our experimental results in the coarse sand show that, for infiltration rates varying between 0.3 and 12 cm/h, finger diameters remain more or less constant. This observation also agrees with existing theories. However, at infiltration rates lower than 0.12 cm/h, the coarse sand experiments show that the wetting fronts became stable. For rates between 0.3 and 0.12 cm/h, the wetting is semi-stable; that is, there is incomplete wetting without distinct development of fingers. A similar trend is observed in the experimental results of sands with grain sizes of, respectively, 0.841-0.594 and 0.594-0.42 mm. This phenomenon has not been observed in previous experimental studies and is not predicted by current wetting front instability theories. Our experimental data under infiltration rates similar to natural precipitation intensities may explain why unstable wetting has rarely been observed in wettable field soils.

Introduction

Worldwide, preferential flow paths are thought to be a major mechanism for groundwater contamination. These paths can be caused by macropores such as soil cracks or old root channels (Bouma, 1980; Beven and Germann, 1982), by spatial variability of hydraulic conductivity, or by unstable wetting fronts. The occurrence of unstable fronts is

of special importance because they may cause preferential flow paths in homogeneous soils which have neither macropores nor large variability of hydraulic properties. Theoretical studies of wetting front instability (Diment and Watson, 1983; Diment et al., 1982; Glass et al., 1989a, c, 1991; Hillel and Baker, 1988; Parlange and Hill, 1976; Philip, 1975a, b; Raats, 1973; Tabuchi, 1961) are supported by the results of laboratory experiments (Baker and Hillel, 1990; Diment and Watson, 1985; Glass et al., 1989b, 1990; Hendrickx et al., 1988a; Hill and Parlange, 1972; Selker et al., 1989, 1992a, b, c; Tamai et al., 1987; White et al., 1976) and field investigations (Hendrickx et al., 1988b; Hendrickx and Dekker, 1991; Hendrickx et al., 1993; Ritsema et al., 1993; Van Ommen et al., 1989).

Theories to explain unstable wetting in homogeneous soils have been presented by Raats (1973), Philip (1975a, b), Parlange and Hill (1976), Diment et al. (1982), and Glass et al. (1989a, 1991). Based on the instability criterion for homogeneous soils, these theories predict instabilities to occur under the following conditions: (1) infiltration of ponded water with compression of air ahead of the wetting front; (2) redistribution of water in the soil profile; (3) water repellent soils; (4) an increase of water content with depth; and (5) continuous nonponding infiltration. In the case of continuous nonponding infiltration, Raats (1973) and Parlange and Hill (1976) predicted instabilities to occur, whereas Philip (1975a) predicted that none would occur. Experimental evidence, however, shows that instabilities do occur in homogeneous soils during nonponding infiltration (Hagerman et al., 1989; Hendrickx and Dekker, 1991; Selker et al., 1989, 1992a, b).

The diameter of the preferential flow paths, or fingers, has been studied through stability analysis by Chuoke et al. (1959), Philip (1975a, b), Parlange and Hill (1976) and Glass et al. (1991). These researchers stated that the critical wavelength necessary to induce unstable wetting yields an estimate of the finger diameter. Glass et al. (1991) showed that for fluxes less than half the saturated hydraulic conductivity, the formulations by Chuoke et al. (1959) and by Parlange and Hill (1976) gave similar results. In three-dimensional systems with dry soils the finger diameter d of nearly saturated fingers can be calculated as:

$$d = 4.8\frac{S_w^2}{K_s(\theta_s-\theta_0)}\left[\frac{1}{1-q/K_F}\right] \qquad \textbf{(1)}$$

where S_w is the sorptivity of the porous medium at water entry value, K_s is the saturated hydraulic conductivity, θ_s is the saturated water content, θ_0 is the initial water content, q is the infiltration rate and 4.8 is a coefficient derived from stability analysis (Glass et al., 1991). K_F is the hydraulic conductivity inside the finger, a value assumed to be close to K_s.

The formula indicates that finger diameters will increase in finer soils where the decrease in the square of the sorptivity values generally is less than the decrease in hydraulic conductivity values. It also indicates that the finger diameter will increase with increasing infiltration rates until the wetting fronts become stable at infiltration rates equal to or higher than the saturated hydraulic conductivity of the soil. Selker et al. (1992a) and Glass et al. (1989b, 1990) have presented experimental data to support the formula for infiltration rates exceeding 7 cm/h. Recently, Liu et al. (1994) modified Eq. [1] slightly for the prediction of

finger diameters in sandy soils at different water contents. The modified formula was confirmed by experiments with fingers emanating from point sources at high infiltration rates. An increase in finger width was observed from approximately 2 cm at an initial air-dry water content to approximately 7 cm at an initial water content of 0.05 cm^3cm^{-3}.

For infiltration rates approaching zero, Eq. [1] predicts a constant small finger diameter, indicating the persistence of unstable wetting under these low rates. However, to date no studies have been carried out to experimentally verify Eq. [1] for low infiltration rates and its conjectured mechanism of unstable wetting in initially dry, wettable homogeneous soils under such low infiltration rates (7-0.1 cm/h). Because low infiltration rates frequently are more representative for precipitation regimes of field soils than the high infiltration rates used in the studies reported in the literature, it is the objective of this investigation to hypothesize about the stability of wetting fronts at low infiltration rates and to verify our hypothesis with three-dimensional laboratory experiments.

Hypothesis

Each infiltration event is an intricate interplay between the forces of capillarity and gravity. In the early stages of infiltration under the influence of steep soil water pressure gradients, the capillary forces predominate, whereas at later times gravity becomes the dominant driving force for flow. Because unstable wetting is a gravity-driven phenomenon (Raats 1973; Parlange & Hill 1976; Philip 1975a, b) , we hypothesize that no instabilities

will occur during the initial stages of the infiltration process when capillary forces are dominant. For the determination of the time during which capillarity controls the infiltration process we use the gravitational characteristic time, t_{grav}, introduced by Philip (1969):

$$t_{grav} = \left(\frac{S(h)}{K_i(h) - K_o(h_o)} \right)^2 \qquad \textbf{(2)}$$

where S(h) is the sorptivity of the soil at supply water pressure h, $K_i(h)$ is the hydraulic conductivity at the supply soil water pressure h, and K_o is the hydraulic conductivity at the initial soil water pressure (h_0) of the soil. Although this characteristic time is somewhat qualitative as it represents only the order of magnitude at which the effect of gravity on infiltration equals that of capillarity (Philip 1969), it is a useful tool to assess the effect of decreasing infiltration rates on the relative contributions of capillary and gravity forces during the infiltration process.

The gravitational characteristic time is an intrinsic soil property that by itself cannot describe the infiltration process. Therefore, we also define an infiltrational characteristic time, t_{infil}, that reflects the characteristics of the infiltration process as it considers the total amount of water available for infiltration, W, and the infiltration rate, i(h).

$$t_{infil} = \frac{W}{i(h)} \qquad \textbf{(3)}$$

For irrigation, t_{infil} is the total amount of irrigation water divided by the irrigation intensity. During storms, t_{infil} is the total amount of precipitation divided by the precipitation intensity.

As long as $t_{infil}<t_{grav}$, capillary forces dominate the flow process. The larger the difference t_{grav}-t_{infil}, the less likely it will be that unstable wetting fronts occur during the infiltration process. Neglecting K_o and using sorptivity and hydraulic conductivity data at zero tension from Stroosnijder (1976), we find characteristic gravitational times of 3, 270, 8300, and 110,000 minutes for, respectively, a coarse sand, a fine sand, a loam, and a clay soil indicating a high probability for unstable wetting to occur in coarse sand and a low one in a clay soil at conditions of near saturation. As most precipitation events do not last longer than a few hours, this result agrees well with observations that coarse sands appear more susceptible to unstable wetting than finer sands.

Using the characteristic times, t_{grav} and t_{infil}, to evaluate the relative contributions of capillarity and gravity when infiltration rates decrease, it is immediately observed from Eq. [3] that for a given amount of water, W, t_{infil} becomes larger as the infiltration rate decreases. Because the infiltration rate is not explicitly present in t_{grav}, Eq. [2], a direct quantitative comparison between the effects of lower infiltration rates on t_{grav} and t_{infil} is not possible. However, a qualitative comparison is feasible by recognizing the fact that lower infiltration rates result in drier soils with lower soil pressures and lower unsaturated hydraulic conductivities (Koorevaar et al., 1983; Marshall and Holmes 1979). When the infiltration rate approaches zero, the soil water pressure will become more negative and stabilize at a value that depends on the depth to the groundwater table (Koorevaar et al., 1983). In a semi-infinite vadose zone, when the soil water pressure becomes more and more negative, the unsaturated hydraulic conductivity will become very small, and t_{grav} will approach infinity.

Therefore, t_{grav} and t_{infil} both become larger as the infiltration rate decreases. Thus, when infiltration rates decrease, capillary forces can become more dominant only if the increase in t_{grav} exceeds the increase in t_{infil}.

As stated before, the absence of i(h) in Eq. [2] prevents a direct evaluation of the relationships between t_{grav}, t_{infil} , and i(h). However, Eqs. [2] and [3] show that both t_{grav} and t_{infil} are functions of the soil water pressure. This fact enables us to indirectly evaluate the desired relationships by studying the increases of the t_{grav} and t_{infil} when the soil water pressure becomes more negative and the soil dries out.

Relationship between Gravitational Characteristic Time and Soil Water Pressure

In order to examine how t_{grav} behaves when the soil water pressure decreases from zero to more negative values, we evaluated the relationship between t_{grav} and soil water pressure for a sand, sandy loam, and sandy clay soil assuming infiltration in a dry soil where $\theta_o \approx 0$ and $K_o(h_o) \approx 0$. Combining the Van Genuchten (1980) model for the unsaturated hydraulic conductivity with a common approximation for the sorptivity (Elrick and Reynolds 1992; Philip 1957; White and Sully 1987) yields the following relationship between t_{grav} and h

$$t_{grav} = \frac{b\ (\theta_h - \theta_o) \int_{-\infty}^{h} K(u)du}{\left[K_s S_e^{0.5}(1-(1-S_e^{1/m})^m)^2\right]^2} \qquad (4)$$

where b is a dimensionless parameter approximately equal to 1.82 (White and Sully 1987), u is a dummy variable of integration, and S_e is the effective saturation, m=1-1/n where n is a shape parameter. Figure 2.1 presents the relationships between t_{grav} and soil water pressure for a sand, sandy loam, and sandy clay soil using Van Genuchten parameters presented by Carsel and Parrish (1988). For all three soils t_{grav} increases non-linearly to large values with modest decreases in soil water pressure so that t_{grav} exceeds five hours at soil water pressures of 0, -9, and -13 cm in, respectively, the sandy clay, sandy loam, and sand. Since five hours is a rather long t_{infil} for many precipitation and irrigation events, Fig. 2.1 illustrates that capillarity quickly dominates the infiltration process when soil water pressures drop. For example, Fig 2.1 shows that during infiltration at a soil water supply pressure of -20 cm capillarity is as dominant in the sand as in the sandy clay soil. Experimental data obtained by Prevedello et al. (1991) during water redistribution in a sand soil confirm that capillary forces start dominating gravitational forces at soil water contents less than nine volumetric percent.

Fig. 2.1. Relationship between the gravitational characteristic time, t_{grav}, and the soil water pressure (h)

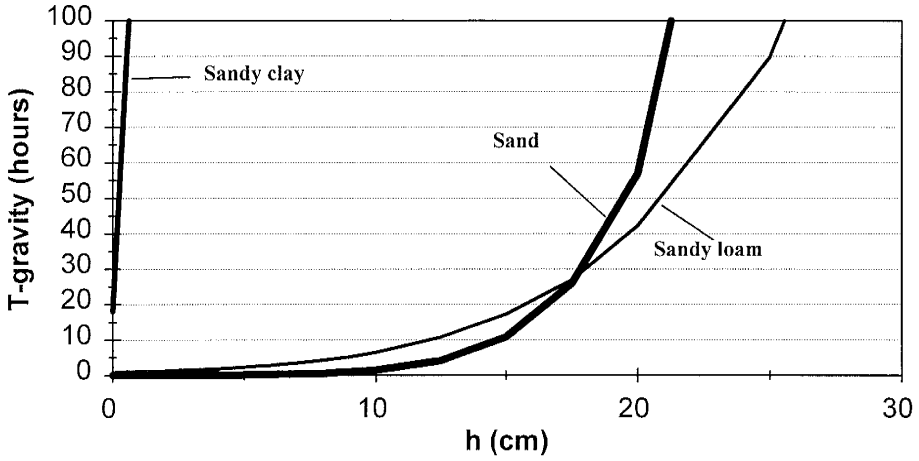

Relationship between Infiltrational Characteristic Time and Soil Water Pressure

The relation between soil water pressure and infiltration rate i(h) is easily determined when gravity completely dominates the infiltration process, since water moves then under a unit gradient and the infiltration rate is equal to the unsaturated hydraulic conductivity. When capillarity plays a role, the hydraulic gradient exceeds unity and, consequently, the infiltration rate will exceed the unsaturated hydraulic conductivity with a factor equal to the hydraulic gradient and t_{infil} will be reduced by that same factor. In Fig 2.2 we plot the relation between soil water pressure and t_{infil} for a sand and sandy loam under different conditions: total water applications of 30 and 60 mm, hydraulic gradients of 1 and 5. We also included from Fig 2.1 the zones where gravity or capillarity dominate. Figure 2.2 demonstrates that relatively small decreases in soil water pressure caused by decreases in the infiltration rate will often result in an infiltration process dominated by capillary forces.

The above analysis strongly indicates that capillarity may play an important role in sandy soils at the low infiltration rates that are common for many precipitation and irrigation events. The huge increases in t_{grav} with relatively small decreases in soil water pressure (Fig. 2.1) suggest that infiltration at lower soil water pressures tends to stabilize wetting fronts because gravity forces become less important. Since lower infiltration rates lead to lower soil water pressures, we have formulated the hypothesis that "wetting fronts caused by low infiltration rates tend to be more stable than those caused by high infiltration rates". The

Fig. 2.2. Relationship between the infiltrational characteristic time, t_{infil}, and the soil water pressure at hydraulic gradients (dH/dz) of 1 and 5 for the (A.) sand and (B.) sandy loam

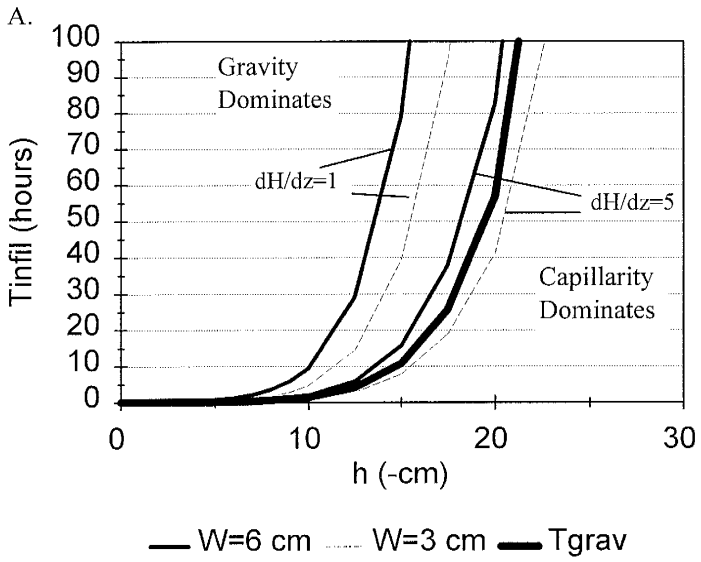

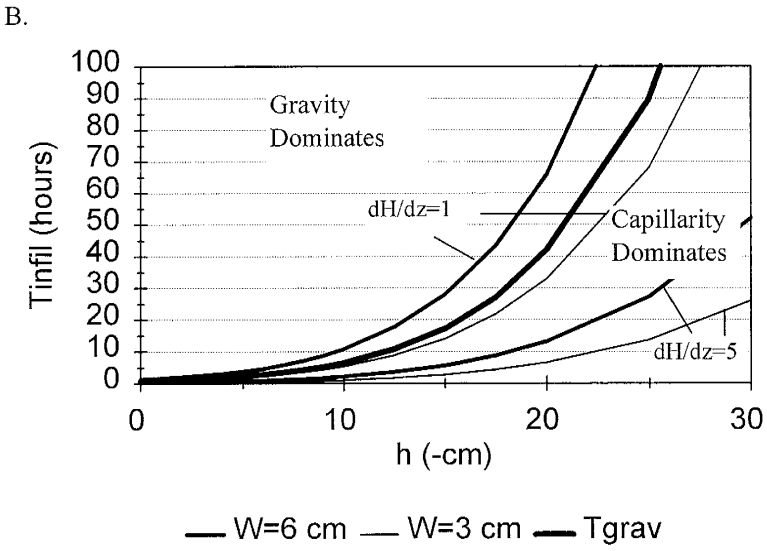

objective of this experimental study is to test this hypothesis under well controlled laboratory conditions.

Materials and Methods

Experimental Sands

Four different grades perlite sand and quartz sand were used: U.S. mesh size No. 14-20 (1.41-.841mm), 20-30 (.841-.594mm), 30-40 (.594-.42mm), and 40-60 (.42-.25mm). The particle size distribution was determined with a sieve analysis (Fig. 2.3). The shapes of the particle size distribution curves indicated that the sands were rather homogeneous. For our experiments we needed to transport, dry, clean, and sieve approximately 10 m^3 sand. Perlite sand was chosen as the experimental material for budgetary reasons since it was made available to us by the Grefco Perlite Mine near Socorro at no cost. Some experiments were repeated in natural quartz sand to corroborate the experimental results observed in perlite sand.

Physical Parameters of the Sands

Perlite is similar to quartz sand, but has a lower specific density of approximately 2.2 g/cm^3 compared to 2.65 g/cm^3 of quartz sand. This leads to a bulk density in the lysimeters

Fig. 2.3. Grain Size Distribution of Perlite and Quartz Sand

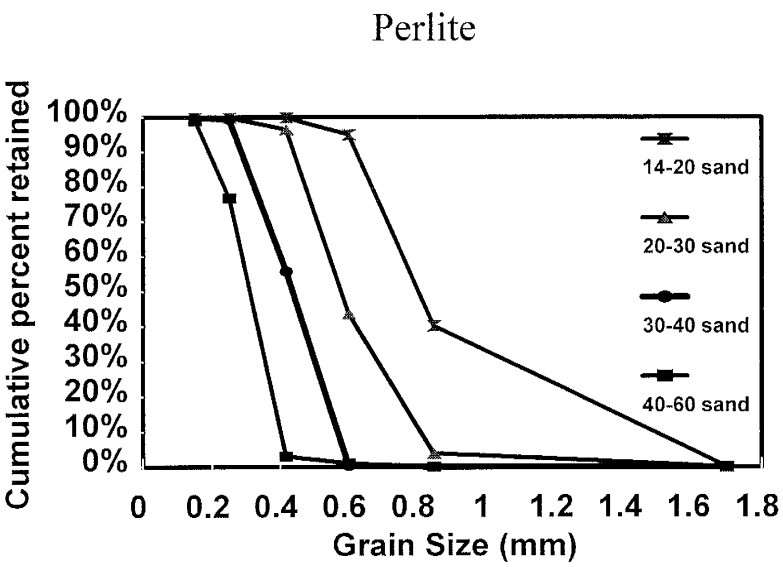

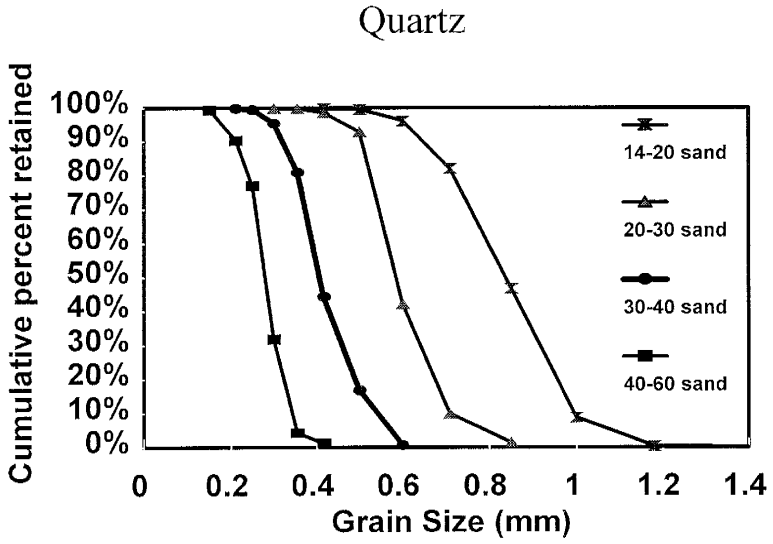

of approximately 1.25 g/cm^3 and a porosity of 45%. Quartz sand has a higher bulk density of 1.54 g/cm^3 and a slightly lower porosity of 42%.

For each grade we determined water retention curves with the hanging water column technique on 100 cm^3 dry samples that were taken in-situ from the lysimeters. The data were fitted with the RETC program of Van Genuchten et al. (1991). The saturated hydraulic conductivity was measured with the constant head method. Water-entry values were estimated gravimetrically from vertical capillary rise experiments (Glass et al., 1990). The sand was packed into a 10 cm diameter PVC column consisting of twenty rings, each 1 cm high. The bottom part of this column was immersed into water until no further rise was observed. Next, the water content of each 1 cm layer was measured. After plotting the water contents versus the average height of the samples, water-entry values were determined, by definition, at the lowest water tension along the saturation portion of the wetting curve (Glass et al., 1989c). The sorptivities of the sand at the water entry value were determined with a tension infiltrometer (Ankeny et al., 1988).

There was some concern that the chemically bound water molecules of the perlite could be set free during drying of samples in the oven. Another concern was that perlite particles may still contain some water in their micropores after air-drying. However, tests revealed this was not the case: perlite sand behaves like quartz sand in the air-dried and oven-dried conditions.

Experiments

The air-dried perlite and quartz sands were used to fill small (diameter 30 cm, height 50 cm) non-weighing lysimeters. Perlite was also used in a large lysimeter (diameter 100 cm, height 150 cm). The small lysimeters were designed after those employed by Glass et al. (1990) by stacking seven 10 cm high rings and filling them with sand. A funnel-extension-randomizer also based on the design of Glass et al. (1990) randomized the falling sand so that microlayering and grading due to particle size segregation was avoided. After filling, the top two layers were taken off and the surface of the column was smoothed. The weight of the two top layers helped to compact the underlying layers to a constant density of approximately 1.25 g/cm^3 for perlite sand and 1.54 g/cm^3 for quartz sand.

In order to study fingers with diameters larger than 30 cm, we used a large lysimeter which consisted of 10 circular slabs, each 15 cm high. The inside diameter of the lysimeter was 100 cm. The slabs, with a gasket in between, were bolted together so that a water- and air-tight connection was obtained. Forty-five outlets in the bottom prevented the air pressure from increasing during the infiltration experiments.

To fill the large lysimeter with perlite, we used a 1 m diameter "funnel-extension-randomizer" as described above. In addition, a 2 ton capacity crane was installed and a large quick-release loader was built to facilitate the filling process. The entire experimental setup involved two stories in our laboratory with a height of 8 meters.

Water Application

A sprinkler system was built by inserting eleven hundred drip needles in a sealed plexi-glass box at grid points 3 cm apart. The needles covered a circular area with 1.2 m diameter. The drop size from the needles (20G1, from Beckon and Dickinson) was measured as approximately 3 mm in diameter, which is close to the drop size of a storm rainfall in the United States (Bubenzer, 1979; Carter et al., 1974; Laws and Parsons, 1943). For low flux experiments, smaller needles (30G1/2) were used to obtain a more uniform water distribution. Two variable-speed, gear-reduction motors were placed on two adjoining sides to control the north-south and east-west movements separately. The offsets in both directions could be adjusted so that we could obtain a random distribution of the water without a repetitious pattern. A Masterflex pump and a syringe pump were used for accurate flow control. The water application rate could be adjusted from 0.05 cm/h to 36 cm/h.

The lysimeters were exposed to infiltration regimes representative for natural precipitation events in New Mexico and elsewhere in the world (Bubenzer, 1979). The infiltration rates varied between 0.068 cm/h to 27 cm/h; the total amounts of applied water between 2.5 to 8 cm.

After water application, the lysimeters were excavated layer by layer to allow visual inspection of the flow pattern. Samples were taken within and outside the fingers to determine bulk density and water content. In each layer we photographed the wetting pattern

for later analysis of total wet area and finger diameter. One hundred and twelve experiments were conducted in initially dry sands under the experimental conditions shown in Table 2.1.

Results and Discussion

Effect of Sand Grain Size on Finger Diameter

The results of the soil physical measurements are presented in Table 2.2. The saturated hydraulic conductivity decreases from 1188 to 180 cm/h in, respectively, the coarse and fine sands, whereas the sorptivity, in general, increases from 11.2 to 17.4 cm/h$^{1/2}$. The sorptivity at water-entry tension was estimated by interpolating the plot of sorptivities versus tensions. The large variability of measured sorptivity near the water-entry tension makes interpolation difficult and may have resulted in the lower sorptivity values for the 40-60 perlite sand.

Visual inspection revealed that all experiments with infiltration rates between 0.3 and 12 cm/h gave rise to fingering. It is not possible to determine the total number of fingers due to the frequent merger of adjacent fingers. However, there were sufficient isolated fingers to allow the determination of finger diameter. The fingers that touched the edge of the column were not considered. Figs 2.4A-2.4D show experimental results in perlite sand for different grain sizes at a depth of 30 cm under water application rates between 4.3 and 12.3

Table 2.1. Summary of Experiments in lysimeters filled with sand of 14-20, 20-30, 30-40, or 40-60 mesh size

	Number of experiments											
	Sand size (US Mesh)											
	14-20			20-30			30-40			40-60		
	Lysimeter type †											
Infiltration rate	S	SQ	L	S	SQ	L	S	SQ	L	S	SQ	L
(cm/hour)												
0.12 - 0.5	6	6	-	5	-	-	5	-	-	3	-	-
0.5 - 3.0	4	-	-	3	-	-	4	-	1	4	-	-
3.0 - 6.0	9	1	1	6	1	-	2	-	1	2	-	1
6.0 - 9.0	14	5	-	1	1	-	-	2	1	-	1	-
9.0 - 12.0	9	-	-	-	2	-	-	1	1	-	-	-
12.0 <	1	-	-	2	-	-	2	-	-	3	-	1
Total	43	12	1	17	4	0	13	3	4	12	1	2

† S means small lysimeter with perlite sand; SQ means small lysimeter with quartz sand; and L means large lysimeter with perlite sand.

Table 2.2. Physical Parameters of the Perlite and Quartz Sand

	Parameters†						
Sand size	K_s	θ_s	θ_r	α	n	Ψ_{we}†	S†
US Mesh	cm/h	m^3m^{-3}	m^3m^{-3}	1/cm	-	cm	$cm/h^{1/2}$
				Perlite			
14-20	1188	.45	.075	.188	3.48	3.5	13.2
20-30	720	.45	.044	.131	4.50	6.0	16.8
30-40	468	.45	.063	.092	5.07	8.0	17.4
40-60	252	.45	.052	.062	5.19	10.0	15.0
				Quartz			
14-20	1008	.42	.075	.135	4.02	3.0	11.2
20-30	648	.42	.047	.129	3.97	5.0	12.8
30-40	360	.42	.08	.08	5.76	8.5	14.0
40-60	180	.42	.042	.061	4.50	11.0	15.4

† K_s is saturated hydraulic conductivity; θ_s is saturated water content; θ_r is residual water content; α and n are empirical parameters that describe the shape of the water retention curve in the Van-Genuchten equation (Van Genuchten 1980); Ψ_{we} is the water-entry value based on the capillary rise experiments; S is the sorptivity at water-entry value based on the capillary rise experiments.

Fig. 2.4. Experimental results at high infiltration rates at a depth of 30 cm: (A.) 14-20 Perlite in small lysimeter under 9 cm/h application rate; (B.) 20-30 Perlite in small lysimeter under 4.3 cm/h application rate; (C.) 30-40 Perlite in large lysimeter under 12.3 cm/h application rate; (D.) 40-60 Perlite in large lysimeter under 9 cm/h application rate

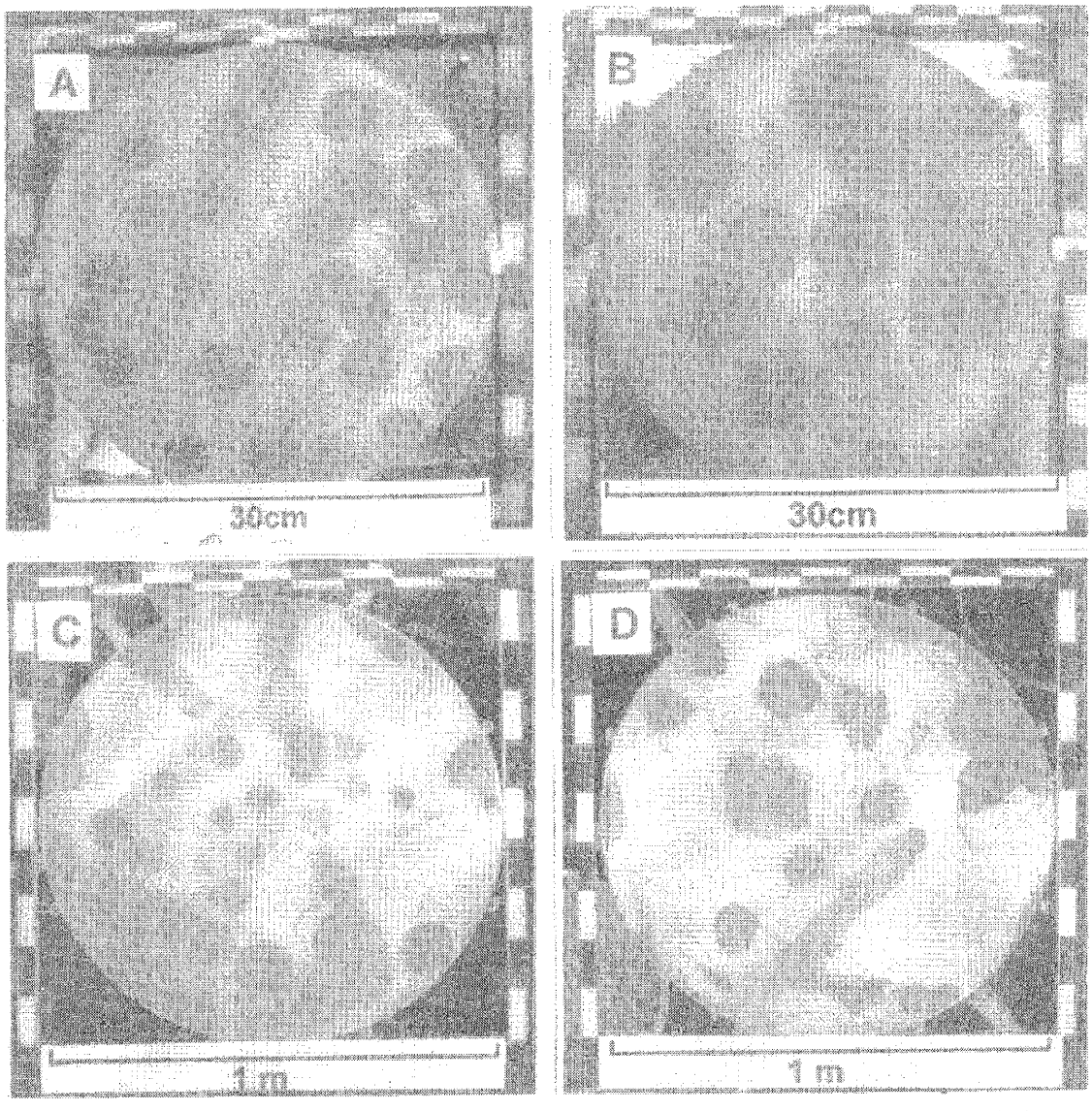

cm/h. It is evident that the finger diameter increases with decreasing grain size which is a verification of Eq. [1] of Glass et al. (1991) under these relatively high infiltration rates.

Effects of Decreasing Infiltration Rates on Finger Diameter

Figure 2.5A presents both the finger diameters observed in the experiment in perlite sands and those predicted by Eq. [1]. It is clear that the equation fails to provide a prediction of finger diameter at water infiltration rates below 1 cm/h. The two finger diameters of 30 cm at an infiltration rate of 0.2 cm/h indicate stable wetting because these fingers cover the entire horizontal cross section of the small lysimeters. The finger diameter behavior at decreasing infiltration rates observed in the 14-20 perlite sand (Fig. 2.5A) is similar to that observed in the quartz sand (Fig. 2.5B). The pictures of Fig. 2.6 illustrate the relation between finger width and infiltration rate in 14-20 perlite and quartz sand. In perlite and quartz sand at rates of 9 and 8.6 cm/h we observed finger diameters of, respectively, 2.5 and 4 cm (Fig. 2.6A and B). At infiltration rates of 0.14 and 0.12 cm/h we observed large finger diameters that almost covered the entire column area (Figs. 2.6C and D). In quartz sand at a rate of 0.29 cm/h we observed a finger diameter of 13 cm (Fig. 2.6E), while a rate of 0.13 cm resulted in a stable wetting front (Fig. 2.6F). The dry ring at the edge is a result of an edge cover used to prevent an edge effect. The above comparison between finger diameters observed in perlite and quartz sand leaves no doubt that the wetting processes in both sands are similar and are not affected by their different physical properties.

Fig. 2.5. Plot of finger diameters* vs. the infiltration rates in the (A) perlite and (B) quartz sand

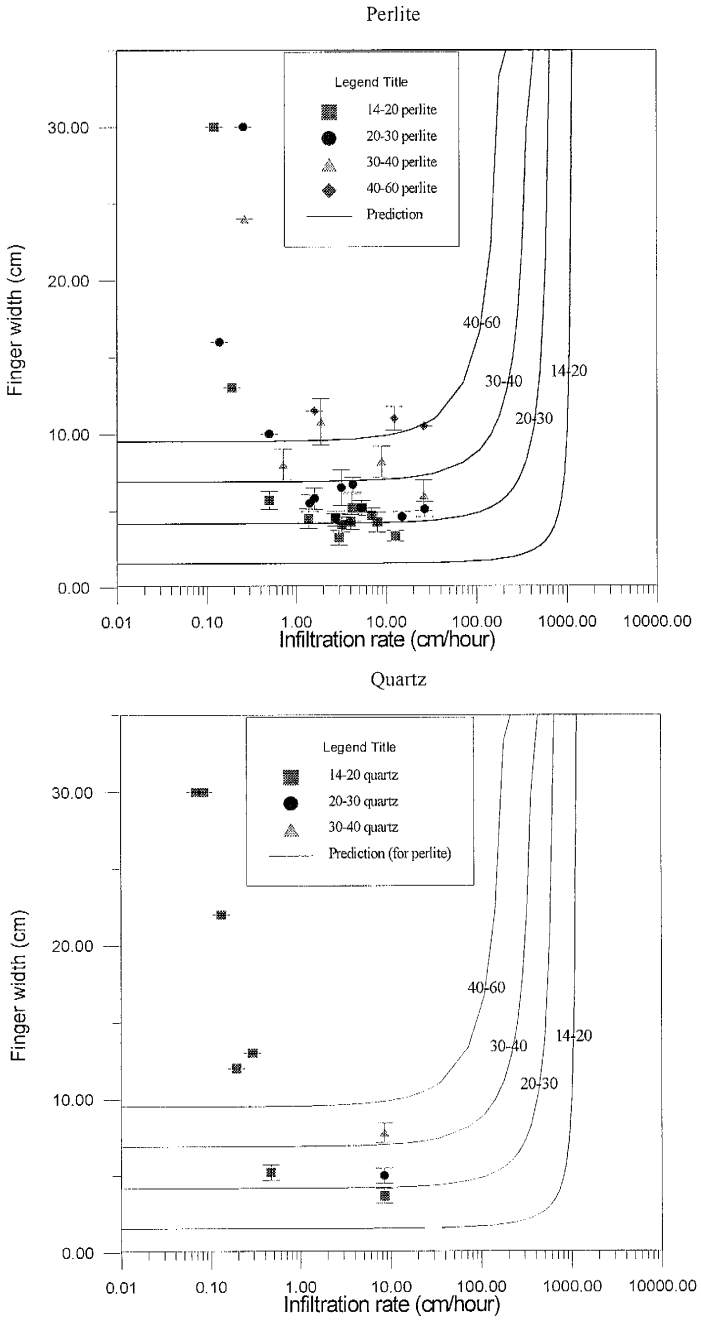

* Finger diameters were measured using tape measure during the column slicing. All the fingers that are joined or attached to the edge were not measured. Standard deviations for average finger size are shown.

Fig. 2.6. Experimental results observed in small lysimeter at high (8.5-9.0 cm/h) and low (0.12-0.29 cm/h) infiltration rates in 14-20 perlite and quartz sand (A) high rate of 9 cm/h in perlite; (B) high rate of 8.6 cm/h in quartz; (C) low rate of 0.14 cm/h in perlite; (D) low rate of 0.12 cm/h in perlite; (E) low rate of 0.29 cm/h in quartz; (F) low rate of 0.13 cm/h in quartz

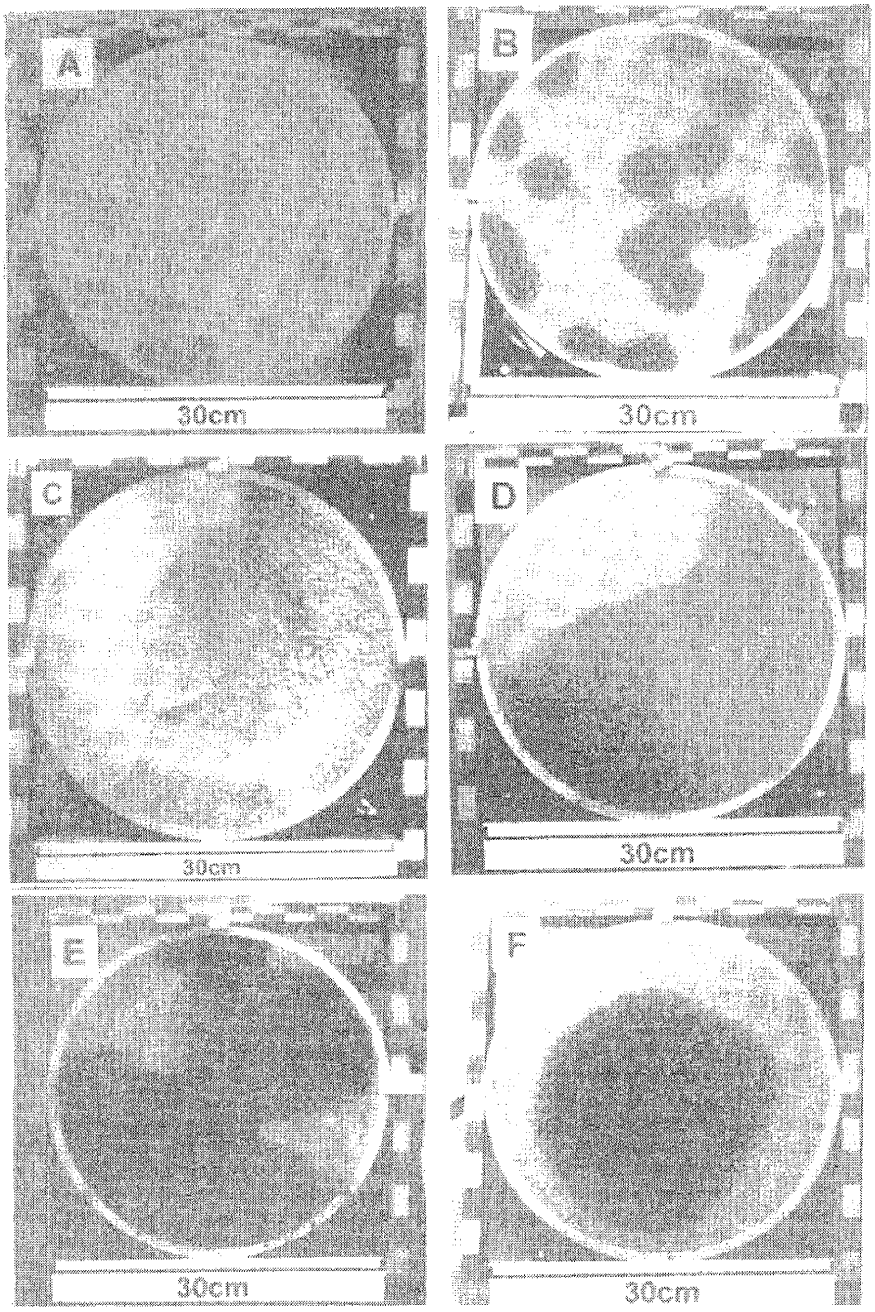

These low infiltration rate experiments increase our understanding of unstable wetting under natural conditions since they simulate the conditions at low precipitation intensities. Figures 2.6A-2.6F show a trend of widening finger diameters at lower infiltration rates. For the 30 cm diameter column, the finger diameters start to increase at rates below 1 cm/h (Figs. 2.6C and 2.6E) and stabilize at a rate of 0.12 cm/h (Figs. 2.6D and 2.6F). For fine grain size sand the stabilization appears to start at a higher infiltration rate of 2 cm/h (Fig. 2.5). The stabilization of wetting fronts at low infiltration rates has not been reported as such, although some investigators observed a change in wetting patterns. For example, Glass et al. (1989b) observed that under low flow rates the fingers tend to have a meandering behavior. This property allows fingers to touch each other, resulting in larger fingers. But they still concluded that under low infiltration rates finger diameters maintain their small size as suggested by Eq. [1].

The experimental results obtained in the 20 quartz sand experiments are similar to those observed in the 92 perlite sand experiments. This indicates that the special properties of perlite sand such as the lower density, chemically bonded water molecules, and micro-porosity in the grains did not affect the results. Table 2.3 shows the finger diameters predicted by Eq. [1] under intermediate flux conditions (> 1 cm/h) using the measured parameters in Table 2.2. The predicted diameters increase when grain size becomes finer; sorptivity increases and saturated conductivity decreases. In general, Eq. [1] is able to predict finger diameters quite well for infiltration rates higher than 1 cm/h. However, the absolute accuracy may be off by a factor of 2. The lack of accuracy is caused by the fact that the

Table 2.3. Predicted and Observed Finger Diameters in Perlite and Quartz Sand

	Diameters in Perlite		Diameters in Quartz	
Sand size	Predicted	Observed	Predicted	Observed
US Mesh	cm	cm	cm	cm
14-20	1.6	3-6	1.4	2.5-5
20-30	4.2	4-7	2.9	4-6
30-40	6.9	6-11	7.0	6.5-9
40-60	10.0	10-18	14.3	-

sorptivity of coarse sand is very hard to measure, especially in the region of the water-entry value. The high uncertainty of sorptivity measurements has been discussed by Selker et al. (1992a) and seems to be a major drawback to a more accurate prediction of finger diameters.

This study confirms our hypothesis that wetting fronts stabilize under low infiltration rates. When gravity dominates the infiltration process at rates lower than the saturated hydraulic conductivity, fingers will occur with a diameter predicted by Eq. [1]. However, when gravity plays little or no part and capillarity dominates, there is no mechanism to cause instability and, as a consequence, the wetting fronts will be stable and no fingers will form. Hendrickx and Yao (1996) apply the experimental results of this study for the prediction of wetting front stability in dry homogeneous field soils using readily available precipitation and soil data.

The effect of gravity becomes negligible under two extreme conditions. The first condition is encountered at infiltration rates equal or higher than the saturated hydraulic conductivity where viscosity dominates the flow process and no fingers are formed. The second condition is found at very low infiltration rates where capillarity dominates the flow processes and gravity effects are virtually absent. The analysis of Glass et al. (1989a, b; 1991) is based on previous work done by Chuoke et al. (1959), Saffman (1986), and Saffman and Taylor (1958) on viscous fingering. As a consequence the analysis of Glass et al (1989a, b) is correct for the prediction with Eq. [1] of the change from stable wetting

to unstable wetting at relatively high rates when gravity starts dominating the effect of viscosity.

However, at low infiltration rates viscous effects are virtually absent and the process becomes dominated by capillary forces, a condition at which Eq. [1] fails to correctly predict wetting front stabilities. Although Glass et al. (1989a, b, 1991) take into account some effects of capillarity following a procedure proposed by Parlange and Hill (1976), their basic analysis remains a study of viscous fingering that cannot account for processes where viscosity does not play a role as in the case of infiltration rates below 1 cm/h. Therefore, Eq. [1] does not correctly predict the stability of wetting fronts at low rates where viscosity effects are absent.

In summary, we have investigated the stability of wetting fronts during infiltration in homogeneous dry sand soils at rates that are representative of natural precipitation intensities. The experimental results demonstrate that, at such low rates, the wetting fronts tend to become stable. The stability analysis by Glass et al. (1991) does not account for this behavior, and can therefore not be used for prediction of wetting front behavior under low infiltration rates in dry homogeneous soils.

References

Ankney, M.D., T.C. Kaspar, and R. Horton. 1988. Design for an automated tension infiltrometer. Soil Sci. Soc. Am. J. 52:893-896.

Baker, R.S., and D. Hillel. 1990. Laboratory tests of a theory of fingering during infiltration into layered soils. Soil Sci. Soc. Am. J. 54:20-30.

Beven, K., and P. Germann. 1982. Macropores and water flow in soils. Water Resour. Res. 18(5):1311-1325.

Bouma, J. 1980. Soil morphology and preferential flow along macropores. Agri. Water Management. 3:235-250.

Bubenzer, G.D., 1979. Rainfall characteristics important for simulation. p. 22-34. *In* Proceedings of rainfall simulator workshop, Tucson, AZ. 7-9 Mar. 1979.

Carsel, R.F., and R.S. Parrish. 1988. Developing joint probability distributions of soil water retention characteristics. Water Resources Research 24:755-769.

Carter, C.E., J.D. Greer, H.J. Braud, and J.M. Floyd. 1974. Raindrop characteristics in south central United States. Trans. ASAE. 17(6):1033-1037.

Chuoke, R.L., P. van Meurs, and C. van der Poel. 1959. The instability of slow, immiscible, viscous liquid and liquid displacements in permeable media. Trans. ACME 216: 188-194.

Diment, G.A., and K.K. Watson. 1983. Stability analysis of water movement in unsaturated porous materials: 2. Numerical studies. Water Resour. Res. 19:1002-1010.

Diment, G.A., and K.K. Watson. 1985. Stability analysis of water movement in unsaturated porous materials: 3. Experimental studies. Water Resour. Res. 21:979-984.

Diment, G.A., K.K. Watson, and P.J. Blennerhassett. 1982. Stability analysis of water movement in unsaturated porous materials: 1. Theoretical considerations. Water Resour. Res. 18:1248-1254.

Elrick, D.E., W.D. Reynolds. 1992. Infiltration from constant-head well permeameters and infiltrometers. p. 1-24. *In* G. C. Topp et al. (ed.) Advances in measurement of soil physical properties : Bring theory into practice. SSSA Spec. Publ. 30. SSSA, Madison, WI.

Glass, R.J., J. King, S. Cann, N. Bailey, J.-Y. Parlange, and T.S. Steenhuis. 1990. Wetting front instability in unsaturated porous media: A three-dimensional study. Transp. Porous Media. 5: 247-268.

Glass, R.J., J.-Y. Parlange., and T.S. Steenhuis, 1991. Immiscible displacement in porous media: Stability analysis of three-dimensional, axisymmetric disturbances with application to gravity-driven wetting front instability. Water Resour. Res. 27:1947-1956.

Glass, R.J., T.S. Steenhuis, and J.-Y. Parlange. 1989a. Wetting front instability: 1. Theoretical discussion and dimensional analysis. Water Resour. Res. 25:1187-1194.

Glass, R.J., T.S. Steenhuis, and J.-Y. Parlange. 1989b. Wetting front instability: 2. Experimental determination of relationships between system parameters and two-dimensional unstable flow field behavior in initially dry porous media. Water Resour. Res.25:1195-1207.

Glass, R.J., T.S. Steenhuis, and J.-Y. Parlange. 1989c. Mechanism for finger persistence in homogeneous, unsaturated, porous media: theory and verification. Soil Sci. 148:60-70.

Hagerman, J.R., N.B. Pickering, W.F. Ritter, and T.S. Steenhuis. 1989. In situ measurement of preferential flow. ASCE National Water Conference and Symposium, Newark, Delaware. pp. 10.

Hendrickx, J.M.H., and L.W. Dekker. 1991. Experimental evidence of unstable wetting fronts in non-layered soils. p. 22-31. *In* Proc. Natl. Symp. Preferential Flow, Chicago, IL. 16-17 Dec. 1991. Am. Soc. Agric. Eng., St. Joseph, MI.

Hendrickx, J.M.H. and T. Yao. 1996. Prediction of wetting front stability in dry homogeneous field soils under non-ponding infiltration. Geoderma, 70:265-280.

Hendrickx, J.M.H., L.W. Dekker, and O.H. Boersma. 1993. Unstable wetting fronts in water repellent field soils. J. of Environmental Quality. 22:109-118.

Hendrickx, J.M.H., L.W. Dekker, and P.A.C. Raats. 1988a. Formation of sand columns caused by unstable wetting fronts. Grondboor en Hamer. 6:173-175. (in Dutch).

Hendrickx, J.M.H., L.W. Dekker, E.J. Van Zuilen, and O.H. Boersma. 1988b. Water and solute movement through a water repellent sand soil with grass cover. pp. 131-146. *In* Wierenga, P.J. and D. Bachelet. Validation of flow and transport models for the unsaturated zone: Conference Proceedings; May 23-26, 1988 Ruidoso, New Mexico. Research Report 88-SS-04 Dept. of Agronomy and Horticulture, New Mexico State University, Las Cruces, N.M. pp. 545.

Hill, D.E., and J.-Y. Parlange. 1972. Wetting front instability in layered soils. Soil Sci. Soc.

Am. Proc. 36:697-702.

Hillel, D., and R.S. Baker. 1988. A descriptive theory of fingering during infiltration into layered soils. Soil Sci. 146:51-56.

Koorevaar, P., G. Menelik, and C. Dirksen. 1983. Elements of soil physics. Elsevier, New York. pp. 230.

Laws, J.O., and D.A. Parsons. 1943. Relation of raindrop size to intensity. Trans. Am. Geophy. Union. 24:452-460.

Liu, Y., T.S. Steenhuis, and J.-Y. Parlange. 1994. Closed-form solution for finger width in sandy soils at different water contents. Water Resour. Res. 30:949-952.

Marshall, T.J, and J.W. Holmes. 1979. Soil physics. Cambridge Univ. Press. pp. 345.

Parlange, J.-Y., and D.E. Hill. 1976. Theoretical analysis of wetting front instability in soils. Soil Sci. 122:236-239.

Philip, J.R., 1957. The theory of infiltration: 4. Sorptivity and algebraic infiltration equations. Soil Sci. 84:257-264.

Philip, J.R., 1969. Theory of infiltration. Advance. Hydroscience 5:215-296.

Philip, J.R. 1975a. Stability analysis of infiltration. Soil Sci. Soc. Am. Proc. 39:1042-1049.

Philip, J.R. 1975b. The growth of disturbances in unstable infiltration flows. Soil Sci. Soc. Am. Proc. 39 :1049-1053.

Prevedello, C.L., P.L. Libardi, and K. Reichardt. 1991. Water flow in homogeneous unsaturated soils: An attempt using a diffusional model to describe gravitational flow. Soil Sci. 152: 184-188.

Raats, P.A.C. 1973. Unstable wetting fronts in uniform and nonuniform soils. Soil Sci. Soc.

Am. Proc. 37:681-685.

Ritsema, C.J., L.W. Dekker, J.M.H. Hendrickx, and W. Hamminga. 1993. Preferential flow mechanism in a water-repellent sandy soil. Water Resour. Res. 29:2183-2193.

Saffman, P.G. 1986. Viscous fingering in Hele Shaw cells. J. Fluid Mech. 173:73.

Saffman, P.G. and G.I. Taylor. 1958. The penetration of a fluid into a porous medium or Hele-Shaw cell containing a more viscous liquid. Proc. Roy. Soc. London. A245:312-331.

Selker, J.S., T.S. Steenhuis, and J.-Y. Parlange. 1989. Preferential flow in homogeneous sandy soils without layering. Paper No. 89-2543, Am. Soc. Agric. Eng.,Winter Meeting, New Orleans. pp. 22.

Selker, J.S., T.S. Steenhuis, and J.-Y. Parlange. 1992a. Wetting front instability in homogeneous sandy soils under continuous infiltration. Soil Sci. Soc. Am. J. 56:1346-1350.

Selker, J.S., P. Leclerq, J.-Y. Parlange, and T.S. Steenhuis. 1992b. Fingered flow in two dimensions. 1. Measurement of matric potential. Water Resour. Res. 28:2513-2521.

Selker, J.S., J.-Y. Parlange, and T.S. Steenhuis. 1992c. Fingered flow in two dimensions. 2. Predicting finger moisture profile. Water Resour. Res. 28:2523-2528.

Stroosnijder, L. 1976. Infiltration and redistribution of water in soils. Publisher Pudoc, Wageningen, The Netherlands. (in Dutch).

Tabuchi, T. 1961. Infiltration and ensuing percolation in columns of layered glass particles packed in laboratory (In Japanese, with a summary in English). Nogyo dobuku kenkyn, Bessatsu (Trans. Agr. Eng. Soc., Japan). 1:13-19.

Tamai, N., T. Asaeda, and C.G. Jeevaraj. 1987. Fingering in two-dimensional, homogeneous, unsaturated porous media. Soil Sci. 144:107-112.

Van Genuchten, M.Th. 1980. A closed-form equation for predicting the hydraulic conductivity of unsaturated soils. Soil Sci. Soc. Am. J. 44:892-898.

Van Genuchten, M.Th., F. J. Leij, and S. R. Yates. 1991. The RETC code for quantifying the hydraulic functions of unsaturated soils. U.S. Salinity Laboratory, U. S. Department of Agriculture, Agricultural Research Service, Riverside, CA.

Van Ommen, H.C., R. Dijksma, J.M.H. Hendrickx, L.W. Dekker, J. Hulshof, and M. van den Heuvel. 1989. Experimental assessment of preferential flow paths in a field soil. J. of Hydrology 105:253-262.

White, I., P.M. Colombera, and J.R. Philip. 1976. Experimental study of wetting front instability induced by sudden change of pressure gradient. Soil Sci. Soc. Am. J. 40:824-829.

White, I., and M.J. Sully. 1987. Microscopic and macroscopic capillary length and time scales from field infiltration. Water Resour. Res. 23:1514-1522.

3. Practical Estimation of Finger Sizes for Field Application

T. Yao, J. -Y. Parlange, T. S. Steenhuis, and J. M. H. Hendrickx

T. Yao and J.M.H. Hendrickx, Hydrology Program, Department of Earth & Environmental Sciences, New Mexico Tech, Socorro, NM 87801;

J.-Y. Parlange and T.S. Steenhuis, Department of Agricultural and Biological Engineering, Cornell University, Ithaca, NY 14853

Abstract

We verified an equation for the prediction of finger sizes in homogeneous soils under unstable wetting conditions. To apply this equation over the full range of infiltration rates, we differentiated two conditions: saturated and unsaturated fingers. For infiltration rates exceeding approximately 1 cm/hr, the finger tip is assumed to be saturated and the equation uses easily determined hydraulic properties close to saturation and at water entry value.

Under these conditions it yields a range of finger size predictions which were found to bound the experimentally observed finger sizes. Under lower infiltration rates, the finger tip is no longer saturated and the hydraulic parameters for finger size prediction are more difficult to obtain. We described an approximate scheme to obtain these parameters from infiltration experiments. The equation correctly predicts finger sizes at infiltration rates less than 1 cm/hr if the proper hydraulic parameters are used. We present a step-by-step approach for practical finger size estimation in field soils.

Introduction

A good understanding of wetting front instability is of crucial importance for the prediction of water movement and solute transport in the vadose zone since it causes preferential flow channels that accelerate water and contaminant transport processes [*e.g. Hendrickx and Dekker*, 1991; *Hendrickx et al.,* 1993*; Parlange et al.*, 1988]. An important characteristic of these channels, also called fingers, is their size.

The diameter of finger flow paths has been studied through linear stability analysis by *Chuoke et al.* [1959], *Philip* [1975a,b], *Parlange and Hill* [1976], and *Glass et al.* [1989a, 1991]. The minimum critical wavelength obtained from stability analysis is the major criterion used for finger size determination. Half of the critical wavelength is equivalent to the finger diameter. *Parlange and Hill* [1976] derived a two-dimensional formula for finger size determination. *Glass et al.* [1991] extended this formula in three dimensions:

$$d = \lambda \frac{S_F^2}{K_F(\theta_F - \theta_0)} \left[\frac{1}{1 - q/K_F}\right] \qquad \textbf{(1)}$$

where λ = 4.8 in three dimensions [*Glass et al.*, 1991] and $\lambda = \pi$ in two dimensions [*Parlange and Hill*, 1976], S_F is the sorptivity of the porous medium at water content of finger tip, K_F is the hydraulic conductivity at water content of finger tip, θ_F is the water content of finger tip, θ_0 is the initial water content, and q is the infiltration rate. The formula has been verified by experimental studies [*Glass et al.,* 1989b, 1990; *Selker et al.*, 1992a; *Ritsema et al.,* 1996].

When fingers are close to saturation under high infiltration rates, *Glass et al.*, [1989a] suggested the following approximation for finger size prediction: θ_F is replaced by θ_s, K_F is replaced by K_s, and S_F is replaced by S_{we} where S_{we} is the sorptivity at water entry tension. Using these parameters, *Glass et al.* [1989b, 1990] and *Selker et al.* [1992a] verified equation (1) for the prediction of finger sizes for high and intermediate infiltration rates (more than 1 cm/hr).

Using hydraulic properties at the water entry tension for the finger properties in equation (1), *Ritsema et al.* [1996] found that equation (1) yields finger size predictions close to those observed in the field. *Liu et al.* [1994] conducted two-dimensional experiments with a point source as water supply and also found a good match between predicted and measured finger diameters using an approximate formula based on equation (1). These studies

demonstrate that equation (1) yields reliable results for high and intermediate infiltration rates.

In laboratory experiments with sand-filled lysimeters, *Yao and Hendrickx* [1996] observed that wetting fronts start to stabilize and finger sizes increase at infiltration rates below 1 cm/hr and become stable at rates below 0.1 cm/hr. Their results were quite different from the finger sizes predicted with equation (1) by *Glass et al.* [1989a] under the assumption of saturated finger tips for all infiltration rates. Therefore, *Yao and Hendrickx* [1996] observed that the approach by *Glass et al.* [1989a] for high and intermediate infiltration rates cannot be used for finger size prediction at low infiltration rates. In this note, we will readdress this issue and propose a practical method to estimate finger sizes using equation (1).

Method and Materials

The use and applicability of equation (1) will be verified using finger diameters observed during 3-dimensional experiments by *Yao and Hendrickx* [1996].

Material and Experiments

Three different grades of perlite sand and quartz sand were used: US mesh size No. 14-20 (1.41-.841mm), 20-30 (.841-.594mm), and 30-40 (.594-.42mm). The air-dried sands

were used to fill small non-weighing lysimeters (diameter 30 cm, height 50 cm). Perlite was also used in a large lysimeter (diameter 100 cm, height 150 cm). The lysimeters were exposed to infiltration rates from 0.068 to 27 cm/hr; total amounts of applied water varied between 2.5 to 8 cm. After water application, the lysimeters were excavated layer by layer to allow visual inspection of the flow pattern. In each layer we photographed the wetting pattern for analysis of total wet area and finger diameter. For experimental details we refer to *Yao and Hendrickx* [1996].

The following soil hydraulic properties have been measured: the unsaturated hydraulic conductivity using the instantaneous profile method [*Watson*, 1966], soil water retention with the hanging water column, and sorptivity. Sorptivity measurements were taken at and close to water entry values using the tension infiltrometer [*Ankney et al.,* 1988]. In this study we only use the hydraulic properties from quartz sands which are similar to those of perlite sands [*Yao and Hendrickx,* 1996]. The hydraulic conductivity model by *Mualem* [1976] and soil water retention model by *van Genuchten* [1980] were used to fit the measured data to soil hydraulic parameters (Table 3.1).

Finger Size Calculation

Under intermediate to high infiltration rates, it is relatively easy to determine soil parameters needed for finger size prediction since the finger tip can be assumed to be close

Table 3.1. Soil hydraulic properties of quartz sands

Sand Size	K_s	K_{we}	θ_r	θ_s	θ_{we}	S_{we}^2	α*	n*	λ	ψ_{we}**
US mesh	– cm/hr –		–	cm^3/cm^3 –		cm^2/hr	1/cm	-	-	cm
14-20	1008	362	0	.42	.36	124.2	.208	2.92	1.22	3
20-30	648	140	0	.42	.32	165.6	.156	2.88	.828	5
30-40	360	109	0	.42	.33	194.4	.09	3.46	.61	8.5

K_s, saturated hydraulic conductivity; K_{we}, hydraulic conductivity at water entry tension; θ_r, residual water content; θ_s, saturated water content; θ_{we}, water content at water entry tension; S_{we}, sorptivity at water entry value; α, n, and λ are curve-fitting parameters for soil hydraulic properties [*van Genuchten*, 1980]; ψ_{we}, soil water tension at water entry value

* Fitted with initial wetting curve

** Estimated from gravimetrically vertical capillary rise experiments [*Yao and Hendrickx*, 1996]

to saturation. Previous research demonstrated that two different sets of parameters can be used: one for hydraulic properties at saturation [*Glass, et al.*, 1989a] and another one for hydraulic properties at the water entry value [*Hillel and Baker*, 1988]. In approach I, θ_F, K_F, and S_F are set to equal to saturated water content, saturated hydraulic conductivity, and sorptivity at water entry value, respectively [*Glass, et al.*, 1989a]. Approach II assumes that finger tips are close to saturation but with water content and hydraulic conductivity at the water entry value [*Hillel and Baker*, 1988]. Table 3.1 lists all the parameters used for our calculation.

Under low infiltration rates, it cannot be assumed that the finger tip is close to saturation. Therefore, equation (1) requires actual measurements of water content at the finger tip (θ_F), the sorptivity at the finger tip (S_F), and the hydraulic conductivity at the finger tip (K_F). These parameters are not readily measurable in the field and need a special laboratory setup. However, with certain assumptions we can obtain estimates of these parameters (approach III).

In approach III, the water content at the unsaturated finger tip is estimated from wetting ratio data from the lysimeter experiments. The wetting ratio (WR) is the ratio of the average wetted area over the total cross-sectional area of the lysimeter. Minimum water content at the finger tips (θ_F) has been estimated as:

$$\theta_F > \frac{K_F\ t\ A}{V_l} \qquad \textbf{(2)}$$

where $K_F = i/WR$, i is the infiltration rate, t is the duration of water application, A is the surface area of the lysimeter, and V_l is the total volume of the lysimeter. This equation yields the average water content in the fingers. Since the water content at the finger tips has been measured to be higher than the average water content taken over the entire finger length [*Glass et al.*, 1989c; *Selker et al.*, 1992b; *Liu et al.*, 1994], equation (2) provides an estimate of the minimum water content at the finger tip. θ_F and its corresponding S_F and K_F values are used to calculate finger sizes with equation (1).

Sorptivity values at different tensions have been calculated with the approximate formula of *Parlange* [1975]:

$$S^2 = \int_{h_i}^{h} [\theta(h) + \theta(H) - 2\theta(h_i)] K(h) dH \qquad \textbf{(3)}$$

where S is the sorptivity, h is the soil water tension at the surface of water supply, h_i is the initial soil water tension, θ is the water content which is a function of the soil water tension, $\theta(h_i)$ is the initial soil water content, H is a dummy variable, and $K(h)$ is the unsaturated hydraulic conductivity. Approach III can only be applied when the fingers do not reach the bottom of the lysimeter. Therefore we excluded experiments from *Yao and Hendrickx* [1996] in which fingers reached the bottom of the lysimeter.

Results and Discussion

Finger Sizes under High and Intermediate Infiltration Rates

Approaches I and II were used to estimate finger sizes. Figures 3.1 through 3.3 show that equation (1) yields reasonable estimates of the finger size in the three experimental sands at infiltration rates from 1 to 30 cm/hr. The observed finger sizes were located between the predicted ones using approaches I and II. Approach I results in an underestimation of finger size in US mesh 14-20 and 20-30 sands but not in 30-40 sand. The deviation seems to be caused by experimental difficulties during our sorptivity measurements in coarse sands. During these experiments, fingering phenomena were observed which resulted in lower sorptivity values. Using these underestimated sorptivity values yields smaller finger size predictions. This problem is more serious for coarse sands. Finger diameters at infiltration rates less than 1 cm/hr cannot be predicted since the assumption of saturated finger tips is not valid under this condition.

Scaling of Finger Diameter

Parlange et al. [1990] showed that Miller's scaling model can be applied to predict finger widths for unstable flow. In similar porous media, the finger width is inversely proportional to the mean grain size:

Figure 3.1. Finger diameter predictions versus experimental observations for 14-20 quartz sand using approaches I, II, and III

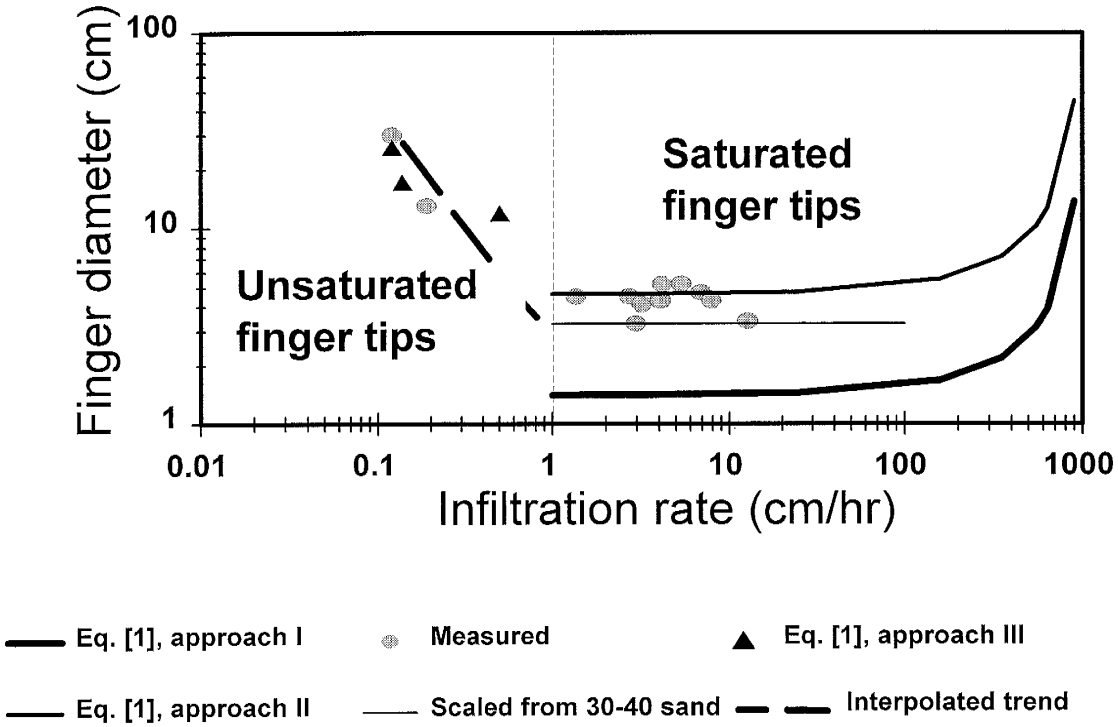

Figure 3.2. Finger diameter predictions versus experimental observations for 20-30 quartz sand using approaches I, II, and III

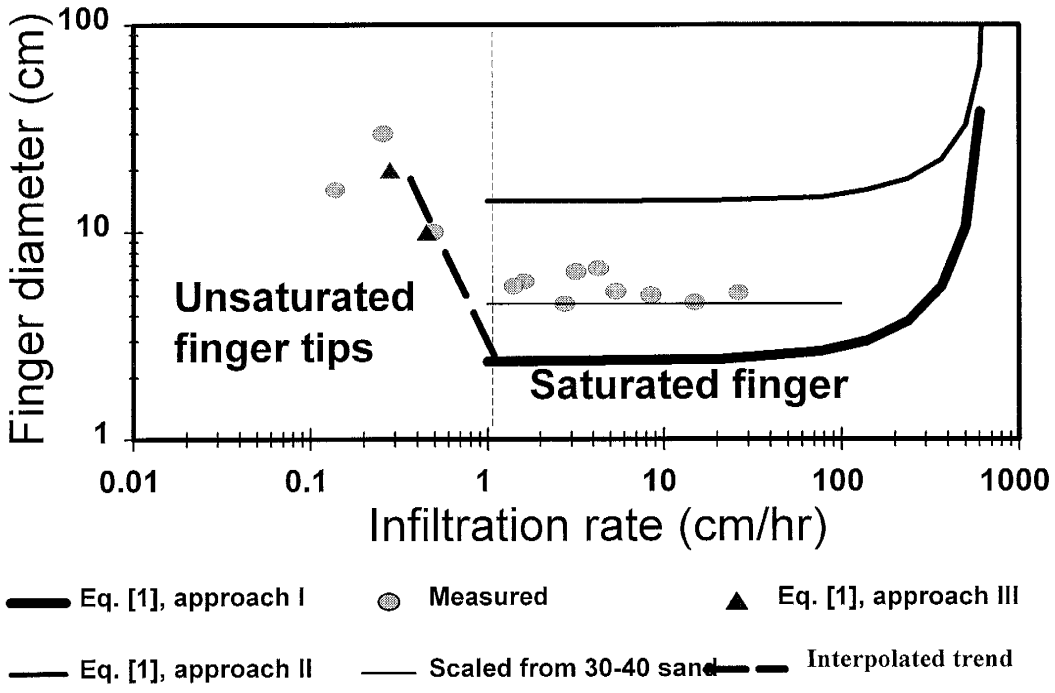

Figure 3.3. Finger diameter predictions versus experimental observations for 30-40 quartz sand using approaches I, II, and III

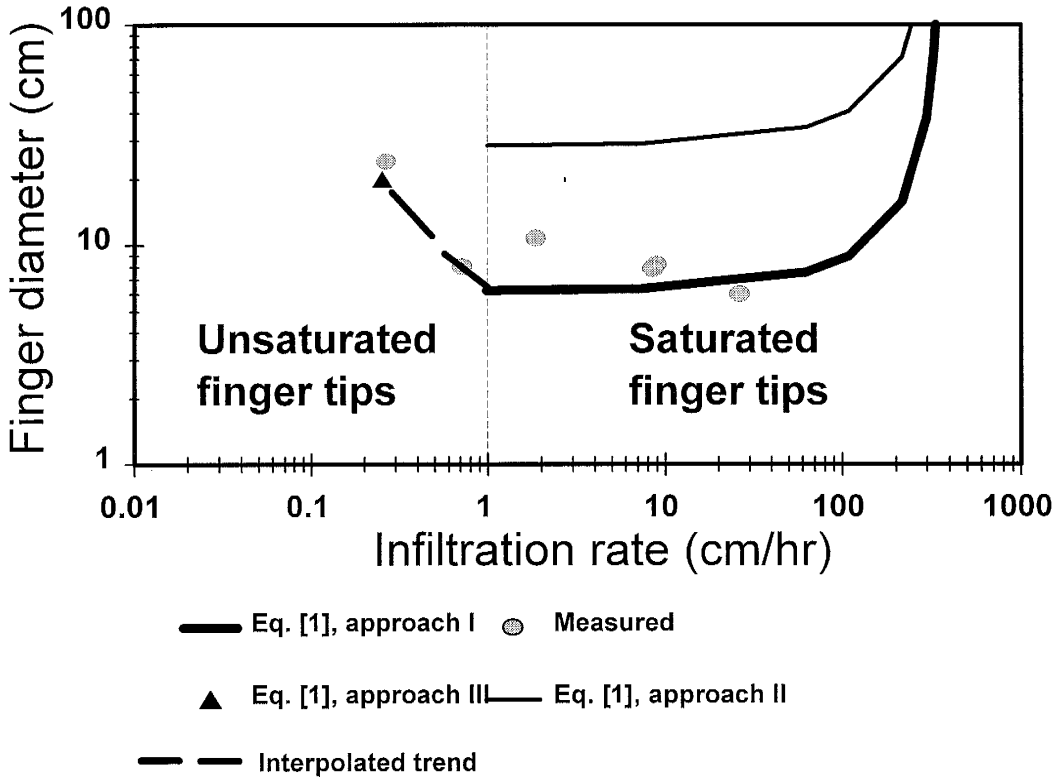

$$D_2 = D_1 M_1 / M_2 \qquad \textbf{(4)}$$

where D_2 is the finger width estimation for soils with mean grain size M_2, and D_1 is the finger width measured for soils with mean grain size M_1. Because sorptivity values are more difficult to obtain for coarse sands than fine sands, we used the results from our US mesh 30-40 sand and scaled the finger sizes for the coarser US mesh 14-20 and 20-30 sands using equation (4). Figures 3.1 and 3.2 demonstrate that the scaled finger diameters give better predictions than the predictions using equation (1) with directly measured soil parameters at intermediate infiltration rates. However, the application is restricted because this scaling relationship can only be applied to similar porous media.

Finger Sizes under Low Infiltration Rates

For infiltration rates less than 1 cm/hr, we used approach III for the prediction of finger sizes. Table 3.2 and Figures 3.1 through 3.3 show finger predictions from equation (1) using the wetting ratio data for three soils. The predictions from equation (1) using the wetting ratio data and parameter approximations from equation (3) demonstrate that equation (1) yields an excellent match between predictions and experimental observations under low infiltration rates. Therefore, we conclude that equation (1) correctly predicts finger sizes from low to high infiltration rates.

Table 3.2. The estimated parameters used in equation (1) and finger size predictions

Sand size (US Mesh)	Infiltration rates (cm/hr)	WR^* (cm^2/cm^2)	θ_F (cm^3/cm^3)	S_F^2 (cm^2/hr)	K_F (cm/hr)	Predicted Finger Size (cm)
14-20	0.5	0.363	0.275	59.4	93.96	11
	0.138	0.628	0.16	8.28	12.46	20
	0.12	1	0.16	8.28	12.46	20
20-30	0.5	0.35	0.238	25.0	35.9	14
	0.138	0.65	0.153	2.99	5.76	16
30-40	0.138	0.882	0.113	1.08	2.02	23

θ_F, water content at finger tips; S_F, Sorptivity at finger tips; K_F, hydraulic conductivity at finger tips

* WR: wetting ratio in the lysimeter experiments

Prediction of Finger Diameter

We propose the following steps to predict finger diameters for the full range of infiltration rates:

1. First the occurrence of unstable wetting fronts needs to be verified using the procedure presented by *Hendrickx and Yao* [1996].

2. Using equation (1), we approximate finger sizes using saturated hydraulic properties and the sorptivity at the water entry value. This step will give minimum finger size predictions at high and intermediate infiltration rates.

3. Using equation (1), we approximate finger sizes using water content, hydraulic conductivity, and sorptivity at water entry tensions. This step will give maximum finger size predictions at high and intermediate infiltration rates.

4. For infiltration rates less than approximately 1 cm/hr, we cannot use equation (1) assuming saturated finger tips. Finger diameters can be calculated using water content measurements at the finger tips with a special laboratory setup. Another option is to estimate water content at the finger tip using equation (2) which requires wetting ratio data from simple infiltration experiments or field observations after precipitation. Obviously, such experiments or observations would also reveal the finger size. The application of equation (1) under these

circumstances could prove useful to assess how well the unsaturated hydraulic conductivity for the soil has been determined.

A more realistic scenario is one where no information is available on wetting ratios or water content at the finger tips. Assuming that the experimental results of *Yao and Hendrickx* [1996] can be extrapolated to other soils, we postulate that wetting fronts are stable at infiltration rates less than 0.1 cm/hr. Finger diameters between infiltration rates 1 to 0.1 cm/hr can be found by linear interpolation (as is shown in Figures 3.1 to 3.3). Since the experimental data from *Yao and Hendrickx* [1996] originate from coarse sands, and wetting fronts tend to stabilize in finer texture soils [*Yao and Hendrickx*, 1998], the linear interpolation is a reasonable approach.

Conclusion

This study shows that equation (1) derived from stability analysis for the prediction of finger sizes can be applied over the full range of infiltration rates. For high and intermediate infiltration rates, finger tips are assumed to be saturated or close to saturation. Then equation (1) can be used with easily measured hydraulic parameters to predict finger sizes. For low infiltration rates, equation (1) is valid if the hydraulic parameters are determined at the water content in the finger tip.

Practitioners can use equation (1) for finger size predictions in homogeneous field soils. At infiltration rates exceeding approximately 1 cm/hr, finger sizes can be assessed from the saturated water content and saturated hydraulic conductivity or from the water content, unsaturated hydraulic conductivity, and sorptivity at the water entry value. At infiltration rates less than 0.1 cm/hr, wetting fronts tend to be stable. At infiltration rates from 1 to 0.1 cm/hr, finger sizes can be found by linear interpolation.

References

Ankney, M.D., T.C. Kaspar, and R. Horton, Design for an automated tension infiltrometer, *Soil Sci. Soc. Am. J., 52*, 893-896, 1988.

Chuoke, R.L., P. van Meurs, and C. van der Poel, The instability of slow, immiscible, viscous liquid-liquid displacements in permeable media, *Trans. AIME, 216*, 188-194, 1959.

Glass, R.J., J. King, S. Cann, N. Bailey, J.-Y. Parlange, and T.S. Steenhuis, Wetting front instability in unsaturated porous media: A three-dimensional study, *Transp. Porous Media., 5*, 247-268, 1990.

Glass, R.J., J.-Y. Parlange, and T.S. Steenhuis, Immiscible displacement in porous media: Stability analysis of three-dimensional, axisymmetric disturbances with application to gravity-driven wetting front instability, *Water Resour. Res., 27*, 1947-1956, 1991.

Glass, R.J., T.S. Steenhuis, and J.-Y. Parlange, Wetting front instability: 1. Theoretical discussion and dimensional analysis, *Water Resour. Res., 25*, 1187-1194, 1989a.

Glass, R.J., T.S. Steenhuis, and J.-Y. Parlange, Wetting front instability: 2. Experimental determination of relationships between system parameters and two-dimensional unstable flow field behavior in initially dry porous media, *Water Resour. Res., 25*, 1195-1207, 1989b.

Glass, R.J., T.S. Steenhuis, and J.-Y. Parlange, Mechanism for finger persistence in homogeneous, unsaturated, porous media: theory and verification, *Soil Sci.,148*, 60-70, 1989c.

Hendrickx, J.M.H., and L.W. Dekker, Experimental evidence of unstable wetting fronts in non-layered soils, in *Proc. Natl. Symp. Preferential Flow, Chicago, IL. 16-17 Dec. 1991, Am. Soc. Agric. Eng.*, St. Joseph, MI, pp.22-31, 1991.

Hendrickx, J.M.H., L.W. Dekker., and O.H. Boersma, Unstable wetting fronts in water-repellent soils, *J. Environ. Qual., 22*, 109-118, 1993.

Hendrickx, J.M.H., and T. Yao, Prediction of wetting front stability in dry field soils using soil and precipitation data, *Geoderma, 70*, 265-280, 1996.

Hillel, D., and R.S. Baker, A descriptive theory of fingering during infiltration into layered soils, *Soil Sci., 146*, 51-56, 1988.

Liu, Y., T.S. Steenhuis, and J.-Y. Parlange, Closed-form solution for finger width in sandy soils at different water contents, *Water Resour. Res., 30*, 949-952, 1994.

Mualem, Y., A new model for predicting the hydraulic conductivities of unsaturated porous media, *Water Resour. Res., 12*, 1248-1254, 1976.

Parlange, J.-Y., On solving the flow equation in unsaturated soils by optimizing: Horizontal infiltration, *Soil Sci. Soc. Am. Proc., 39*, 415-417, 1975.

Parlange, J.-Y., and D.E. Hill, Theoretical analysis of wetting front instability in soils, *Soil Sci. 122*, 236-239, 1976.

Parlange, J.-Y., R.J. Glass, and T.S. Steenhuis, Application of scaling to the analysis of unstable flow phenomena, in *D. Hillel, and D. E. Elrick, Scaling in soil physics: Principles and applications, Soil Sci. Soc. Am. Spec. Publ., 25*, 53-57, 1990.

Parlange, J.-Y., T.S. Steenhuis, R.J. Glass, T.L. Richard, N.B. Pickering, W.J. Waltman, N.O. Bailey, M.S. Andreini, and J.A. Throop, The flow of pesticides through preferential paths in soils, *New York's Food and Life Science Quarterly, 18 (1/2)*, 20-23, Cornell University, Ithaca, NY, 1988.

Philip, J.R., Stability analysis of infiltration, *Soil Sci. Soc. Am. Proc., 39*, 1042-1049, 1975a.

Philip, J.R., The growth of disturbances in unstable infiltration flows, *Soil Sci. Soc. Am. Proc., 39*, 1049-1053, 1975b.

Ritsema, C.J., T.S., Steenhuis, J.-Y. Parlange, and L.W. Dekker, Predicted and observed finger diameters in field soils, *Geoderma, 70*, 185-196, 1996.

Selker, J.S., T.S. Steenhuis, and J.-Y. Parlange, Wetting front instability in homogeneous sandy soils under continuous infiltration, *Soil Sci. Soc. Am. J., 56*, 1346-1350, 1992a.

Selker, J.S., J.-Y. Parlange, and T.S. Steenhuis, Fingered flow in two dimensions. 2. Predicting finger moisture profile, *Water Resour. Res., 28*, 2523-2528, 1992b.

van Genuchten, M.T., A close form equation for predicting the hydraulic conductivity of unsaturated soils, *Soil Sci. Soc. Am. J., 44*, 892-898, 1980.

Watson, K.K., An instantaneous profile method for determining the hydraulic conductivity of unsaturated porous materials, *Water. Resour. Res., 2*, 709-715, 1966.

Yao, T., and J.M.H. Hendrickx, Stability of wetting fronts in homogeneous soils under low infiltration rates, *Soil Sci. Soc. Am. J., 60*, 20-28, 1996.

Yao, T., and J.M.H. Hendrickx, Stability analysis of the unsaturated water flow equation: 2. Experimental verification, submitted to *Water Resour. Res.*, 1998.

4. Prediction of Wetting Front Stability in Dry Field Soils Using Soil and Precipitation Data

Jan M.H. Hendrickx and Tzung-mow Yao

Hydrology Program, Department of Earth and Environmental Sciences,

New Mexico Tech, Socorro, NM 87801

Abstract

A need exists for information regarding the stability of wetting fronts in field soils because they increase the vulnerability for groundwater contamination. In this study, we develop a simple approach for the evaluation of wetting front stability in dry soils. We show that the stability of wetting fronts in the top layer of a soil depends both on the type of soil and the intensity of the precipitation. Our approach distinguishes stability criteria for wetting events that are different for a high, intermediate, and low infiltration rate. At *high infiltration rates*, wetting fronts are stable if the infiltration rate exceeds or equals the saturated hydraulic conductivity of the soil. The stability criterion for *low infiltration rates* (less than

approximately 0.2 cm/h for sand soils) is based on two characteristics times: a gravitational time and an infiltration time. The gravitational time, t_{grav}, indicates when gravity and capillarity each contribute equally to the process of infiltration. The infiltration time, t_{infil}, is the duration of the infiltration event. Experimental and literature data show that in well-sorted laboratory sands, wetting fronts are stable when $t_{infil}<0.002\ t_{grav}$. This expression can also be expressed as $Wi<0.002\ S^2$ with W the total amount of precipitation, i its intensity, and S the sorptivity at a slightly positive soil-water pressure. For *intermediate infiltration rates,* wetting fronts remain stable as long as W is smaller than the amount of water needed to wet a distribution layer near the surface. The application of the stability criteria is demonstrated with a case study from the Sevilleta dunes near Socorro, NM.

Introduction

An abundance of theoretical and experimental studies shows that unstable wetting is a phenomenon that does occur in field soils and increases the vulnerability for groundwater contamination (Hendrickx et al., 1993; Starr et al., 1978). Theoretical work on wetting front instability (Diment and Watson, 1983; Diment et al., 1982; Glass et al., 1989a, c, 1991; Hillel and Baker, 1988; Parlange and Hill, 1976; Philip, 1975a, b; Raats, 1973; Tabuchi, 1961) is supported by laboratory experiments (Baker and Hillel, 1990; Diment and Watson, 1985; Glass et al., 1989b, 1990; Hendrickx et al., 1988a; Hill and Parlange, 1972; Selker et al., 1989, 1992; Tamai et al., 1987; White et al., 1976; Yao and Hendrickx, 1996) and has been confirmed by field investigations (Dekker and Ritsema, 1994; Hendrickx et al., 1988b;

Hendrickx and Dekker, 1991; Ritsema and Dekker, 1994; Ritsema et al., 1993; Van Dam et al., 1990; Van Ommen et al., 1989). However, in spite of this wealth of information on the physics of unstable wetting, few efforts have been undertaken to predict the stability of wetting fronts in field soils. Starr et al. (1978, 1986) investigated unstable wetting in a layered field soil under ponded conditions while Hendrickx et al. (1993) and Ritsema et al. (1993) showed fingers in water-repellent field soils under a natural precipitation regime.

There is a pressing need for an easily applicable instability criterion that can be used by practitioners dealing with the protection of groundwater supplies. This special issue on fingered flow contains two papers that develop stability criteria for field soils. The first approach by Ritsema et al. (1996) is based on the theory of Parlange and Hill (1976), while our approach is to synthesize relevant research results on unstable wetting fronts in the development of criteria for wetting front instability.

Review of Previous Research

The literature and our own experimental data (Yao and Hendrickx, 1996) suggest that the infiltration rate and the presence of a surface fine sand layer are key elements in determining if the wetting front is stable or unstable. In analyzing the effect of flow rate, three infiltration rates are distinguished: high, intermediate, and low. *High infiltration rates exceeding saturated hydraulic conductivity* are common in flood irrigated soils and in non-irrigated soils during high intensity rainstorms. At these rates, wetting fronts are stable, as

shown by laboratory experiments (Glass et al., 1989b) and by Rice et al. (1991) who observed little preferential flow in a continuously ponded loam soil, whereas preferential flow was observed in the same soil under intermittent flooding. *Intermediate infiltration rates* (defined as rates between saturated conductivity and the rate of a gentle rainstorm), almost always result in finger formation in sandy soils. This was demonstrated by laboratory experiments (Glass et al., 1989b; Selker et al., 1992; Yao and Hendrickx, 1996), in a lysimeter study under natural precipitation (Hendrickx and Dekker, 1991), and by observations of unstable wetting patterns in Dutch and German dune sands after nonponding precipitation events (Dekker and Ritsema, 1994). Under *low infiltration rates,* capillary forces dominate over gravity forces and fingers do not form. For example, Fig. 4.1 shows that the finger diameter in a coarse 14-20 quartz sand (1.41-0.841 mm) increases from 4 cm at an infiltration rate of 8.6 cm/hour to 22 cm at a rate of 0.13 cm/hour. Such a large increase in finger diameter by itself does not prove that the wetting front has become stable since the finger diameter is larger than the width of the chamber. However, the experimental data presented in Figure 5 by Yao and Hendrickx (1996) show that at infiltration rates less than 0.2 cm/h, finger diameters increase more than 100% for each 10% decrease in infiltration rate. In other words, such low infiltration rates result in finger diameters frequently one order of magnitude larger than the thickness of the soil layer in which the infiltration takes place.

Figure 4.1. **Increase of finger diameter in a coarse 14-20 sand with decreasing infiltration rates: (a) wetting pattern at depth 20 cm after application of 4 cm water at rate of 8.6 cm/hour, (b) wetting pattern at depth 20 cm after application of 5 cm water at rate of 0.13 cm/hour**

(a) **(b)**

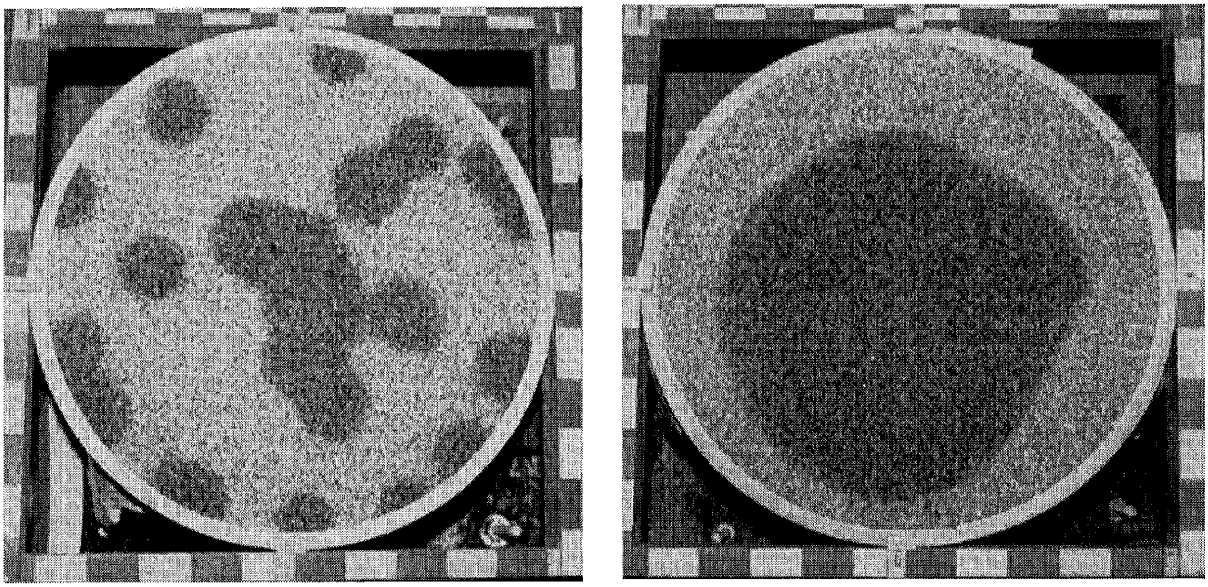

Layered Versus Non-Layered Soils

Three-dimensional infiltration experiments for the investigation of wetting front instabilities have been conducted in either layered (e.g., Glass et al., 1989b) or non-layered systems (Selker et al., 1992; Yao and Hendrickx, 1996). In layered systems, water has been applied through a fine top layer into a coarse bottom layer in which instabilities were observed. In non-layered systems, water has been applied through a sprinkler system at a rate less than the saturated hydraulic conductivity of the soil. The major difference between these two systems is the top boundary condition of the layer in which instabilities have been observed. Non-layered systems have a flux-type boundary condition with a flux equal to the infiltration rate. In layered systems, the top boundary condition of the bottom layer in which the instability occurs is a pressure head equal to the water entry pressure. The two different top boundary conditions appear to cause different relationships between the infiltration rate and the stability of wetting fronts. For example, when a low infiltration rate (0.08 cm/h) is applied to a homogeneous non-layered dry coarse sand, a stable wetting front results. However, the same infiltration rate applied to a layered system with a fine layer on top of the same dry coarse sand causes an unstable wetting front in the coarse sand (Fig. 4.2). Although much experimental and theoretical work has been done on infiltration through layered soils (e.g., Glass et al., 1989c; Hill and Parlange, 1972; Hillel and Baker, 1988; Starr et al., 1978), the exact infiltration mechanism is still not known. For example, a distinct difference between layered and non-layered systems appears to be the way in which water is distributed laterally before entering the fingers. In non-layered systems, lateral water movement has to

Figure 4.2. Wetting pattern in (a) non-layered and (b) layered system at an infiltration rate of 0.08 cm/h

(a) **(b)**

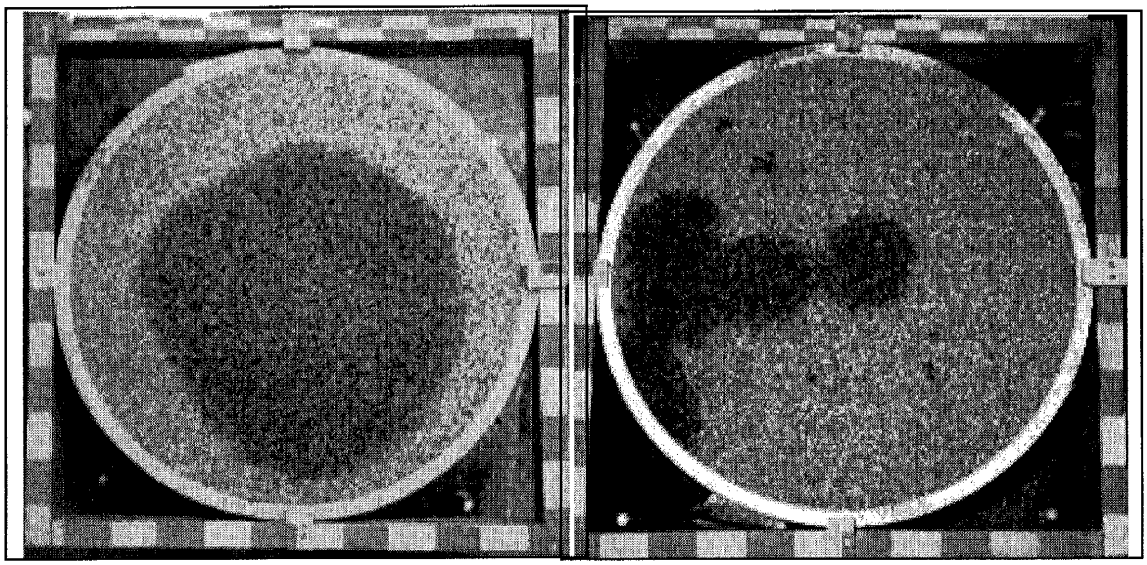

take place in the same layer that experiences the instability. Thus, a distribution layer is formed near the soil surface.

Three Stability Criteria

In the previous section, we discussed three characteristic infiltration regimes: one with high infiltration rates of the same order of magnitude as the saturated hydraulic conductivity, a condition in which viscous forces dominate the infiltration process; one with such low infiltration rates that capillary forces become dominant; and one regime in which gravity forces play a major role to the extent that gravity-driven fingers may occur. In this section, we will present a stability criterion for each of these three regimes. One of the important parameters is the *gravitational characteristic time* t_{grav} as introduced by Philip (1969):

$$t_{grav} = \left(\frac{S_i}{K_i - K_o} \right)^2 \qquad \textbf{(1)}$$

where S_i and K_i are, respectively, the sorptivity and the hydraulic conductivity at the supply soil-water pressure, and K_o is the hydraulic conductivity at the initial soil-water pressure. Philip (1969) indicates that this characteristic time is somewhat qualitative as it represents only *the order of magnitude* at which the effect of gravity on infiltration equals that of capillarity. In order to use t_{grav} for the prediction of unstable wetting fronts we will examine

at which fraction of this characteristic time gravity forces are sufficiently reduced to prevent instabilities.

Stability Criterion for High Infiltration Rates

Theoretical analysis and experimental evidence have shown that the wetting front becomes stable if the infiltration rate exceeds the saturated hydraulic conductivity of the soil. Therefore, the stability criterion for high infiltration rates becomes (Glass and Nicholl, 1996) :

$$i \geq K_{sat} \qquad \textbf{(2)}$$

If this condition is met, one should check whether an increase of soil-air pressure may cause unstable wetting to occur in the field. For higher precipitation rates, criterion Eq. [2] indicates that unstable wetting is more likely to occur in coarse than in fine soils.

Stability Criterion for Low Infiltration Rates

Philip (1975a) and Raats (1973) derive their stability criterions from the delta-function model for one-dimensional infiltration during wetting processes in which gravity plays an important role. The approach proposed in this section focuses on wetting processes in which capillarity is the dominant force and gravity effects are negligible so that no gravity-driven instabilities can occur.

Application of Eq. [1] to field soils is not straightforward because the supply and initial soil-water pressures during infiltration need to be known. Therefore, Eq. [1] is reformulated in such a manner that it can be used for field assessments of unstable wetting. For infiltration into dry soil, we can replace (K_i - K_o) in Eq. [1] by the infiltration rate, i, assuming that the conductivity of the wet soil is much higher than the dry soil and that the water flows under unit gradient. Eq. [1] is then rewritten as

$$t_{grav} = \left(\frac{S}{i} \right)^2 \qquad \textbf{(3)}$$

where S is the sorptivity measured at a slightly positive soil-water supply pressure for which data are available of many soils .

The gravitational characteristic time, by itself, cannot predict instabilities. Therefore, an *infiltration characteristic time*, t_{infil}, is introduced that reflects the characteristics of the infiltration process,

$$t_{infil} = \frac{W}{i} \qquad \textbf{(4)}$$

where W is the total amount of water available for infiltration. For irrigation, t_{infil} is the duration of the irrigation event. During storms, t_{infil} is the total amount of precipitation divided by the average precipitation intensity. In principle, if $t_{infil} \ll t_{grav}$ gravity forces are not able to dominate the flow process and cause unstable wetting fronts. If $t_{infil} \gg t_{grav}$ gravity dominates the flow process and unstable wetting fronts may occur. The question that arises

now is "what happens when t_{grav} and t_{infil} are of the same order of magnitude?" Previously, Talsma (1969) assumed that gravity effects can be neglected at times less than $0.02t_{grav}$. We examined our and other three-dimensional lysimeter experiment results in homogeneous non-layered soils for determination of the time where gravity causes instabilities by plotting, in Fig. 4.3, t_{infil} against t_{grav}. Examination of the data obtained by Yao and Hendrickx (1996) in three-dimensional infiltration experiments in perlite and quartz sands reveals that gravity effects were negligible and stable wetting fronts resulted for times less than $0.002t_{grav}$, which is one order of magnitude smaller than Talsma (1969). The observation in Fig. 4.3, marked by a question mark, is an experiment that resulted in a wetting pattern not entirely stable nor entirely unstable. The experimental data reported by Selker et al. (1992) are all located in the lower left-hand corner of Fig. 4.3, far away from the stable zone.

The experimental data presented in Fig. 4.3, show that wetting fronts are stable as long as

$$t_{infil} < 0.002\ t_{grav} \qquad \textbf{(5)}$$

The validity of this equation is limited to the well-sorted sands used in the experiments by Selker et al. (1992) and Yao and Hendrickx (1996). One important question that needs to be addressed is whether this linear relationship also holds for natural soils that are less uniform.

Figure 4.3. Plot of characteristic gravitational times (t_{grav}) versus characteristic infiltration times (t_{infil}) observed in three-dimensional experiments

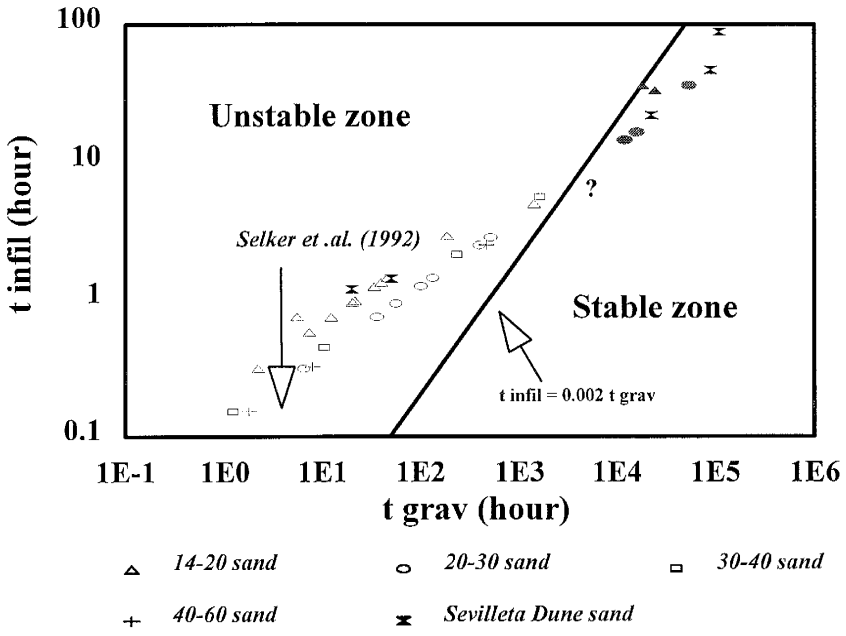

Another question is whether it is indeed necessary to relate t_{infil} and t_{grav} since Fig. 4.3 suggests that stable wetting fronts occur for t_{grav}>1500 hours. The sudden increase of finger diameter for t_{grav}>1500 hours in Fig. 4.4 seems to confirm this suggestion, at least for the experimental data obtained in well-sorted sands. Although the relationship between t_{grav} and t_{infil} clearly needs more study, Eq. [5] seems, for now, a reasonable criterion. Inserting Eqs. [3] and [4] into Eq. [5], we find, after rearranging,

$$Wi < 0.002\ S^2 \qquad \textbf{(6)}$$

This stability criterion for low infiltration rates will be useful for quick evaluation of the probability for stable wetting. However, application of this criterion "as is" may lead to erroneous results when low infiltration rates change into intermediate ones. For example, for precipitation rates of 1 cm/hour criterion Eq. [6] leads to the conclusion that clay and loam soils which have typically a lower sorptivity than sand soils, are more susceptible for unstable wetting than sand soils. Although this conclusion by itself may be correct, theoretical analysis combined with experimental field and laboratory evidence indicates that unstable wetting in finer-textured soils results in finger diameters at least an order of magnitude larger than those found in coarse sands (Glass et al., 1989b; Yao and Hendrickx, 1996) and, thus, in a pseudo-stable wetting front. Therefore, an additional stability criterion is needed for intermediate infiltration rates.

Figure 4.4. Relation between the gravitational time and the finger diameter in experiments by Yao and Hendrickx (1996)

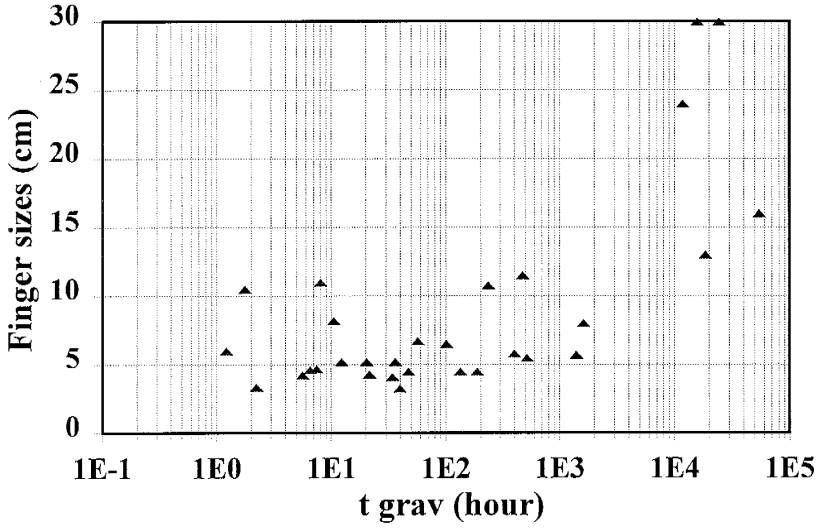

Stability Criterion for Intermediate Infiltration Rates

In addition to an increase in finger diameter, we also observed, during our lysimeter experiments in finer-textured soils, an increase in the thickness of the distribution layer that feeds the fingers. Thus, a larger amount of water is needed to initiate fingered flow in a fine-textured soil than in a coarse-textured one. A plot of observed finger diameters against observed thicknesses of the distribution layer (Fig. 4.5) reveals a strong correlation between the two variables. Therefore, it appears that the equation presented by Glass et al. (1989a) for prediction of finger diameter can also be used for an estimation of the thickness of the distribution layer. The equation is

$$d = 4.8 \frac{S_w^2}{K_F(\theta_s - \theta_o)} \cdot \frac{1}{1 - i/K_F} \qquad (7)$$

where S_w is the sorptivity of the soil at water entry value, θ_s is the saturated water content, θ_o is the initial water content, i is the infiltration rate, and 4.8 is a coefficient derived from stability analysis (Glass et al., 1991). K_F is the hydraulic conductivity inside the finger, a value that is assumed to be close to K_s. Because the wetting front in the distribution layer is stable, Eq. [7] can provide an estimate of the **minimum** amount of water (W_{min}) that needs to infiltrate before unstable wetting fronts can form:

Figure 4.5. Relation between finger diameter and thickness of the distribution layer observed in experiments by Yao and Hendrickx (1996) and in this study.

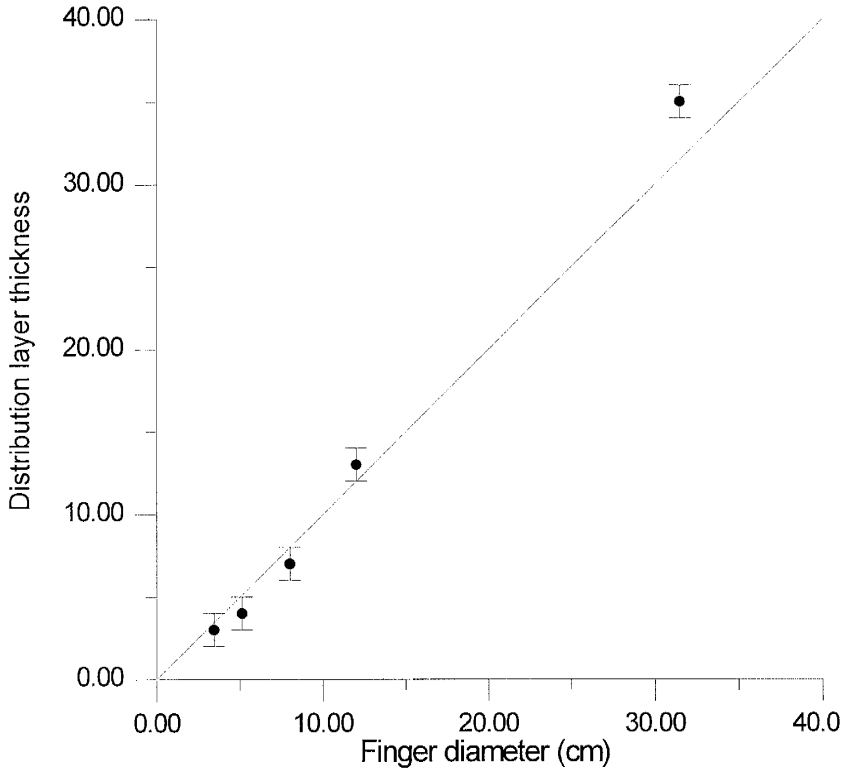

$$W_{\min} = d(\theta_d - \theta_o) \qquad \textbf{(8)}$$

where θ_d is the volumetric water content of the distribution layer. This criterion should be used whenever criterion Eq. [6] indicates that instabilities may develop. For precipitation rates less than approximately 10% of the saturated hydraulic conductivity and $K_F \approx K_s$, the stability criterion for intermediate infiltration rates in dry non-layered soils becomes

$$W < 4.8 \frac{\theta_d}{\theta_s} \frac{S_W^2}{K_s} \qquad \textbf{(9)}$$

Using data from Yao and Hendrickx (1996) we find that in their well-sorted 14-20 and 40-60 sands, 0.1 and 1.5 cm of water, respectively, is needed for instabilities to develop. This indicates that even a very small amount of water may be sufficient to trigger unstable wetting fronts in these soils if applied at an appropriate rate.

Estimation of Sorptivity at the Water Supply Pressure

For the evaluation of criterion Eq. [9], knowledge of the sorptivity at the water supply pressure is critical. Its value can be obtained directly from measurements or indirectly from the water retention and unsaturated hydraulic conductivity curves. Water-entry soil-water pressures can be directly measured in vertical capillary rise experiments (e.g., Glass et al., 1990), while the sorptivity at the appropriate water-entry value can be directly measured with a disk permeameter. When direct measurements are not possible, an indirect method must

be employed using water retention drying curves and unsaturated hydraulic conductivity curves that are available for many soils (Van Genuchten et al., 1992). The water retention drying curve provides an estimate of the air-entry soil-water pressure (h_{ae}) by plotting the log of the soil-water pressure versus the log of the volumetric water content and fitting a straight line to the data (Campbell, 1985). From the air-entry soil-water pressure, the water-entry soil-water pressure (h_{we}) can be determined as (Brakensiek, 1977; Freyberg et al., 1980) :

$$h_{we} = 0.76 h_{ae} \qquad \textbf{(10)}$$

Knowing the water-entry pressure, the sorptivity at this pressure can be calculated with a common approximation (Elrick and Reynolds, 1992; Philip, 1957; White and Sully, 1987):

$$S(h_{we}) = \sqrt{b(\theta_{h_{we}} - \theta_o) \int_{-\infty}^{h_{we}} K(h)dh} \qquad \textbf{(11)}$$

where b is a dimensionless parameter approximately equal to 1.82 (White and Sully, 1987).

For example, using the hydraulic properties of a typical dune sand in the Netherlands (Ritsema and Dekker, 1994; Wösten et al., 1987) we find h_{ae} equals -32 cm and from Eq. [10] h_{we} is -24 cm. Using Eq. [11] we find that $S(h_{we})$ is approximately 2.5 $cm.h^{-1/2}$. Wösten et al. (1987) give K_s as 4.15 cm/h and θ_s as 0.35 cm^3/cm^3. The volumetric water contents in the distribution layers of the dune sands used in the lysimeter experiments described earlier by Hendrickx and Dekker (1991) varied between 3.6 to 6.2 volumetric %. With Eq. [9], we calculate that only 0.7 to 1.3 cm of water is sufficient to induce unstable wetting in these

Dutch dune sands. This may explain the relatively frequent observations of irregular wetting patterns along the seashores of the Netherlands and Germany (e.g., Hendrickx and Dekker, 1991).

Layered Soils

The stability criterion of Eq. [9] applies to dry homogeneous non-layered soils. A stability criterion for layered soils, where a fine less permeable layer overlays a coarse more permeable layer, can be expressed as

$$W_l < W_t + W_b \qquad \textbf{(12)}$$

where W_l is the minimum amount of water needed to trigger unstable flow in the layered system, W_t is the amount of water needed to wet the top layer to such an extent that at the layer interface the water entry pressure of the bottom layer is exceeded, and W_b is the minimum amount of water needed to induce unstable wetting in the bottom layer. According to the theory (e.g., Hillel and Baker, 1988), fingers form instantaneously at the interface and W_b equals zero. However, since experimental evidence (e.g., Hill and Parlange, 1972) indicates that sometimes distribution layers develop at the interface, it seems reasonable to assume that W_b varies from zero to an amount calculated with Eq. [9]. More research is needed for refinement of the minimum amount of water needed to trigger unstable wetting.

Case Study: the Sevilleta Dunes

In the following case study of the Sevilleta dunes, located 30 km north of Socorro (NM, U.S.A.), we demonstrate in which manner precipitation and soil data can be used to predict unstable wetting in dry field soils. According to the theory and field observations in Dutch dune sands, the Sevilleta dunes appear a prime site for the occurrence of unstable wetting since, at the beginning of the July rains, a thick top layer of dry sand receive relatively large amounts of precipitation. Nevertheless, field observations after periods with precipitation failed to detect the uneven wetting. This led to the laboratory research discussed earlier.

The occurrence of wetting front stability in the Sevilleta dunes can now be evaluated as follows. First, we derive the soil-water pressure at water-entry from the wetting curve (Fig. 4.6). Its value of -18 cm is somewhat lower than 0.75 times the value of the air-entry soil-water pressure, i.e., -25 cm. From Fig. 4.7, we find S_w as 12 cm.hour$^{-1/2}$ and in our laboratory experiments we measured θ_d as approximately 0.11. Stability criterion Eq. [9] indicates that at least 4.4 cm water is needed before instabilities can be triggered; this is reflected by the horizontal line in Fig. 4.8. Next, we impose the stability criterion for high infiltration rates (Eq. [2]) by drawing a vertical line where the infiltration rate equals the saturated hydraulic conductivity of 43 cm/hour. Finally, we finish the graph by drawing the line representing stability criterion Eq. [5]: Wi<2.0. The grey area in Fig. 4.8 covers W-i combinations that will likely result in unstable wetting.

Figure 4.6. The wetting and drying water retention curves for Sevilleta dune sand

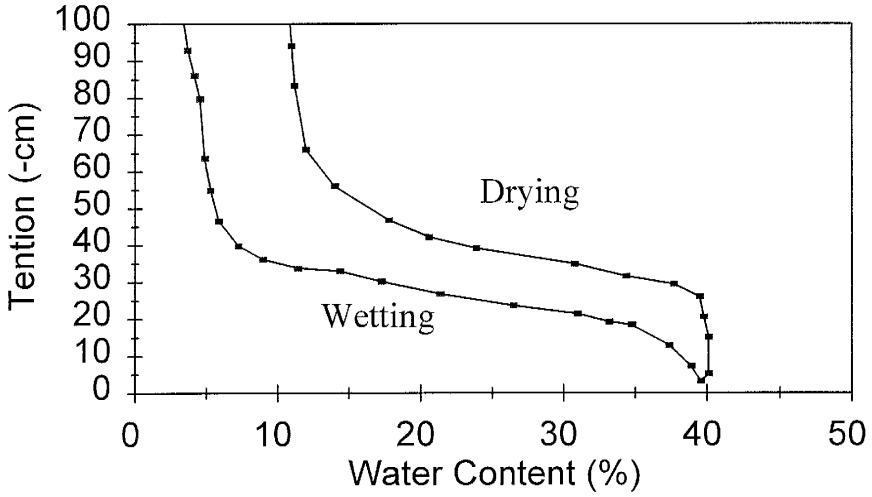

Figure 4.7. The relationship between sorptivity and soil-water tension for Sevilleta dune sand

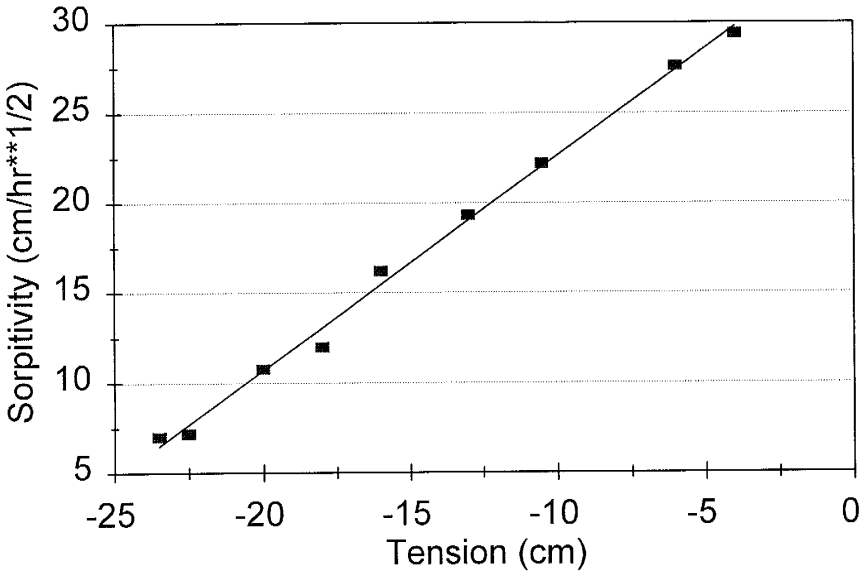

Figure 4.8. **Application of stability criteria [2], [5], and [9] for the Sevilleta dunes near Socorro**

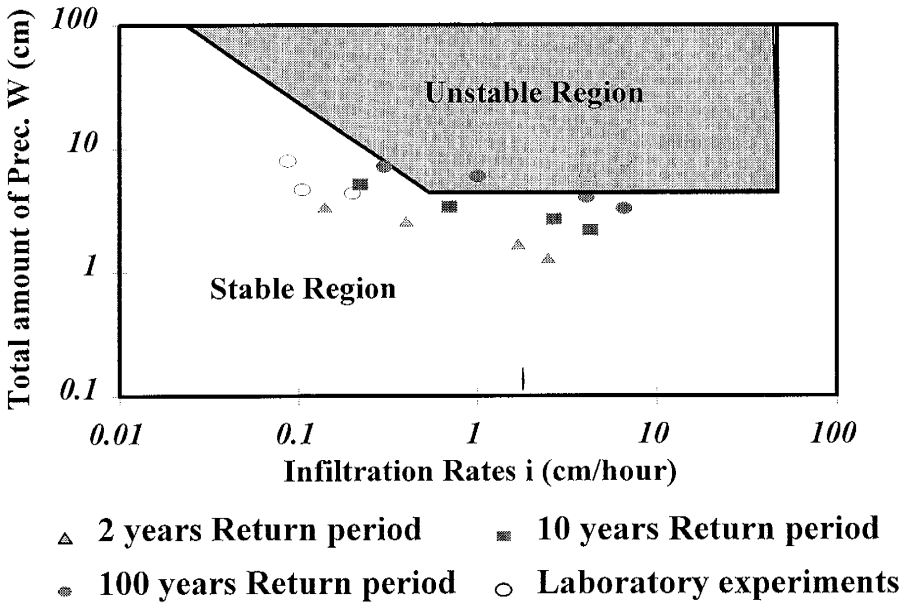

The precipitation regime is analyzed using standard rate-duration-frequency curves for point precipitation for durations of 0.5, 1, 6, and 24 hours for return periods of 2, 10, and 100 years. Fig. 4.8 shows the prevalent W-i combinations for the area. For example, for a 2-year return period, the total amount of precipitation in 0.5 hour is 2.5 cm with an intensity of 1.25 cm/hour; for a 100-year return period the total amount of precipitation in 6 hours is 6 cm with an intensity of 1 cm/hour. Figure 4.8 shows that unstable wetting is rare in the Sevilleta dunes. All precipitation events with a 2- and 10-year return period are located in the stable region of the graph. Even three precipitation events with a return period of 100 years fall into the stable region.

For verification of the predicted unstable conditions in Fig. 4.8, we conducted five laboratory experiments in a large lysimeter (diameter 1 m, depth 1.5 m) filled with Sevilleta dune sand following a procedure described by Yao and Hendrickx (1996). Three experiments were conducted at low infiltration rates of 0.2, 0.1, and 0.09 cm/h with a total amount of applied water of 4.4, 4.7, and 8 cm, respectively. Two experiments were conducted at intermediate infiltration rates of 4.2 and 6.7 cm/h with a total amount of applied water of 6 and 8 cm, respectively. As shown in Fig. 4.8, the low rate experiments were predicted to result in stable wetting and the intermediate ones in unstable wetting. Visual observations of the wetting patterns in the large lysimeter seem to confirm our predictions on the basis of the three stability criteria. In Fig. 4.9, the percent wetted area is plotted versus the depth. A steep decrease of wetted area indicates a stable wetting front, while a gradual decrease indicates

Figure 4.9. **The relationship between percent wetted area and depth for five infiltration experiments in a large lysimeter filled with Sevilleta dune sand**

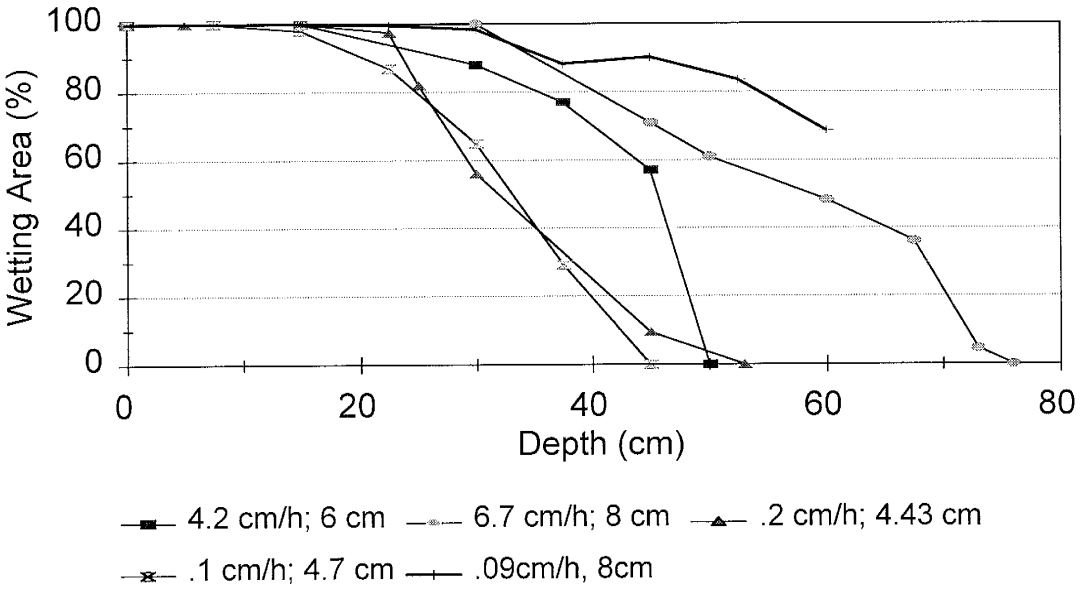

an unstable one. For example, the steep lines found during the application of 4.4 and 4.7 cm of water at rates of 0.2 and 0.1 cm/h, respectively, clearly indicate stable wetting. However, the gradual decrease of wetted area during the application of 8 cm of water at a rate of 6.7 cm/h indicates unstable wetting. Indeed, application of 8 cm at a rate of .09 cm/h resulted in a different relationship between wetted area and depth. Unfortunately, lack of dry sieved dune sand prevented us in obtaining data to a greater depth, but the trend indicates that the much lower rate resulted in a more stable wetting front. The application of 6 cm of water at 4.2 cm/h seemed to create a wetting front that is neither stable nor unstable. In Fig. 4.10, several horizontal cross-sections are presented. Sections a and b from the two intermediate rate experiments exhibit more instability than section c from a low rate experiment. Overall, this case study shows that the three stability criteria used in our approach for the prediction of wetting front stability in dry field soils can help explain field observations and assess the risk for occurrence of unstable wetting.

Flow Diagram for Evaluation of Wetting Front Stability

Combination of the three stability criteria with the results of previous research in water-repellent soils, leads to our approach for the prediction of wetting front stability (Fig. 4.11). The required soil data are water repellency, water retention, and hydraulic conductivity. The precipitation data are the total amount of precipitation and its intensity for

Figure 4.10. **Unstable wetting patterns observed in the large diameter lysimeter in Sevilleta dune sand: (a) wetting pattern at depth 50 cm after application of 8 cm water at rate of 6.7 cm/hour, (b) wetting pattern at depth 37.5 cm after application of 6 cm water at rate of 4.2 cm/hour, (c) wetting pattern at depth 52 cm after application of 8 cm water at a rate of 0.087 cm/h**

(A) **(B)**

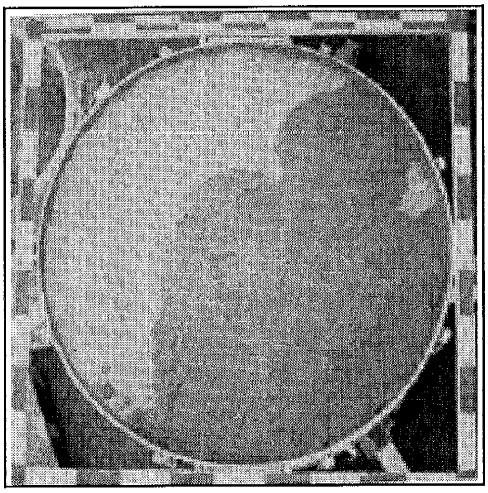

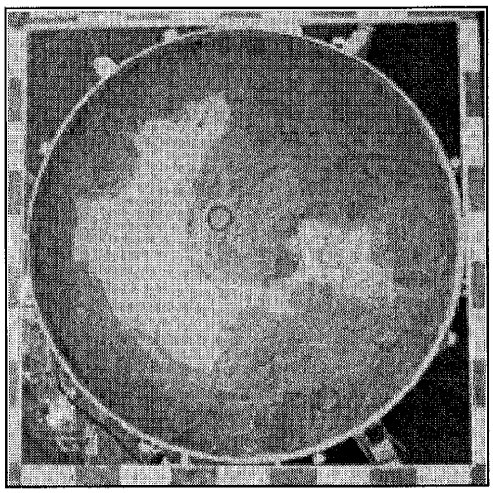

(C)

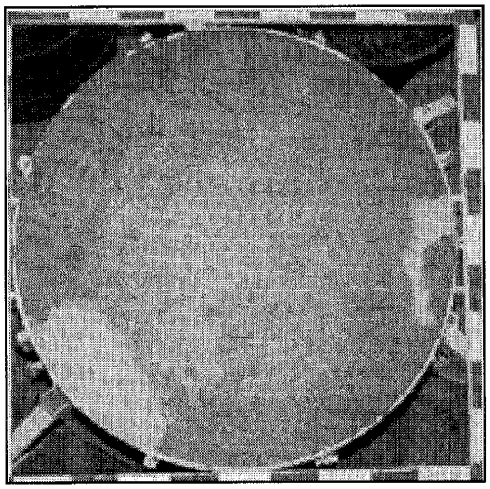

Figure 4.11. Flow diagram for the prediction of unstable wetting fronts in dry field soils

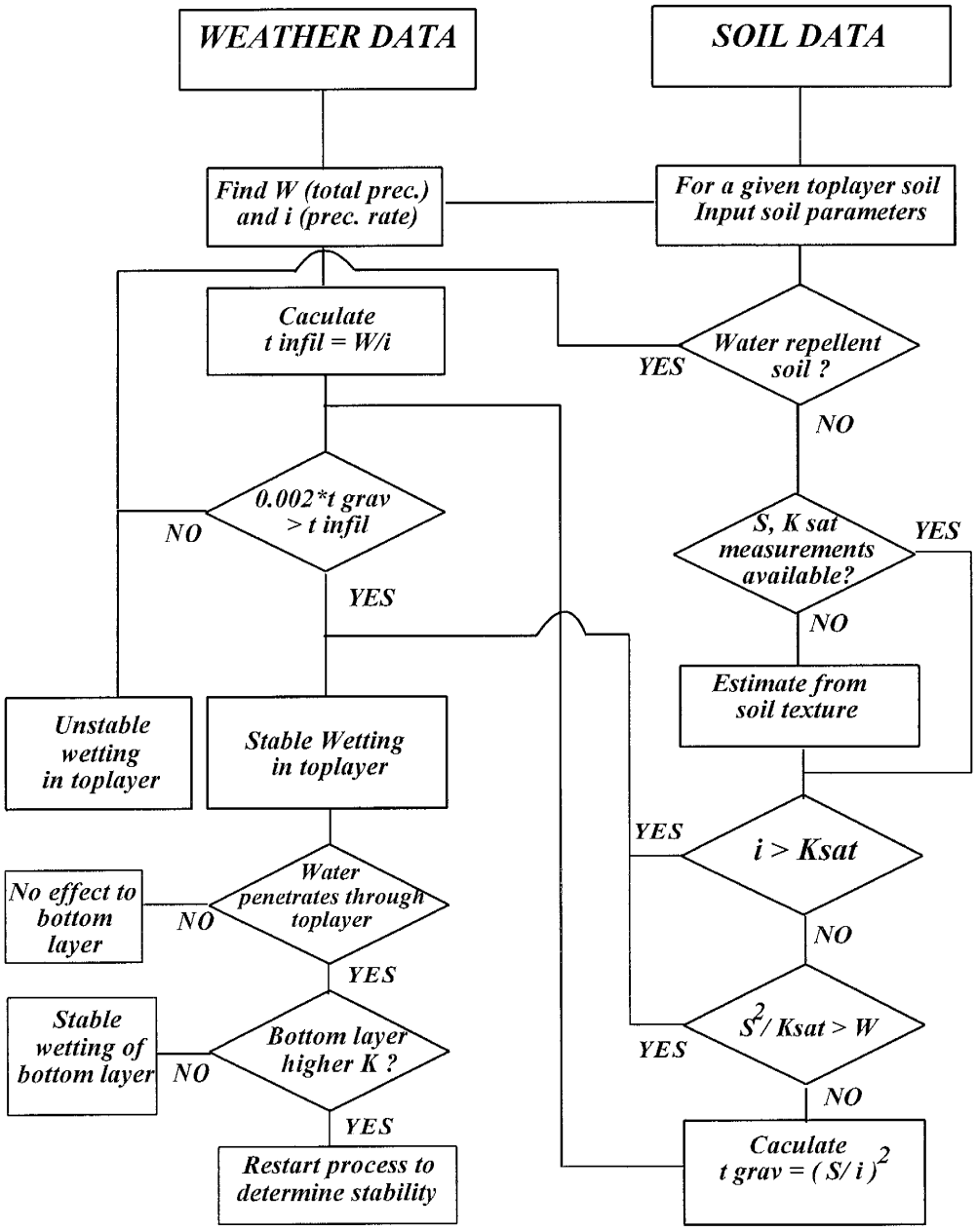

the return period of interest. Previous research has shown that water repellency always results in unstable wetting fronts. If the soil is not water repellent, the three stability criteria are evaluated. If the wetting front in the top layer is stable and the front reaches the next layer, the process to determine wetting front stability is restarted. If the wetting front in the top layer is unstable, it is likely that the instability continues into the next soil horizon. Although the proposed diagram is rather simple and does not include processes such as air compression or redistribution after infiltration, we believe that it will be useful in helping to identify situations where fingered flows can occur.

References

Baker, R.S., and D. Hillel. 1990. Laboratory tests of a theory of fingering during infiltration into layered soils. Soil Sci. Soc. Am. J. 54:20-30.

Brakensiek, D.L. 1977. Estimating the effective capillary pressure in the Green-and-Ampt infiltration equation. Water Resour. Res. 13:680-682.

Campbell, G.S. 1985. Soil physics with Basic. Transport models for soil-plant systems. Developments in Soil Science 14. Elsevier, Amsterdam, The Netherlands. 150 pp.

Dekker, L.W., and C.J. Ritsema. 1994. Fingered flow: The creator of sand columns in dune and beach sands. Earth surface processes and landforms 19:153-164.

Diment, G.A., and K.K. Watson. 1983. Stability analysis of water movement in unsaturated porous materials: 2. Numerical studies. Water Resour. Res. 19:1002-1010.

Diment, G.A., and K.K. Watson. 1985. Stability analysis of water movement in unsaturated porous materials: 3. Experimental studies. Water Resour. Res. 21:979-984.

Diment, G.A., K.K. Watson, and P. J. Blennerhassett. 1982. Stability analysis of water movement in unsaturated porous materials: 1. Theoretical considerations. Water Resour. Res. 18:1248-1254.

Elrick, D.E., W.D. Reynolds. 1992. Infiltration from constant-head well permeameters and infiltrometers. p. 1-24. *In* G. C. Topp et al. (ed.) Advances in measurement of soil physical properties : Bring theory into practice. SSSA Spec. Publ. 30. SSSA, Madison, WI.

Freyberg, D.L., J.W. Reeder, J.B. Franzini, and I. Remson. 1980. Application of the Green-and-Ampt model to infiltration under time-dependent surface water depths. Water Resour. Res. 16:517-528.

Glass, R.J., J. King, S. Cann, N. Bailey, J.-Y. Parlange, and T.S. Steenhuis. 1990. Wetting front instability in unsaturated porous media: A three-dimensional study. Transp. Porous Media. 5: 247-268.

Glass, R.J., and M.J. Nicholl. 1996. Physics of gravity fingering of immiscible fluids within porous media: An overview of current understanding and selected complicating factors. Geoderma, 70:133-163.

Glass, R.J., J.-Y. Parlange, and T.S. Steenhuis. 1991. Immiscible displacement in porous media: Stability analysis of three-dimensional, axisymmetric disturbances with application to gravity-driven wetting front instability. Water Resour. Res. 27:1947-1956.

Glass, R.J., T.S. Steenhuis, and J.-Y. Parlange. 1988. Wetting front instability as a rapid and far-reaching hydrologic process in the vadose zone. J. of Cont. Hydrology 3:207-226.

Glass, R.J., T.S. Steenhuis, and J.-Y. Parlange. 1989a. Wetting front instability: 1. Theoretical discussion and dimensional analysis. Water Resour. Res. 25:1187-1194.

Glass, R.J., T.S. Steenhuis, and J.-Y. Parlange. 1989b. Wetting front instability: 2. Experimental determination of relationships between system parameters and two-dimensional unstable flow field behavior in initially dry porous media. Water Resour. Res. 25:1195-1207.

Glass, R.J., T.S. Steenhuis, and J.-Y. Parlange. 1989c. Mechanism for finger persistence in homogeneous, unsaturated, porous media: Theory and verification. Soil Sci. 148:60-70.

Hendrickx, J.M.H., L.W. Dekker, and P.A.C. Raats. 1988a. Formation of sand columns caused by unstable wetting fronts. Grondboor en Hamer 6:173-175. (in Dutch).

Hendrickx, J.M.H., L.W. Dekker, E.J. Van Zuilen, and O.H. Boersma. 1988b. Water and solute movement through a water-repellent sand soil with grasscover.In: Wierenga, P.J. and D. Bachelet. 1988. Validation of flow and transport models for the unsaturated zone: Conference Proceedings; May 23-26, 1988 Ruidoso, New Mexico. pp. 131-146. Research Report 88-SS-04, Dept. of Agronomy and Horticulture, New Mexico State University, Las Cruces, NM 545 p.

Hendrickx, J.M.H., and L.W. Dekker. 1991. Experimental evidence of unstable wetting fronts in non-layered soils. *In* Proc. Natl. Symp. Preferential Flow, Chicago,IL. 16-17 Dec. 1991. Am. Soc. Agric. Eng., St. Joseph, MI. pp. 22-31.

Hendrickx, J.M.H., L.W. Dekker, and O.H. Boersma. 1993. Unstable wetting fronts in water-repellent soils. J. of Env. Qual. 22:109-118.

Hill, D.E., and J.-Y. Parlange. 1972. Wetting front instability in layered soils. Soil Sci. Soc. Am. Proc. 36:697-702.

Hillel, D., and R.S. Baker. 1988. A descriptive theory of fingering during infiltration into layered soils. Soil Sci. 146:51-56.

Parlange, J.-Y., and D.E. Hill. 1976. Theoretical analysis of wetting front instability in soils. Soil Sci. 122:236-239.

Philip, J.R., 1957. The theory of infiltration: 4. Sorptivity and algebraic infiltration equations. Soil Sci. 84:257-264.

Philip, J.R., 1969. Theory of infiltration. Advances in Hydroscience 5:215-296.

Philip, J.R. 1975a. Stability analysis of infiltration. Soil Sci. Soc. Am. Proc. 39:1042-1049.

Philip, J.R. 1975b. The growth of disturbances in unstable infiltration flows. Soil Sci. Soc. Am. Proc. 39:1049-1053.

Raats, P.A.C. 1973. Unstable wetting fronts in uniform and nonuniform soils. Soil Sci. Soc. Am. Proc. 37:681-685.

Rice, R.C., D.B. Jaynes, and R.S. Bowman. 1991. Preferential flow of solutes and herbicides under irrigated fields. Transactions of the ASAE 34:914-918.

Ritsema, C.J., and L.W. Dekker. 1994. Soil moisture and dry bulk density patterns in bare dune sands. J. Hydrology 154:107-131.

Ritsema, C.J., L.W. Dekker, J.M.H. Hendrickx, and W. Hamminga. 1993. Preferential flow mechanism in a water-repellent sand soil. Water Resour. Res. 29:2183-2193.

Ritsema, C.J., T.S. Steenhuis, J.-Y. Parlange, L.W. Dekker. 1996. Predicted and observed finger diameters in field soils. Geoderma, 70: 185-196.

Selker, J.S., T.S. Steenhuis, and J.-Y. Parlange. 1989. Preferential flow in homogeneous sandy soils without layering. Paper No. 89-2543, American Society of Agricultural Engineering, St. Joseph, MI. pp. 22.

Selker, J.S., T.S. Steenhuis, and J.-Y. Parlange. 1992. Wetting front instability in homogeneous sandy soils under continuous infiltration. Soil Sci. Soc. Am. J. 56:1346-1350.

Starr, J.L., H.C. DeRoo, C.R. Frink, and J.Y. Parlange. 1978. Leaching characteristics of a layered field soil. Soil Sci. Soc. Am. J. 42:386-391.

Starr, J.L., J.-Y. Parlange, and C.R. Frink. 1986. Water and chloride movement through a layered field soil. Soil Sci. Soc. Am. J. 50:1384-1390.

Tabuchi, T. 1961. Infiltration and ensuing percolation in columns of layered glass particles packed in laboratory. (In Japanese, with a summary in English). Nogyo dobuku kenkyn, Bessatsu (Trans. Agr. Eng. Soc., Japan) 1:13-19.

Talsma, T. 1969. In situ measurements of sorptivity. Aust. J. of Soil Res. 7:269-276.

Tamai, N., T. Asaeda, and C.G. Jeevaraj. 1987. Fingering in two-dimensional, homogeneous, unsaturated porous media. Soil Sci. 144:107-112.

Van Dam, J.C., J.M.H., Hendrickx, H.C. van Ommen, M.H. Bannink, M.Th. van Genuchten, and L.W. Dekker. 1990. Simulation of water and solute transport through a water-repellent sand soil. J. Hydrology 120:139-159.

Van Genuchten, M.Th., Leij, F.J. & Lund, L.J. (Eds.). 1992: Indirect methods for estimating the hydraulic properties of unsaturated soils. Proceedings of the International Workshop on Indirect Methods for Estimating the Hydraulic Properties of Unsaturated Soils, Riverside, CA, October 11-13, 1989. U.S. Salinity Laboratory, Agricultural Research Service, U.S. Dept. of Agriculture, Riverside, California, U.S.A. pp. 718.

Van Ommen, H.C., R. Dijksma, J.M.H. Hendrickx, L.W. Dekker, J. Hulshof, and M. van den Heuvel. 1989. Experimental assessment of preferential flow paths in a field soil. J. Hydrology 105:253-262.

White, I., P.M. Colombera, and J.R. Philip. 1976. Experimental study of wetting front instability induced by sudden change of pressure gradient. Soil Sci. Soc. Am. J. 40:824-829.

White, I., and M.J. Sully. 1987. Microscopic and macroscopic capillary length and time scales from field infiltration. Water Resour. Res. 23:1514-1522.

Wösten, J.H.M., M.H. Bannink, and J. Beuving. 1987. Water retention and hydraulic conductivity of soils in the Netherlands: The Staring Series. Report 1932 STIBOKA, Wageningen, The Netherlands. (in Dutch).

Yao, T., and J.M.H. Hendrickx. 1996. Stability of wetting fronts in homogeneous soils under low infiltration rates. Soil Sci. Soc. Am. J. 60:20-28.

5. An Approximate Analytical Solution of the Richards' Equation Using Actual Soil Hydraulic Properties

X.H. Du[1], T. Yao[2], W.D. Stone[3], and J.M.H. Hendrickx[2]

[1]Hydrology Program, Department of Earth & Environmental Science, New Mexico Tech, Socorro, NM 87801; presently at Electrical Engineering Department, Pennsylvania State University, State College, PA 16801

[2]Hydrology Program, Department of Earth & Environmental Science and, New Mexico Tech, Socorro, NM 87801;

[3]Department of Mathematics, New Mexico Tech, Socorro, NM 87801

Abstract

There are few analytical solutions of the Richards' equation that can be solved using actual soil hydraulic properties. We have developed a method to solve the one-dimensional Richards' equation under the conditions of constant soil water content at the top boundary and uniform initial soil water content deeper in the profile. The hydraulic conductivity and

diffusivity can be any differentiable functions of water content. We used the large time traveling wave solution as our base solution and added two extra functions of time, $\alpha(t)$ and $\beta(t)$, which can describe the downward propagation of the wetting front from early to large times. The function $\alpha(t)$ describes the change of the wetting front shape with time while $\beta(t)$ represents the wetting front travel distance from the surface. The functions $\alpha(t)$ and $\beta(t)$ are determined by two parameters, V_0 and V_2, which are calculated using the soil water content profile at large times. Compared to other methods reported in the literature, our method requires relatively simple calculations and can be applied at all times. The applicability of our method was verified by comparing its results to analytical solutions and numerical simulations of infiltration into a clay and sand soil.

Introduction

Solutions of the one-dimensional Richards' equation are important for the study of unsaturated flow in porous media. Unfortunately, it is difficult to obtain exact analytical solutions because the dependencies of the hydraulic conductivity $K(u)$ and diffusivity $D(u)$ on soil water content u are nonlinear. Philip (1957a) presented an analytical series solution in terms of powers of $t^{1/2}$ which is accurate and converges rapidly for early times. However, it fails for large times since this series solution becomes divergent as time goes to infinity. Assuming the existence of a traveling wave solution, Philip (1957b) provided a traveling wave solution that is accurate for large times ($t \to \infty$), but fails at early times. Combining these results could provide solutions for early and large times, but not for intermediate times.

Parlange (1971) theoretically verified the existence of the traveling wave solution and provided a method to solve the Richards' equation. However, his method involves an iterative scheme which was complicated by a triple-integral equation form. His solution can be simplified for large times ($t \to \infty$) and then coincides with the traveling wave solution by Philip (1957b).

The work of Philip and Parlange has been followed by many other studies that have presented analytical solutions of the Richards' equation. However, these studies are based on predetermined forms of the diffusivity and conductivity curves. For example, Parlange and Fleming (1984), Hogarth et al. (1989), and Ross and Parlange (1994) assumed that K and D obey a power law. Warrick et al. (1991) expressed $K(u)$ and $D(u)$ as rational functions of water content u. Srivastava and Yeh (1991) assumed exponential expressions of K and D. Barry et al. (1993) selected a special moisture characteristic curve. Recently, Parlange et al. (1997) presented a new approximate technique that can solve Richards' equation for arbitrary soil properties and surface boundary conditions. The objective of this study is to develop an analytical solution of the Richards' equation for all times without being confined to predefined relationships between diffusivity or conductivity and soil water content.

Theory

The Richards' equation governing one-dimensional vertical flow in unsaturated soil can be written as:

$$\frac{\partial u}{\partial t} = \frac{\partial}{\partial z}\left(D(u)\frac{\partial u}{\partial z} - K(u)\right) \quad (1)$$

where t is the time, z is the vertical coordinate with positive downward direction, u is the volumetric water content, $K(u)$ is the hydraulic conductivity, and $D(u)$ is the diffusivity. In this study, we consider the following boundary and initial conditions:

$$u(0,t) = u_1 \quad (2)$$

$$u(z,0) = u_0 \quad (3)$$

$$u(\infty,t) = u_0 \quad (4)$$

where u_1 is the water content at the top boundary, and u_0 is the initial water content.

To obtain a solution of Eq. [1] subject to conditions [2], [3], and [4], we first derive the traveling wave solution for large times, and then develop a solution that can be applied to the whole time domain (from early to large times).

Traveling Wave Solution for Large Times

Philip (1957b) postulated the existence of the traveling wave solution based on physical reason and Parlange (1971) developed the theory that proved it exists. We take it

for granted that the traveling wave solution exists for large times.

Following Philip (1957b) and Parlange (1971), the traveling wave solution has the following form:

$$u = u(\eta) \tag{5}$$

where

$$\eta = z - V_1 t \tag{6}$$

and

$$V_1 = \frac{K(u_1) - K(u_0)}{u_1 - u_0} \tag{7}$$

Thus, V_1 is the velocity of the wetting front. Substituting Eq. [5] into Eq. [1] yields

$$-V_1 \frac{du}{d\eta} = \frac{d}{d\eta}[D(u)\frac{du}{d\eta} - K(u)] \tag{8}$$

Integrating both sides of Eq. [8] once and considering the condition

$$\frac{du}{d\eta}\Big|_{\eta \to \infty} = 0 \tag{9}$$

we obtain

$$\frac{du}{d\eta} = \frac{[K(u) - K(u_0)] - V_1(u - u_0)}{D(u)} \tag{10}$$

As expected, Eq. [10] is equivalent to the result previously obtained by Philip (1957 b; Eq. [38]).

Integrating both sides of Eq. [10] and considering boundary condition [2], Parlange (1971) provided the following solution of Eq. [10]:

$$\eta(u) = \int_u^{u_f} \frac{D(u)}{V_1(u - u_0) - [K(u) - K(u_0)]}\, du \tag{11}$$

where $u_f = u_1 - \epsilon$. The quantity ϵ is small and positive and needs to be introduced because $\eta(u)$ often has a singularity at u_1 (Philip, 1969). u_f is assumed to be the water content corresponding to the upper end point of the traveling wave wetting front. Numerical integration of Eq. [11] yields a unique relationship between u and η which is valid for large times. We denote this relationship:

$$u = F(\eta) \tag{12}$$

Using the soil hydraulic properties of Yolo light clay (Moore, 1939) with $\epsilon = 0.001$, we find the wetting front at large times as demonstrated in Fig. 5.1a and 5.1b.

Figure 5.1.a. Steady state traveling wetting front solution $u=F(\eta)$

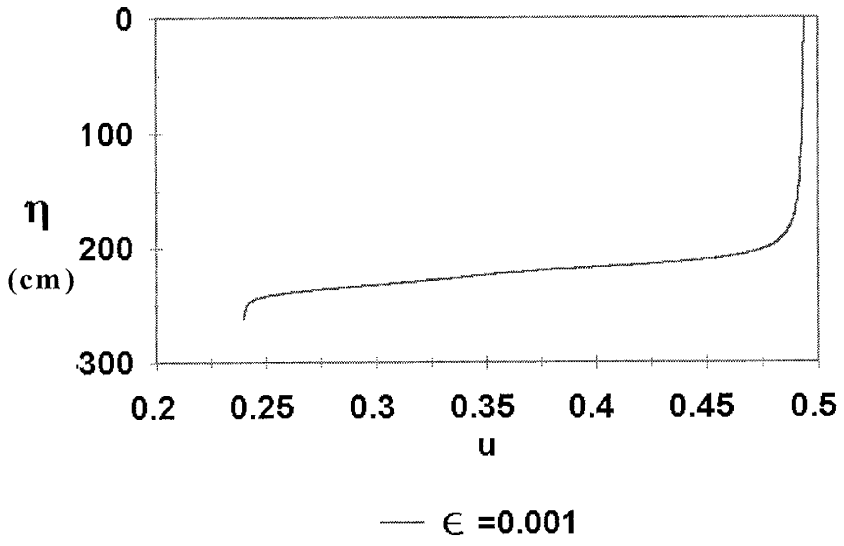

Figure 5.1.b. Steady state traveling wetting front solution $u=F(z-V_1t)$ for different times

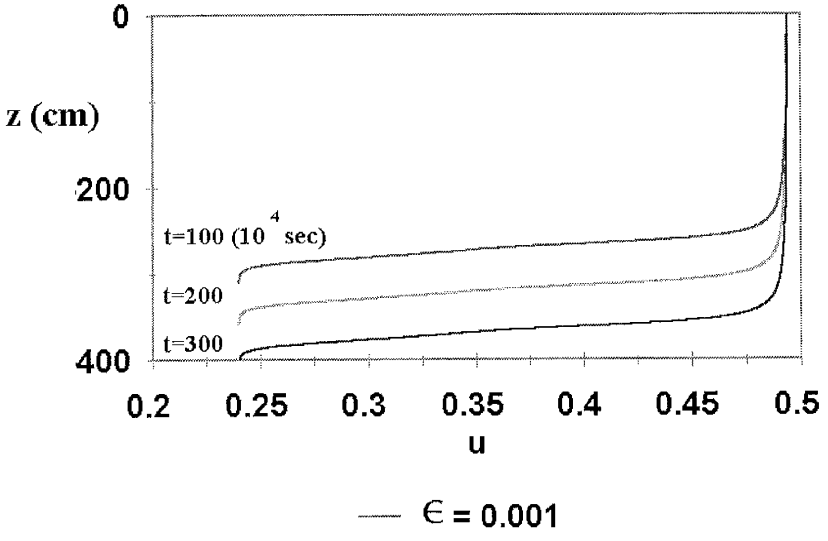

Transient Solution for the Whole Time Domain

The traveling wave solution Eq. [12] expresses the concept that the wetting front at large time is moving with a fixed shape and advances at a constant velocity V_I (Fig. 5.1b). From its initial conditions (Eqs. [2] and [3]), the wetting front changes its shape and downward velocity until it reaches this traveling state. In this section, a solution will be derived to describe the shape and downward velocity of the wetting front during its transition from initial to traveling state. First we replace variable η (the wave form for large times) by a new variable s (the wave form for all times) where

$$s = \alpha(t)(z-\beta(t)) \tag{13}$$

so that

$$z = \frac{s}{\alpha(t)} + \beta(t) \tag{14}$$

These functions are used to establish the relationship between water content u and depth z, more specifically, the location and shape of the wetting front. The shape of the wetting front changes from horizontal at initiation of infiltration to the shape at large times described with Eq. [12] and depicted in Fig. 5.2 (also see Fig. 9 in Philip 1969). The function $\alpha(t)$ converts the shape of the wetting front at large times to the one at early and intermediate times. For large times, $\alpha(t)=1$ so that the shape of function [13] approaches that of the steady traveling wave (see Eq. [6]). For small times, if z goes to 0, the value $\alpha(t)$ has to yield an almost

Figure 5.2. Traveling wetting fronts at different times and their relationship to $\alpha(t)$ and $\beta(t)$

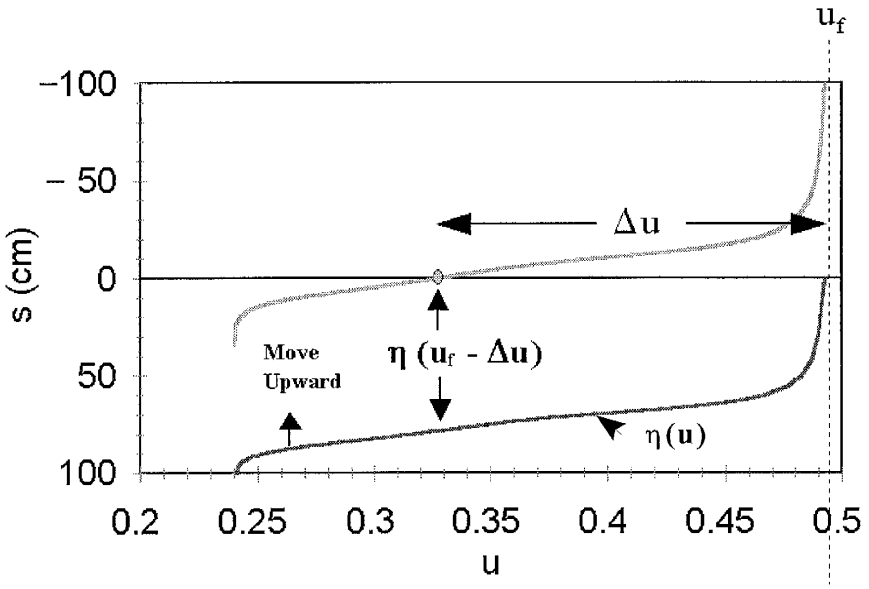

horizontal wetting front. Therefore, $\alpha(t)$ has to approach infinity (see Eq. [14]). For small times we need to examine the shape of the wave form s near the soil surface. Therefore, it is necessary to move the large time wave form η upward to the position where $s(u)$ is close to 0 (see Fig. 5.2). The upward shift makes

$$s(u) = \eta(u) - \eta(u_f - \Delta u) \tag{15}$$

Note that the minus sign indicates an upward shift because the z-coordinate is taken positive downward. Eq. [15] leads to

$$s(u_f - \Delta u) = 0 \tag{16}$$

Under condition [16], $\beta(t)$ becomes approximately equal to the depth of the wetting front at small times since $\alpha(t)$ in Eq. [14] is still very large. Combining the relationship $z = it/u_1$ with the linear relationship between sorptivity, S, infiltration rate, i, and square root of time, $S = it^{1/2}$ (Philip, 1969), we find at the early stage of infiltration that

$$\beta(t) = \frac{S}{u_1}\sqrt{t} \tag{17}$$

In Fig. 5.3, it is demonstrated in which manner wave form s (Eq. [13]) results in wetting front shapes that are representative for the entire time domain. For early and intermediate times, $\beta(t)$ describes the transient behavior of the wetting front velocity; for large times, $\beta(t) = V_1 t$ (see Eq. [6]).

Figure 5.3. Wetting front position adjustment at small times from the change of Δu

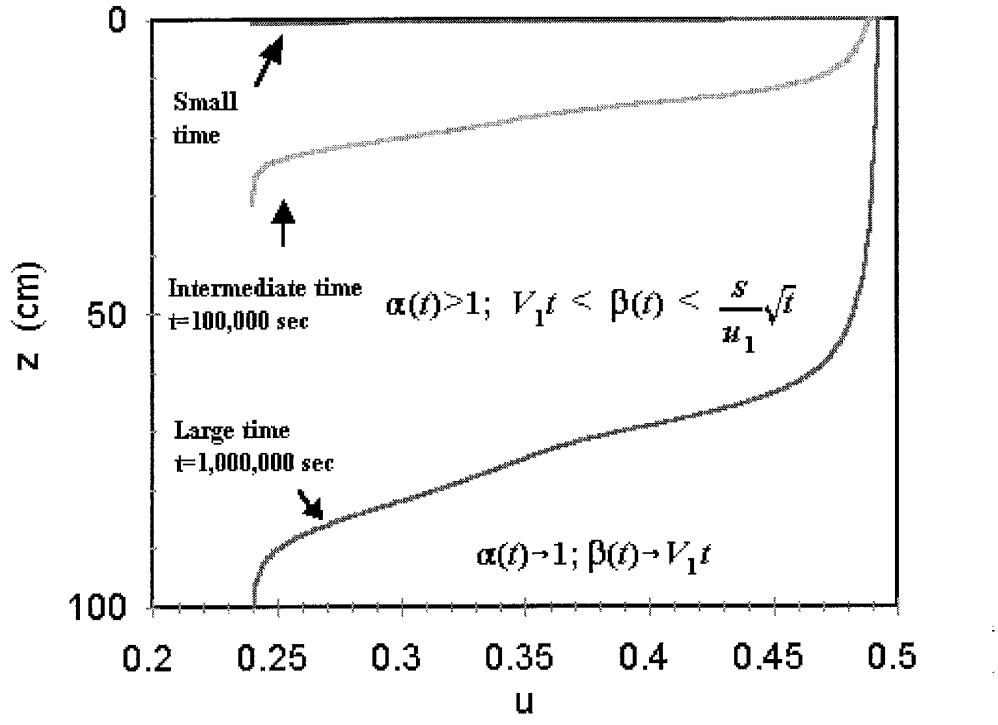

We assume that the transient solution is similar to Eq. [12] and has the following form:

$$u = F(s) \tag{18}$$

Approximate Transient Solution

We obtain the unknown functions $\alpha(t)$ and $\beta(t)$ by analysis of the residual caused by the approximation of the solution [18]. The residual analysis is standard in finite-element analysis. Here we borrow the concept of residuals and apply it in an analytical manner.

Substituting Eq. [18] into Eq. [1], we obtain the residual $R(u)$:

$$\begin{aligned} R(u) &= \frac{\partial u}{\partial t} - \frac{\partial}{\partial z}\left(D(u)\frac{\partial u}{\partial z} - K(u)\right) \\ &= \left[\frac{\alpha'(t)}{\alpha(t)}s - (\alpha^2(t) - \alpha(t))K'(u) + V_1\alpha^2(t) - \alpha(t)\beta'(t)\right]\frac{dF}{ds} \end{aligned} \tag{19}$$

In order to solve for the unknown functions $\alpha(t)$ and $\beta(t)$, we assume that two points s_2 and s_3 can be found which will minimize the residual function $R(u)$. By substituting s_2 and s_3 into Eq. [19] we have:

$$\frac{\alpha'(t)}{\alpha(t)}s_2 + K'(u_2)(\alpha(t) - \alpha^2(t)) + V_1\alpha^2(t) - \alpha(t)\beta'(t) = 0 \tag{20}$$

$$\frac{\alpha'(t)}{\alpha(t)} s_3 + K'(u_3)\,(\alpha(t) - \alpha^2(t)) + V_1\alpha^2(t) - \alpha(t)\beta'(t) = 0 \qquad (21)$$

where $u_2 = F(s_2)$, and $u_3 = F(s_3)$. Subtracting Eq. [21] from Eq. [20] yields:

$$\frac{\alpha'(t)}{\alpha(t)} (s_2 - s_3) + [K'(u_2) - K'(u_3)]\,(\alpha(t) - \alpha^2(t)) = 0 \qquad (22)$$

Eq. [22] can be simplified by defining

$$V_0 = \frac{K'(u_3) - K'(u_2)}{s_2 - s_3} \qquad (23)$$

Thus, parameter V_0 is a constant for a given soil. Substituting Eq. [23] into Eq. [22] yields a first order differential equation

$$\frac{\alpha'(t)}{\alpha^2(t)\,[\alpha(t) - 1]} = -V_0 \qquad (24)$$

At $t = 0$, the wetting front is a sharp front. This means $\alpha(t) \to \infty$ as $t \to 0$. Under this initial condition, Eq. [24] has the following solution:

$$\frac{1}{\alpha(t)} + \ln\left(1 - \frac{1}{\alpha(t)}\right) = -V_0 t \tag{25}$$

$\alpha(t) \to 1$ as $t \to \infty$. This implies that the shape of the wetting front changes gradually from a steep wetting front to the traveling wave form (Fig. 5.2). Thus, the parameter V_0 indicates how fast the wetting front reaches the constant traveling-wave shape (steady-state shape) in a given soil. The smaller V_0 is, the longer the transient time will be. Usually finer soils have a smaller V_0. For Yolo clay, V_0 is about 1.0×10^{-6} (second^{-1}). For coarse sand (US mesh 14-20), V_0 is about 0.5 (second^{-1}).

Substituting Eq. [25] into Eq. [20] or Eq. [21], we have:

$$\beta'(t) = V_2 \frac{\alpha'(t)}{\alpha^2(t)} + V_1 \tag{26}$$

where

$$V_2 = \frac{s_2 K'(u_3) - s_3 K'(u_2) - V_1(s_2 - s_3)}{K'(u_3) - K'(u_2)} \tag{27}$$

Solving Eq. [26] with the initial condition $\beta(0)=0$, we have:

$$\beta(t) = V_1 t - \frac{V_2}{\alpha(t)} \tag{28}$$

Thus, the parameter V_2 describes the transient behavior of the downward velocity of the wetting front and V_2 is always negative to keep the wetting front moving downward. If $V_2 = 0$, then the downward velocity of the wetting front is equal to the traveling velocity V_1 (see Eq. [7]). A more negative V_2 indicates that the transient velocity of the wetting exhibits a greater change. By Eq. [28], $\beta(t)$ becomes linear ($\beta(t)$-$V_1 t \rightarrow$ constant) with time when $\alpha(t)$ becomes constant (Fig. 5.4). We plotted the ($\beta(t)$-$V_1 t$) *vs. t* relationship instead of $\beta(t)$ *vs.t* since the linearlization of the $\beta(t)$ function is a gentle process that cannot be clearly seen by plotting $\beta(t)$ *vs. t*. If $\beta(t)$ becomes linear with time, the ($\beta(t)$-$V_1 t$) function will become constant with time. From Fig. 5.4, we can observe that the transient behavior of the shape and the downward velocity of the wetting front take place during the same early and intermediate time intervals.

For the calculation, s_2 and s_3 can be determined as follows. First, we substitute Eqs. [24] and [26] into Eq. [19] to obtain

$$\frac{R(u)}{dF/ds} = V_0 s\alpha(1-\alpha) + \alpha(1-\alpha)K'(u) + V_1\alpha^2 - \alpha(V_0 V_2 + V_1 - V_0 V_2\alpha) \qquad (29)$$

Then, Eqs. [23] and [27] are substituted into Eq. [29] to obtain:

$$R(u) = \left(\frac{s_2 K'(u_3) - s_3 K'(u_2)}{s_2 - s_3} - K'(u) - \frac{K'(u_3) - K'(u_2)}{s_2 - s_3} s\right)\alpha(\alpha-1)\frac{dF}{ds} \qquad (30)$$

We minimize the $R(u)$ function by minimizing the right hand side of Eq. [30]. For the

Figure 5.4. The $\alpha(t)$-t and $(\beta(t)$-$V_1t)$-t curves for Yolo light clay

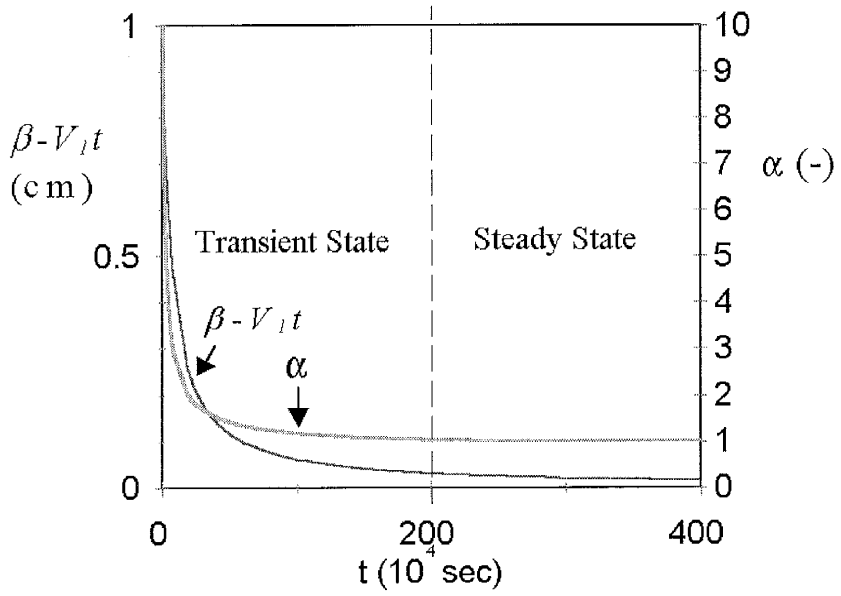

optimization we can omit the $\alpha(\alpha\text{-}1)$ term in Eq. [30] and find s_2 and s_3 by minimizing the remaining function of $R(u)$.

Simplified Transient Solution

For the simplified solution we assume that $K'(u)$ has a linear relationship with u which allows us to place u_2 and u_3 at equal partition points between u_0 and u_1. This procedure immediately yields the values for s_2 and s_3. First we discuss the geometrical meaning of V_0 and V_2. From Eq. [25], the parameter V_0 determines the shape function $\alpha(t)$. We rewrite Eq. [23] as:

$$V_0 = \left[\frac{K'(u_3) - K'(u_2)}{u_2 - u_3}\right]\left[\frac{u_2 - u_3}{s_2 - s_3}\right] = m\ p \qquad (31)$$

where m and p are constants for a particular soil and determined by the relationship shown in the first and second bracket in Eq. [31], respectively. The relationship between u and s is determined by function $F(s)$ or Eq. [11], which is the soil water content profile at large times. This means that the parameter V_0 describing the transient behavior of the wetting front from early to large times can be determined by the soil water content profile at large times and the hydraulic conductivity curve $K(u)$. As shown in Fig. 5.5, the term $(u_2 - u_3) / (s_2 - s_3)$ in Eq. [31] is the slope of the secant line connecting points (u_2, s_2) and (u_3, s_3). For soils with water content profiles that are almost straight lines at the wetting fronts, $(u_2 - u_3) / (s_2 - s_3)$ should not be sensitive to the choice of s_2 and s_3. Therefore, if $K'(u)$ *vs.* u is close to a linear

Figure 5.5. The soil water content profile at large times with locations of the parameters u_L, u_1, u_2, u_3, s_2, and s_3

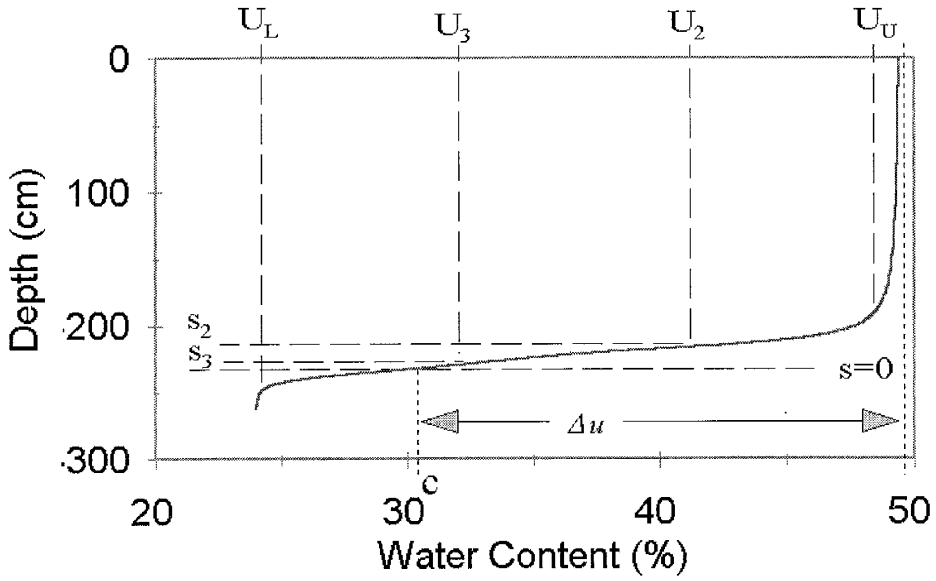

relationship (this assumption is equivalent to neglecting the third and higher order terms in the Taylor expansion of $K(u)$ at some wetting front point), we can arbitrarily choose s_2 and s_3 with little change to the value of V_0.

To discuss the sensitivity of V_2 to the choice of s_2 and s_3, we assume that $K'(u)$ *vs.* u and u *vs.* s are linear functions: $K'(u) = mu + b$ and $u = ps + c$ for $u_L \le u \le u_U$, where (u_L, u_U) is the linear portion of the wetting front (see Fig. 5.6). Under this assumption, Eq. [27] can be rewritten as:

$$V_2 = \frac{m\,c + b - V_1}{V_0} \tag{32}$$

From Eq. [32], V_2 is independent from the choice of s_2 and s_3. However, c is the intercept of the line (u_2, s_2) *vs.* (u_3, s_3) at $s=0$ in the s *vs.* u plot (Fig 5.3), and thus a function of Δu. If Δu is small, the c value becomes large and V_2 will be positive. This contradicts the fact that the V_2 parameter dominates the small time behavior and should remain negative as described in Eq. [28]. In addition, if we choose a small Δu, the $\beta(t)$ function will become negative at small times, which contradicts its positive number nature.

The calculated results for Yolo light clay show that there is only a small difference between the approximated and simplified solutions if we choose $u_2=u_0+2(u_1-u_0)/3$ and $u_3=u_0+(u_1-u_0)/3$, i.e., the equal partition points between u_0 and u_1. This difference is due to the assumption for the simplified method that $K'(u)$ has a linear relationship with u. Figure

Figure 5.6. **Comparison between the two methods of choosing s_3 and s_4 in Yolo light clay. The solid lines are the result of choosing s_3 and s_4 optimally (approximate transient solution), and the dotted lines are the results of choosing s_3 and s_4 at equal partition points (simplified transient solution). The dotted lines are all close to the solid lines.**

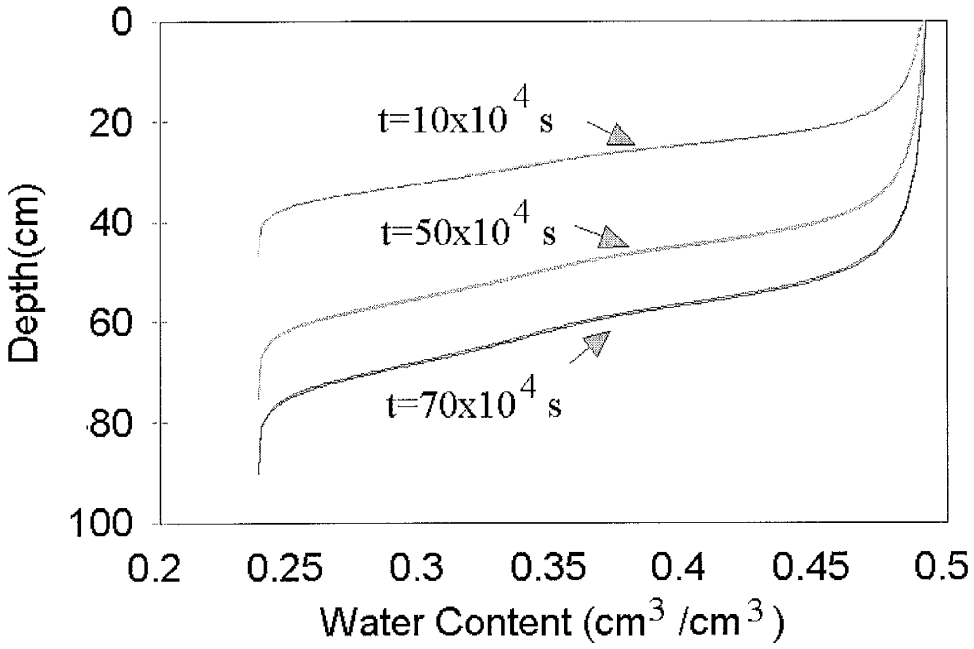

5.6 shows similar results are obtained whether optimized s_2 and s_3 are chosen, or whether they are chosen at equal partition points between u_0 and u_1.

From the above, we know that the transient behavior of the wetting front is described by the functions $\alpha(t)$ and $\beta(t)$, which are determined by two parameters, V_0 and V_2, respectively. From Eq. [27] and Eq. [31], V_0 and V_2 are determined by the soil water content profile at large times and the hydraulic conductivity curve $K(u)$. This means that if we know the soil water content profile at large times, we can obtain V_0 and V_2 by using Eq. [27] and Eq. [31]; next we can obtain the transient propagation of the wetting front.

By applying the simplified scheme described above, we can obtain the transient parameters V_0 and V_2 directly from the soil water content profile of the wetting front at large times and the hydraulic conductivity curve. Suppose we have the curve $K'(u)$ *vs.* u as shown in Fig. 5.7 and the soil water content profile of the wetting front at large times as shown in Fig. 5.8. We can draw straight lines approximate to these two curves. Let the slope and interception of the straight line in Fig. 5.7 be m and b, respectively, and the slope and the interception at $s=0$ of the line in the Fig. 5.8 be $-1/p$ and c, then by Eq. [31],

$$V_0 = |\boldsymbol{p}\cdot\boldsymbol{m}| \tag{33}$$

and V_2 can be determined by Eq. [32].

Figure 5.7. ***K′(u)-u*** **curve of Yolo clay. Draw a straight line which is most approximate to the curve. The interception of the straight line with the vertical axis is *b*, and its slope is *k*.**

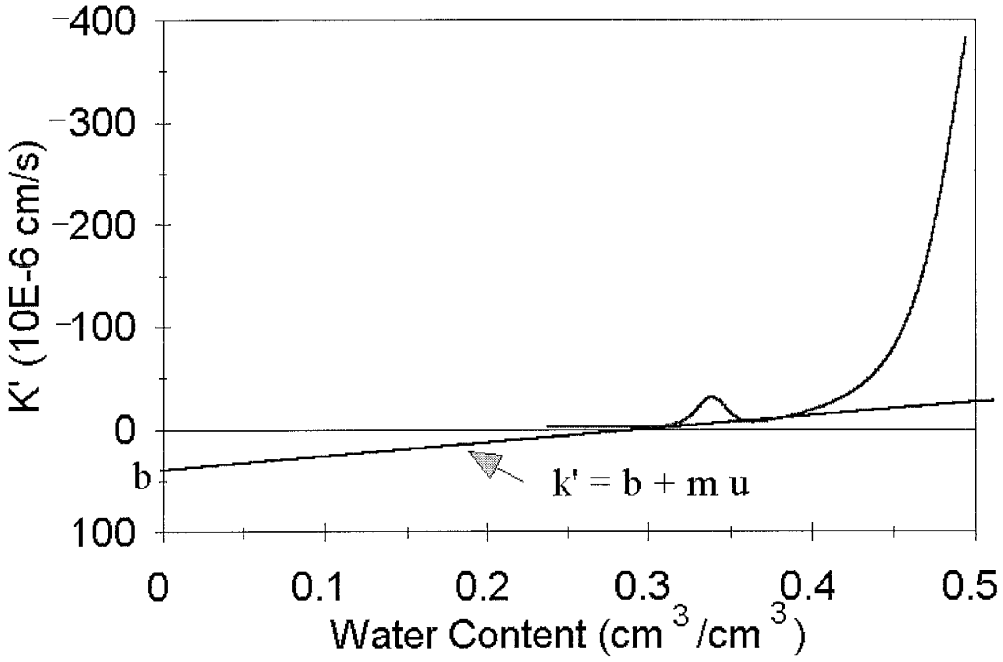

Figure 5.8. The traveling soil water content profile at large times as used for the determination of the *p* and *c* values in the expression *u=ps+c*

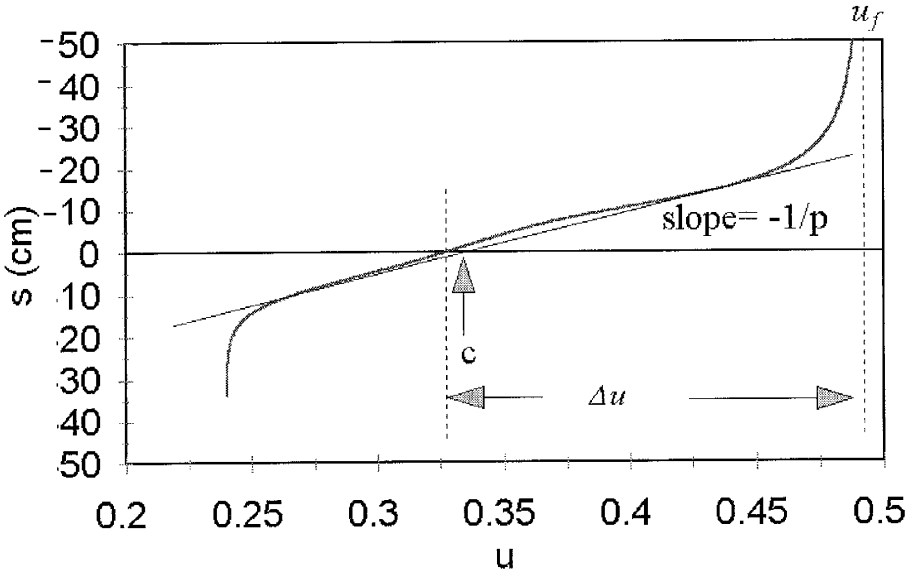

Application of The Transient Solutions

In this section, we present step-by-step instructions for the application of the approximated and simplified transient solutions. We have taken Yolo light clay as the demonstration soil to enable comparison with the previously published solutions by Philip (1957a,b) and Parlange (1971).

Approximate Transient Solution

Step 1. Obtain the unsaturated hydraulic conductivity and diffusivity curves of the soil. We use the conductivity and diffusivity data presented by Parlange (1971) for Yolo light clay.

Step 2. Calculate V_1 using Eq. [7]. For our example, taking u_1= 0.495, u_0 = 0.24 and Δu = 0.2 yields $V_1 = 0.48\times10^{-4}$ cm/s.

Step 3. By solving Eq. [11], we obtain the traveling soil water content profile as the relationship between u and η. We have used Simpson's method to integrate Eq. [11] for Yolo light clay. The result is shown in Fig. 5.8.

Step 4. Eqs. [12] and [18] indicate that the relationship between u and η found in Step 3 is identical to the relationship between u and s. Each s yields a u which in turn yields a $K'(u)$

and *dF/ds* (see Eq. [10]). We can optimize s_2 and s_3 to minimize the *R(u)* function using Eqs. [10], [11], and [26]. These two points, s_2 and s_3, can be obtained by an incremental search method or optimization scheme in the water content interval u_L - u_1. For each s_2 and s_3 , we have used 1,000 increments in the water content range of u_L-u_1 to search for a pair of s_2 and s_3 values that can minimize the *R(u)* function.

Step 5. From the curve obtained in step 3, find the corresponding water content value u_2 and u_3, respectively. For our example, u_2 = 0.3308, and u_3 = 0.3311.

Step 6. Using Eqs. [23] and [27], V_0 and V_2 can be obtained. For our example, V_0 = 1.0×10^{-6} s^{-1}, and V_2 = -3.185 cm.

Step 7. For any time *t*, by solving Eq. [25], we can obtain the corresponding $\alpha(t)$. For example, if we want to know the soil water content profile at $t = 10\times10^4$ seconds for Yolo light clay, we find $\alpha(t)$ = 1.2 from Eq. [25].

Step 8. From Eq. [29] $\beta(t)$ is obtained. For our example, $\beta(t)$ = 7.454 cm at $t = 10\times10^4$ s.

Step 9. By combining Eq. [13] and the curve obtained in step 3, we can obtain the soil water content profile at any time.

Simplified Transient Solution

Steps 1, 2, and *3* are the same as in the optimal method.

Step 4. Measure the slope p and intercept c of the function $u=ps+c$ which represents the traveling soil water content profile (Fig. 5.8). For our example, we choose Δu=0.2, $p = -6.89\times10^{-3}$ cm^{-1} and $c = 0.327$.

Step 5. Let u_2 and u_3 be the equal partition points of the interval (u_0, u_f), then find the slope k and the intercept b of the secant line connecting points $(K'(u_2), u_2)$ and $(K'(u_3), u_3)$ on the $K'(u)$-u curve. For our example, we chose u_0=0.24 , and u_f=0.495 , then u_2= 0.41 and u_3=0.3263. From Fig. 5.7, $K'(u_2) = 0.2266\times10^{-4}$ cm/s and $K'(u_3) = 0.09\times10^{-4}$ cm/s. So, $m = [K'(u_2) - K'(u_3)]/(u_2 - u_3) = 1.611\times10^{-4}$ cm/s and $b = K'(u_2)-k\,u_2 = -0.4295\times10^{-4}$ cm/s.

Step 6. Calculate V_0 and V_2 using Eqs. [31] and [32]. For our example, $V_0 = 1.11\times10^{-6}$ s^{-1} and $V_2 = -3.45$ cm.

Steps 8 and *9* are the same as in the optimal method.

The parameters obtained by the approximate and simplified solutions are very similar

(see Table 5.1). We compared our soil water content profiles using the simplified method, (Fig. 5.9a), with those calculated by Philip (1969) in his Fig. 5.2 at times 10^4, $4x10^4$, $10x10^4$, $20x10^4$, $35x10^4$, $50x10^4$, $70x10^4$, $100x10^4$, $150x10^4$, and $200x10^4$ s (Fig. 5.9b) as well as with the profile calculated by Parlange (1971) in his Fig. 1 at time $70x10^4$ s. Those water content profiles are identical with our results, which demonstrates the usefulness of the analytical solution presented in this study.

Sensitivity of Solutions to the Choice of Δu and its Influence

The approximate analytical solution presented in this study performs well at large times since it uses the traveling wave solution as its base solution. For small times, we can get reasonable results if Δu is large enough. As shown in Fig. 5.3, a large Δu keeps the major part of the wetting front slightly above the soil surface at t=0. Although this is an image, it has some physical significance since infiltration will not start until some water pressure has built up at the soil surface. Table 5.2 shows the results of parameters V_2, β, and S_{40} (defined as the s value at soil water content = 40%) from small Δu to large Δu for Yolo light clay. The reasonable V_2 (<0) and β (>0) values can be obtained only when Δu is greater than 0.11.

To analyze the wetting front behavior at small times on the choice of Δu, we follow these steps: For small times, from Eq. [30]

Table 5.1. The parameters for Yolo clay under the conditions: u_0=0.2376 and u_1=0.4947

	V_0 (10^{-6} s^{-1})	V_1 (10^{-4} cm/s)	V_2 (cm)
Approximate Transient Solution	1.0	0.487	-3.19
Simplified Transient Solution	1.1	0.487	-3.45

Figure 5.9. Soil water content profiles for different times determined with our method (a) and with Philip's (1969) method (b)

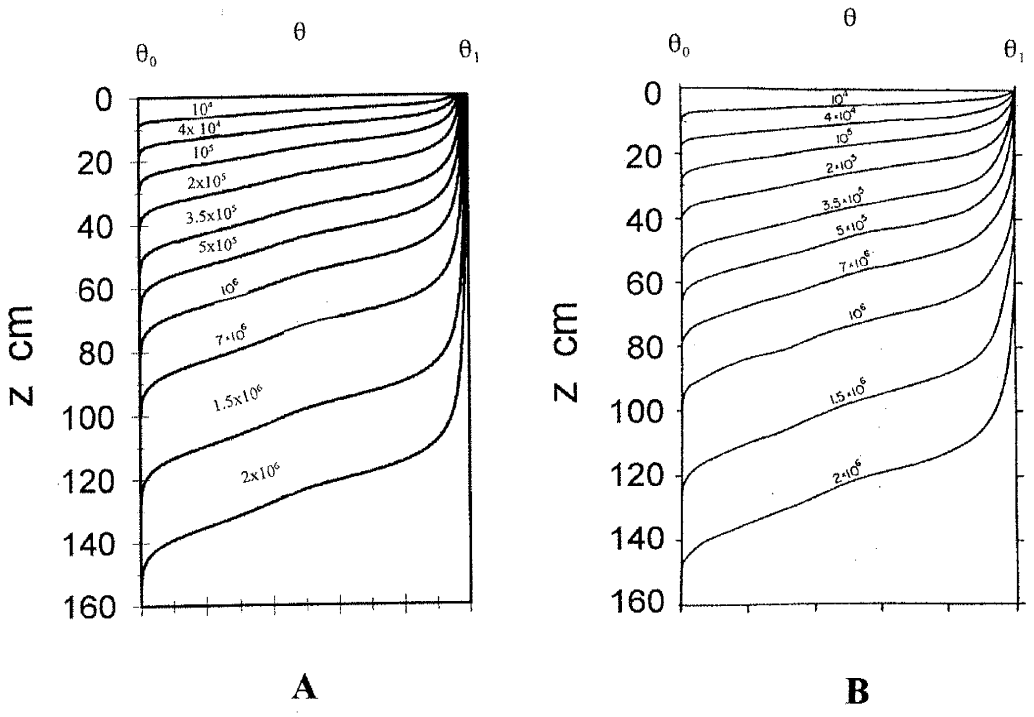

Table 5.2. The parameters for Yolo light clay with different Δu at t=100 sec (small time)

Δu (-)	s_{40}* (cm)	V_2 (cm)	β (cm)
0.001	217.14	192	-2.74
.01	27.85	2.74	-0.034
.1	1.15	-23.96	0.347
.2	-10.74	-35.8	0.516
.24	-14.3	-39.4	0.568

* s value at soil water content = 40%

$$\alpha(t) \cong \frac{1}{\sqrt{2V_0 t}} \tag{34}$$

and from Eqs. [33] and [34]

$$\beta(t) \cong -V_2\sqrt{2V_0}\sqrt{t} \tag{35}$$

The cumulative infiltration I at small times can be approximated as:

$$I = \beta(t)\theta_s \tag{36}$$

At small times, from the definition, $I=St^{1/2}$ (Philip, 1969), where S represents the sorptivity. We can substitute Eq. [35] and this relationship into Eq. [36] to get

$$S \cong -V_2\sqrt{2V_0} \tag{37}$$

This relationship can be verified through calculation. We use the soil hydraulic properties from Yolo light clay. The sorptivity value was calculated using the approximate formula by Parlange (1975):

$$S^2 = \int_{hi}^{h} [\theta(h) + \theta(H) - 2\theta_i] K dH \tag{38}$$

At zero water tension, the calculated sorptivity value for Yolo light clay is 0.012 cm/sec$^{1/2}$. From our approach, V_2 has the range from -1.1 to -36 cm for the Δu range of 0.11 to 0.2. With $V_0 = 1.11*10^{-6}$ s^{-1}, we calculate sorptivity from Eq. [37] and have the range of S from

0.0016 to 0.054 cm/sec$^{1/2}$. The calculated sorptivity, 0.012 cm/sec$^{1/2}$, falls in this range and demonstrates that the small time behavior of our solution can be approximated if the appropriate Δu is used.

Finally, we examined the sensitivity of solutions to the choices of Δu. For Δu from 0.001 to 0.2, as Fig. 5.10 shows, for Yolo light clay there are no differences of the z *vs.* θ profiles between Δu=.001 and Δu= 0.2 for the full time range. Larger Δu will give more reasonable parameters, such as V_2 and β, at the small time range. However, even if Δu is wrongly chosen to be a small number, the final profiles are the same for all times because the s value is larger for smaller Δu and the unreasonable negative $\beta(t)$ at small time will adjust the wetting front position to where it should be.

Comparison with Numerical Simulation

In order to verify the applicability of this model, we compare our calculated results with the numerical simulation using HYDRUS50 (Vogel, et al.,1996). We chose both Yolo light clay and US mesh 14-20 sieved natural quartz sand. We use the optimal scheme for our analysis. The results are shown in Figs. 5.11a and 5.11b. It can be clearly seen that our solution gives a good approximation of the wetting front profile at all times. Another advantage of our method is that the solutions are determined by algebraic Eqs. [18], [25], and [28], so that the errors at early times do not influence the accuracy of later results.

Figure 5.10. **Soil water content profiles for Yolo light clay with two different Δu values 0.001 and 0.2 from small to large times. At the same time, results are identical for different Δu values and the lines are overlapped**

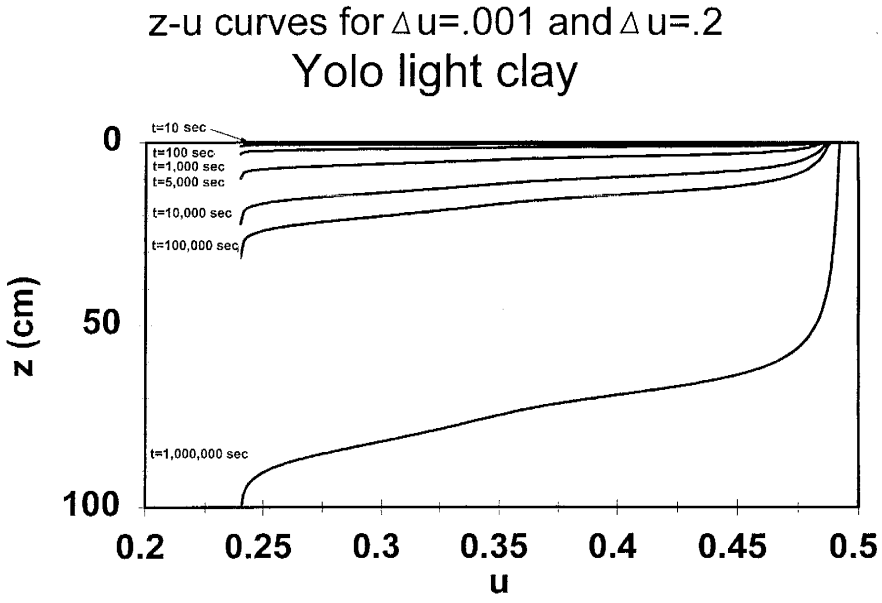

Figure 5.11. Soil water content profiles for different times determined with our method and with numerical simulation for (a) Yolo light clay and (b) US mesh 14-20 sand

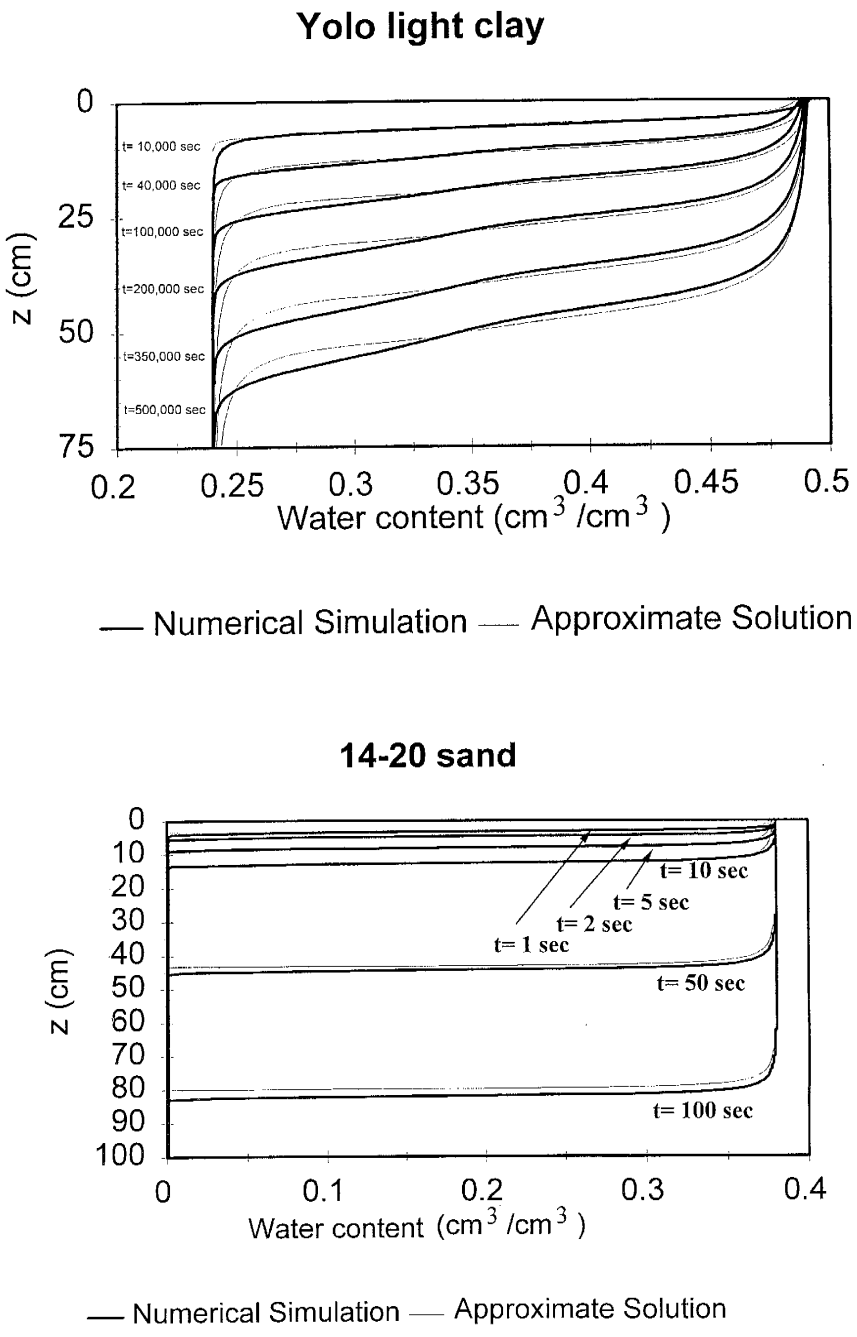

Conclusions

1) The transient behavior of the soil water content profile during infiltration from early to large times can be represented by two functions of time, $\alpha(t)$ and $\beta(t)$. Function $\alpha(t)$ describes the change of the wetting front shape with time and $\beta(t)$ describes the depth of the wetting front below the soil surface. The two functions of time, $\alpha(t)$ and $\beta(t)$, can be calculated from Eqs. [25] and [28], which contain two parameters, V_0 and V_2.

2) The two parameters V_0 and V_2 can be obtained from the soil water content profile at large times and the hydraulic conductivity curve by using the approximate solution. If the relationship $K'(u)$ *vs.* u is approximately linear, the simplified solution can be used. Then, V_0 and V_2 are obtained by measuring the slope and interception of the soil water content profile at infinite time and the slope and interception of $K'(u)$ *vs.* u curves.

3) The results from the methods presented in this study are --for Yolo light clay-- as accurate as those from other methods previously reported in the literature (Philip, 1969; Parlange, 1971). However, our method covers the entire infiltration process from early to large times and its implementation is relatively simple.

4) By comparing the results from our approximate method and numerical simulation for both clay and sand soils, we prove the usefulness of our method for a wide range of soils at all times.

References

Barry, D.A., J.-Y. Parlange, G.C. Sander, and M. Sivaplan. 1993. A class of exact solutions for Richards' equation. J. of Hydrol, 142:29-46.

Hogarth, W.J., J.-Y. Parlange, and R.D. Braddock. 1989. First integrals of the infiltration equation: 2. Nonlinear conductivity. Soil Sci. 148:165-171.

Moore, R.E. 1939. Water conduction from shallow water tables. Hilgardia. 12: 383-426.

Parlange, J.-Y. 1971. Theory of water-movement in soil: I. One-dimensional infiltration. Soil Sci. 111:170-174.

Parlange,J.-Y. 1975. On solving the flow equation in unsaturated soils by optimizing: Horizontal infiltration. Soil Sci. Soc. Am. Proc. 39: 415-417.

Parlange, J-Y., D.A. Barry, M.B. Parlange, W.L. Hogarth, R. Haverkamp, P.J. Ross, L. Ling, and T.S. Steenhuis. 1997. New approximate analytical technique to solve Richards equation for arbitrary surface boundary conditions. Water Resour. Res. 33: 903-906.

Parlange, J.-Y., and J.F. Fleming. 1984. First integral of the infiltration equation: 1. Theory. Soil Sci. 137:391-394.

Philip, J.R. 1957a. The theory of infiltration: 1. The infiltration equation and its solution. Soil Sci. 83:345-357.

Philip, J.R.. 1957b. The theory of infiltration: 2. The profile at infinity. Soil Sci. 83:435-448.

Philip, J.R. 1969. Theory of infiltration. Advances in Hydroscience 5:215-296.

Ross, P.J., and J.-Y. Parlange. 1994. Investigation of a method for deriving unsaturated soil

hydraulic properties from water content profiles. Soil Sci. 157:335-340.

Srivastava, R., and T.-C. Yeh. 1991. Analytical solution for one-dimensional, transient infiltration toward the water table in homogeneous and layered soils. Water Resour. Res. 27:753-762.

Vogel, T., K. Huang, R. Zhang, and M. Th. van Genuchten. 1996. The HYDRUS code for simulating one-dimensional water flow, solute transport, and heat movement in variably-saturated media. Version 5.0. Research Rep. No. 140. U.S. Salinity Laboratory, Riverside, California.

Warrick, A.W., A. Islas, and D.O. Lomen. 1991. An analytical solution to Richards' equation for time-varying infiltration. Water Resour. Res. 27:763-766.

6. Stability Analysis of the Unsaturated Water Flow Equation: 1. Mathematical Derivation

X.H. Du[1], T. Yao[2], W.D., Stone[3], and J.M.H. Hendrickx[2*]

[1]Hydrology Program, Department of Earth & Environmental Science and Geophysical Research Center, New Mexico Tech, Socorro, NM 87801; presently at Electrical Engineering Department, Pennsylvania State University, State College, PA 16801

[2]Hydrology Program, Department of Earth & Environmental Science and Geophysical Research Center, New Mexico Tech, Socorro, NM 87801

[3]Department of Mathematics, New Mexico Tech, Socorro, NM 87801

Abstract

This paper provides a theoretical stability analysis of gradual wetting fronts based on perturbation analysis. A general solution of the one-dimensional vertical flow Richards' equation is used as the basic flow on which three-dimensional perturbations are introduced. By locally linearizing the three-dimensional Richards' equation, a linear partial differential equation is obtained which governs the perturbation variables. The stability of each point at the wetting front is considered in the local coordinate system. The analysis of this

perturbation equation at these points of the wetting front provides not only the relationship between the finger sizes and the infiltration rates at the top surface, but also the traveling speeds of the fingers rooted from these points. The stability of the wetting front is determined by two factors: finger sizes and downward velocities of fingers. If the size of the finger rooting from some point is large, then this point is considered to be stable whatever the downward velocity is; if the size of the finger is not large, but the downward velocity of the finger is smaller than that of the stable wetting front, then the finger will be covered eventually by the distribution layer and this point remains stable. Instability will occur only when the finger size is small and the downward velocity of the finger is larger than that of the stable wetting front. Under these conditions, the finger will remain ahead of the stable wetting front at all times. For any homogeneous soil profile with uniform initial water content, this model can predict instability and finger characteristics over the full range of infiltration rates.

Introduction

Knowledge of the conditions that cause unstable wetting fronts is essential for the prediction of water and solute fluxes through field soils and vadose zones. Field data presented by *Hendrickx and Dekker* [1991], *Hendrickx et al.* [1993], *Ritsema et al.* [1993], *Starr et al.* [1978, 1986], *Van Dam et al.* [1990], and *Van Ommen et al.* [1989] demonstrate that preferential flow paths resulting from unstable wetting in field soils decrease travel times of solutes and increase the vulnerability for aquifer contamination. Unfortunately, the

conditions that cause unstable wetting fronts are not well understood because the highly nonlinear behavior of the unsaturated flow equation makes a "general attack ... very difficult" [*Philip*, 1975a]. Therefore, *Raats* [1973] and *Philip* [1975a,b] limited their hydrodynamic stability analysis to the relatively simple delta-function model of infiltration that is appropriate for the special case where the soil water diffusivity is concentrated at the wet end of the soil water content range [*Philip,* 1957, 1973]. This model applies well to initially dry coarse-textured soils with sharp wetting fronts and high infiltration rates, but is less suitable to describe the processes occurring in many other soils that have gradual wetting fronts and lower infiltration rates. As a consequence the stability criterion for delta-function soils first postulated by *Raats* [1973] and later derived by *Philip* [1975a] cannot be used with confidence for the prediction of unstable wetting in many field soils. Gradual wetting fronts were used by *Diment and Watson* [1982] for their hydrodynamic stability analysis using numerical simulation [*Diment and Watson*, 1983]. They found no evidence of unstable wetting under conditions of redistribution, heterogeneous, and layered systems where instability was expected. They stated that the absence of unstable phenomena was caused by a relatively high initial water content (5 cm^3/cm^3) that significantly damped out instabilities. They concluded that additional work is required in developing stability analysis for non-sharp gradual fronts that can handle very low initial water content conditions.

Philip [1975b] derived an equation to estimate finger widths in delta-function soils while *Parlange and Hill* [1976] derived one for real soils. According to Philip's equation, soil texture or initial water content will have no effect on finger widths. However, *Parlange*

and Hill [1976] predict that fingers widen when the soil texture is finer or the initial soil water content is higher. These predictions have been confirmed by theoretical and experimental work of *Glass et al.* [1989a,b, 1990, 1991], *Liu et al.* [1994, 1995], *Selker et al.* [1992], *Hendrickx and Yao* [1996], and *Yao and Hendrickx* [1996]. The effect of infiltration rate on finger diameter has also been investigated. It was experimentally verified that the finger diameter increases as the flow rate through the soil increases resulting in stable wetting fronts for flow rates equal or higher than the saturated hydraulic conductivity [*Glass et al.*, 1989b]. Experimental work by *Yao and Hendrickx* [1996] showed that finger diameters also increase when the flow rates decrease, thus resulting in stable wetting fronts at low infiltration rates.

A comprehensive hydrodynamic stability analysis of the Richards' equation that can be applied to all soils and covers all infiltration rates from high ones equal or exceeding saturated soil hydraulic conductivity to low ones approaching zero, is needed for a better understanding of unstable flow in field soils. Therefore, the objectives of this study are (1) to conduct a stability analysis of the unsaturated flow equation that applies to all soils and (2) to derive a model for the estimation of finger characteristics at all infiltration rates.

Mathematical Model

We assume that the complex process of finger formation at wetting fronts can be analyzed as the superposition of two different flow regimes: a perturbation flow

superimposed on a stable flow. The stable flow is described using a solution of the one-dimensional Richards' equation that is valid for all times and for all soils [*Du et al.*, 1998]. The equation governing the perturbation flow is obtained in this study by a local linearization of the three-dimensional Richards' equation. Half the wavelength of the perturbation waveform corresponds to the finger diameter [*Parlange and Hill*, 1976]. If the perturbation disappears with time, the wetting front is stable; otherwise, the wetting front is unstable. The finger diameters are obtained from the profile of the perturbation flow.

Stable Flow Solution

The solution of the one-dimensional Richards' equation by *Du et al.* [1998] is used as the basic flow equation on which the perturbation is performed. Here we will present only those features of the solution which are necessary for the stability analysis.

The Richards' equation governing one-dimensional vertical flow in unsaturated soil can be written as:

$$\frac{\partial u}{\partial t} = \frac{\partial}{\partial z}\left(D(u)\frac{\partial u}{\partial z} - K(u)\right) \qquad (1)$$

where t is the time, z is the vertical coordinate with positive downward direction, u is the volumetric water content, $K(u)$ is the hydraulic conductivity, and $D(u)$ is the diffusivity. In

this study, we consider the following boundary and initial conditions

$$u(0,t) = u_1 \tag{2}$$

$$u(z,0) = u_0 \tag{3}$$

$$u(\infty,t) = u_0 \tag{4}$$

where u_1 is the water content at the top boundary, and u_0 is the initial water content.

Du et al. [1998] define a variable s

$$s = \alpha(t)\,(z - \beta(t)) \tag{5}$$

This function is used to establish for all times the relationship between water content u and depth z, i.e., the location and shape of the stable wetting front. The function $\alpha(t)$ converts the shape of the wetting front at large times to the one at early and intermediate times. For large times, $\alpha(t)$=1. The function $\beta(t)$ provides the depth of the wetting front from the point s=0 to the soil surface. For early and intermediate times, $\beta(t)$ describes the transient behavior of the wetting front velocity; for large times, $\beta(t)=V_1\,t$ where

$$V_1 = \frac{K(u_1) - K(u_0)}{u_1 - u_0} \tag{6}$$

Thus, V_1 is the velocity of the stable wetting front at large times. *Du et al.* [1998] show that the solution has the following form:

$$u = F(s) \tag{7}$$

and F is a function determined by the solution of:

$$\frac{du}{ds} = \frac{[K(u) - K(u_0)] - V_1(u - u_0)}{D(u)} \tag{8}$$

subject to

$$u(0,t) = u_f \tag{9}$$

where $u_f = u_1 - \epsilon$. The quantity ϵ is small and positive and needs to be introduced to avoid the singularity problem at u_1 [*Philip*, 1969]. The unknown functions $\alpha(t)$ and $\beta(t)$ are obtained by substituting (7) into (1) to obtain the residual $R(u)$:

$$\begin{aligned} R(u) &= \frac{\partial u}{\partial t} - \frac{\partial}{\partial z}\left(D(u)\frac{\partial u}{\partial z} - K(u)\right) \\ &= \left[\frac{\alpha'(t)}{\alpha(t)}s - (\alpha^2(t) - \alpha(t))K'(u) + V_1\alpha^2(t) - \alpha(t)\beta'(t)\right]\frac{dF}{ds} \end{aligned} \tag{10}$$

In order to minimize $R(u)$, it follows that

$$-\frac{\alpha'(t)}{\alpha(t)}s + \alpha(t)\beta'(t) - \alpha(t)K'(u) \approx \alpha^2(t)(V_1 - K'(u)) \tag{11}$$

Equation (11), applied to sharp and gradual wetting fronts, will be used in our perturbation

analysis.

Perturbed Flow Equation

A standard perturbation technique [*Nayfeh*, 1981] is applied to the three-dimensional Richards' equation:

$$\frac{\partial \theta}{\partial t} = \nabla \cdot [D(\theta) \nabla \theta] - \frac{\partial K(\theta)}{\partial z} \qquad (12)$$

where θ is the water content. We use θ to denote the solution of the three-dimensional Richards' equation in order to distinguish from the one-dimensional solution u. The perturbed (13) is obtained by substituting $\theta = u(s) + \varepsilon v(x,y,z,t)$ into (12) and neglecting any higher order terms of ε. The $u(s)$ term is a solution in three-dimension but it is independent of x and y, and z and t are related by s while $\varepsilon v(x,y,z,t)$ is three-dimensional and depends on x, y, z, and t; v is the perturbation function and ε is a small number to perturb the function. The three-dimensional perturbation is used in order to obtain three-dimensional finger characteristics in our analysis. The resulting perturbation equation to first order in ε is

$$\frac{\partial v}{\partial t} = D(u)\frac{\partial^2 v}{\partial z^2} + \left[2D'(u)\frac{\partial u}{\partial z} - K'(u)\right]\frac{\partial v}{\partial z}$$
$$+ \left[D''(u)\left(\frac{\partial u}{\partial z}\right)^2 + D'(u)\frac{\partial^2 u}{\partial z^2} - K''(u)\frac{\partial u}{\partial z}\right]v$$
$$+ D(u)\left[\frac{\partial^2 v}{\partial x^2} + \frac{\partial^2 v}{\partial y^2}\right] \qquad \textbf{(13)}$$

Equation (13) can be used to study the general perturbation behavior at the wetting front which is the outcome of superposing all perturbations with various wavelengths. We cannot obtain characteristics of a single finger from the analysis in the space domain. However, the general disturbance can be represented by the sum of any number of basic modes of disturbance through a Fourier integral. It is possible to analyze the stability of these disturbances and their associated characteristics in the Fourier modes which compose these disturbances. This process is known as spectral analysis. In order to conduct the spectral analysis to obtain information regarding a particular waveform, we convert (14) from the space domain into the frequency domain by Fourier Transform. Afer this transformation, it becomes possible to study the instability characteristics of a particular finger with a single wavelength. The Fourier Transform of (13) is taken with respect to x and y:

$$\frac{\partial V}{\partial t} = D(u)\frac{\partial^2 V}{\partial z^2} + \left[2D'(u)\frac{\partial u}{\partial z} - K'(u)\right]\frac{\partial V}{\partial z}$$

$$+ \left[D''(u)\left(\frac{\partial u}{\partial z}\right)^2 + D'(u)\frac{\partial^2 u}{\partial z^2} - K''(u)\frac{\partial u}{\partial z} - (\omega_x^2 + \omega_y^2)D(u)\right]V \tag{14}$$

where function V is the Fourier transform of v. Next, variable z in (14) is replaced by variable s (see (5)).Then, by using (11), we find

$$\frac{\partial V}{\partial t} = \alpha^2(t)D(u)\frac{\partial^2 V}{\partial s^2} + \alpha^2(t)\left[2D'(u)\frac{\partial u}{\partial s} + V_1 - K'(u)\right]\frac{\partial V}{\partial s}$$

$$+ \left[\alpha^2(t)D''(u)\left(\frac{\partial u}{\partial s}\right)^2 + \alpha^2(t)D'(u)\frac{\partial^2 u}{\partial s^2} - \alpha(t)K''(u)\frac{\partial u}{\partial s} - \omega^2 D(u)\right]V \tag{15}$$

where

$$\omega^2 = \omega_x^2 + \omega_y^2 \tag{16}$$

$$\omega = 2\pi/\lambda \tag{17}$$

Parameter ω is the wave number, and λ is the wavelength of the sinusoidal perturbation.

Equation (15) is a second order linear parabolic partial differential equation with real coefficients. Since the superposition principle is valid for linear systems, the stability of (15) can be considered under the following conditions:

$$V(s_p,t) = \delta(t-t_0) \tag{18}$$

$$V(s,t) = 0 \qquad for \quad t < t_0 \tag{19}$$

$$V(\infty,t) = 0 \tag{20}$$

where $\delta(t-t_0)$ is the impulse function that introduces the disturbance, and t_0 and s_p are respectively the time and the position at which the disturbance occurs. The reason of using boundary condition (18) will be explained below. Equations (19) and (20) express the assumptions that the wetting front is stable before the disturbance occurs and that the disturbance never reaches infinite depth.

The perturbation process is schematically shown in Figures 6.1(a) and 6.1(b). In the Fourier domain (Figure 6.1(a)), the impulse function $\delta(t-t_0)$ was introduced at point s_p and time t_0, and the perturbation is represented by an impulse of frequency ω with a amplitude to infinity. In the space domain, this particular frequency disturbance can be transformed

Figure 6.1. **Schematic plots to demonstrate the disturbance *δ(t)* in the frequency or Fourier domain (A) and the equivalent disturbance in the space domain (B). Coarse line represents the wetting front before perturbation. Fine line represents the wetting front after perturbation**

(A)

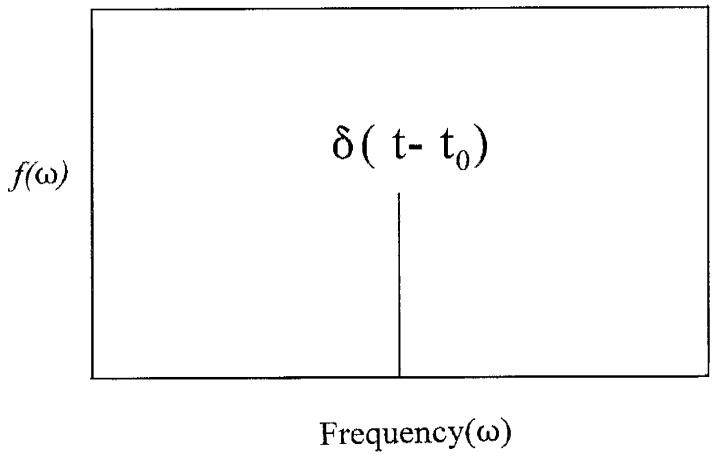

(B)

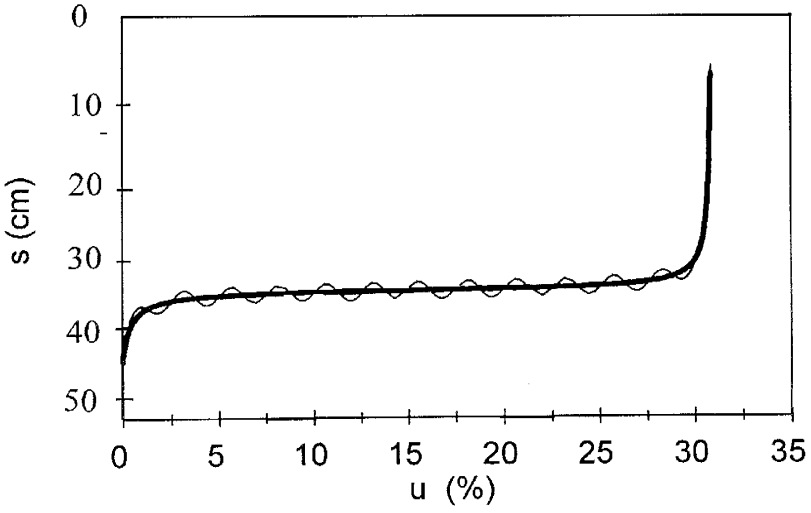

back to a periodic perturbation function (Figure 6.1(b)). The perturbation $sin(\omega u)$ that causes the sinusoidal perturbation to the original wetting front profile is generated at a particular time t_0. The stability at each point of the wetting front according to this particular sinusoidal disturbance will be studied in later sections.

Why is the impulse function $\delta(t-t_0)$ used as the boundary condition in (18)? If we use a perturbation function $f(t)$ that allows for the reoccurrence and amplitude change of the perturbation with time, equation (18) becomes

$$V(s_p,t) = f(t) \tag{21}$$

The general solution $V_{general}(s,t)$, comes from the solution of (15) with boundary conditions (19), (20), and (21), and has the following relationship:

$$V_{general}(s,t) = V(s,t) * f(t) \tag{22}$$

where $V(s,t)$ is the solution that comes from the solution of (15) with boundary conditions (18), (19), and (20). Since (22) is only a convolution relationship and function $f(t)$ is finite and assumed to be a decreasing function with time, the stability behavior of the general perturbation condition can be determined by studying the stability behavior of solution $V(s,t)$. This explains why the impulse function $\delta(t-t_0)$ can be used in (18) without losing the generality in our stability analysis.

For the purpose of obtaining perturbation characteristics, we assume that, at some

time t_0, perturbations will occur at some point s_p of the wetting front. We will find that for the same perturbation issued at different points s_p, different stability scenarios develop. For some points, perturbations will disappear as time increases; these points are stable. For other points, perturbations may exist for a long time once they are introduced; these points are unstable. Fingers will root from these unstable points where fingers can persist ahead the wetting front. The stable condition requires that the Fourier transformed perturbation function $V(s,t) \to 0$ as $t \to \infty$. Equation (15) can be simplified by considering the fact that fingers only will develop under the dominance of gravity [*Hendrickx and Yao*, 1996], i.e. at relatively large times where $\alpha(t)$ approximates unity [*Du, et al.*, 1998]. Equation (15) then becomes

$$\frac{\partial V}{\partial t} = D(u)\frac{\partial^2 V}{\partial s^2} + \left[2D'(u)\frac{\partial u}{\partial s} + V_1 - K'(u)\right]\frac{\partial V}{\partial s} + \left[D''(u)\left(\frac{\partial u}{\partial s}\right)^2 + D'(u)\frac{\partial^2 u}{\partial s^2} - K''(u)\frac{\partial u}{\partial s} - \omega^2 D(u)\right]V \tag{23}$$

Now consider the stability in the local region near s_p. We assume that in a small local region near s_p, $u \approx u_p = u(s_p)$, $du/ds \approx [du/ds]_{s=sp}$, and $d^2u/ds^2 \approx [d^2u/ds^2]_{s=sp}$. Then (23) becomes:

$$\frac{\partial V}{\partial t} = D_p\frac{\partial^2 V}{\partial s^2} + A_p\frac{\partial V}{\partial s} + \left[B_p - \omega^2 D_p\right]V \tag{24}$$

where

$$D_p = D(u_p) \tag{25}$$

$$A_p = 2D'(u_p)\frac{du}{ds}\Big|_{s=s_p} + V_1 - K'(u_p) \tag{26}$$

$$B_p = D''(u_p)\left(\frac{du}{ds}\Big|_{s=s_p}\right)^2 + D'(u_p)\frac{d^2u}{ds^2}\Big|_{s=s_p} - K''(u_p)\frac{du}{ds}\Big|_{s=s_p} \tag{27}$$

Let

$$V = e^{(B_p - D_p\omega^2)t}W \tag{28}$$

where W is a finite function. The exponent $(B_p - D_p\omega^2)$ allows the disturbance V to either increase with time $(B_p - D_p\omega^2 > 0)$ or decrease with time $(B_p - D_p\omega^2 < 0)$. Substitution of (28) into (24) yields a diffusion-convection equation:

$$\frac{\partial W}{\partial t} = D_p\frac{\partial^2 W}{\partial s^2} + A_p\frac{\partial W}{\partial s} \tag{29}$$

Boundary conditions (18), (19) and (20) are transformed into

$$W(s_p,t) = e^{-(B_p - D_p\omega^2)t_0}\,\delta(t-t_0) \tag{30}$$

$$W(\infty,t) = 0 \tag{31}$$

$$W(s,t) = 0 \qquad \text{for } t < t_0 \tag{32}$$

Equation (29) with the boundary conditions (30), (31), and (32) will be used to generate stability criteria and finger characteristics in the next section.

Instability Criteria and Finger Characteristics

Criteria for Instability

Equation (29) is the one-dimensional diffusion-convection equation, its solution subject to conditions (30), (31), and (33) is finite. This implies that V in (28) goes to zero if and only if

$$B_p - D_p\omega^2 < 0 \tag{33}$$

So, the wetting front is stable if

$$\omega > \sqrt{\frac{B_p}{D_p}} \tag{34}$$

the opposite of (34) is not a sufficient condition to cause an unstable wetting front since we also have to consider the relative speeds of the disturbance and the stable wetting front. The reason is that not every disturbance that develops into a small finger will continue to grow. If the traveling speed of a finger is slower than the traveling speed of the stable wetting front, the finger will be covered by the wetting front. This is a process that is typical for the distribution layer (Figure 6.2). If the traveling speed of a small finger is faster than of the stable wetting front, the finger will continue to grow and will fully develop. The speed of the stable wetting front V_1 at large times is given by (6). Inspection of the diffusion-convection (29) shows that the traveling speed of a finger rooting from point s_p, relative to the stable wetting front based upon the one-dimensional stable solution, is $-A_p$. Thus, from (26), the traveling speed of the finger relative to the soil profile, V_f, is

$$V_f(p) = -A_p + V_1 = K'(u_p) - 2D'(u_p)\frac{du}{ds}\Big|_{s=s_p} \tag{35}$$

In $V_f(p)$, we write the velocity of a finger as a function of the perturbation point p to emphasize the dependence of finger velocity on the location of a perturbation on the wetting front. In other words, the velocities of fingers are different if they root from different points at the wetting front.

Figure 6.2. Schematic relation between finger and distribution layer

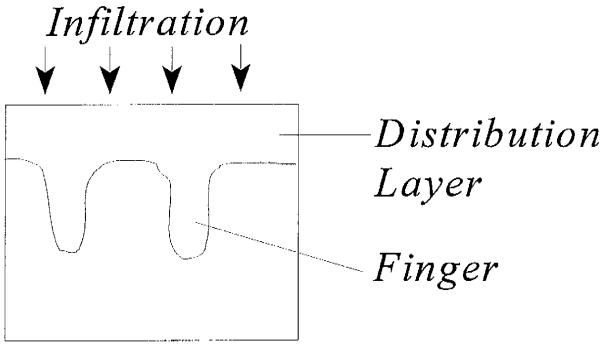

The necessary condition for full finger development is $V_f > V_1$, so that:

$$K'(u_p) - 2D'(u_p)\frac{du}{ds}\Big|_{s=s_p} > V_1 \qquad (36)$$

The stability of the wetting front at a point s_p when $\omega < (B_p / D_p)^{1/2}$ is determined by the interactions between D_p, B_p, and A_p. We distinguish two scenarios. (i). The downward velocity of the finger ($-A_p + V_1$) is less than that of the stable wetting front (V_1), then the finger will eventually be overcome by the stable wetting front and as a consequence this point becomes stable; (ii). If the downward velocity of the finger ($-A_p + V_1$) is larger than that of the stable wetting front (V_1), the finger will remain ahead of the stable wetting front for a long time and the point is unstable.

Thus, the complete criteria for instability are $\omega < (B_p / D_p)^{1/2}$ and $A_p < 0$. These criteria make it possible to determine for each wavelength λ (see (17)) whether an instability will occur

$$\lambda > 2\pi\sqrt{\frac{D_p}{B_p}} \qquad (37)$$

This criterion shows that a small perturbation (λ small) will not result in a finger. The perturbation has to exceed a critical size or wavelength to cause an unstable wetting front.

Finger Velocity and Diameter

The discussion in the previous section indicates that the disturbance with the fastest

downward velocity will have the greatest probability to develop into a persistent finger [*Chu and Parlange*, 1962; *Philip*, 1975]. Therefore, we use (35) to find the water content u* at the location on the wetting front where the finger velocity is the greatest, i.e. $V_f(u^*)$ is the maximum $V_f(u_p)$ in the interval $u_0 < u_p < u_1$.

$$V_f(u*) = K'(u*) - 2D'(u*)\frac{du}{ds}\Big|_{u=u*} \tag{38}$$

The critical or smallest finger diameter rooting from the location on the wetting front where water content equals u* is

$$D_c(u*) = \pi \cdot \sqrt{\frac{D*}{B*}} \tag{39}$$

where

$$D* = D(u*) \tag{40}$$

$$B* = D''(u*)\left(\frac{du}{ds}\Big|_{u=u*}\right)^2 + D'(u*)\frac{d^2u}{ds^2}\Big|_{u=u*} - K''(u*)\frac{du}{ds}\Big|_{u=u*} \tag{41}$$

To find the finger characteristics for different water contents at the top boundary (Equation (2)), we first generate wetting front profiles using (7) and (8) with actual soil hydraulic properties. Next, we use (36) to determine at a given water content for all points

on the wetting front whether a perturbation rooting from a given point will persist or fade away. Finally, the finger velocity and diameter at each unstable point on the wetting front are obtained using (38), (39), (40), and (41). Then, we obtain the relationship between the infiltration rate and the diameter of the finger which has the largest downward velocity by putting

$$i = K(u_1) \tag{42}$$

where i is the infiltration rate. Equation (42) assumes an unit gradient, i.e. water flow is driven by gravity. This assumption is quite reasonable for the study of unstable wetting fronts since fingers can only form when gravity dominates the infiltration process [*Hendrickx and Yao*, 1996]. Our instability analysis is based on an analysis of the infiltration process at large times since we have put $\alpha(t)=1$ to arrive at (23). In the companion paper [*Yao and Hendrickx*, 1998], we will illustrate a step by step numerical scheme that determines wetting front stability and finger characteristics.

Stability Analysis at Different Regions of the Wetting Front

We want to investigate at what location on the wetting front the instability actually occurs. We use (36) as the criterion to determine if fingers can start and persist ahead of the stable wetting front. In Figure 6.3, we postulate four regions for our analysis. We can easily observe in Figure 6.3 that $du/ds \approx 0$ in regions I and IV. This implies that $B_p \rightarrow 0$ and $D_c \rightarrow \infty$

Figure 6.3. Four regions of the soil water content profile

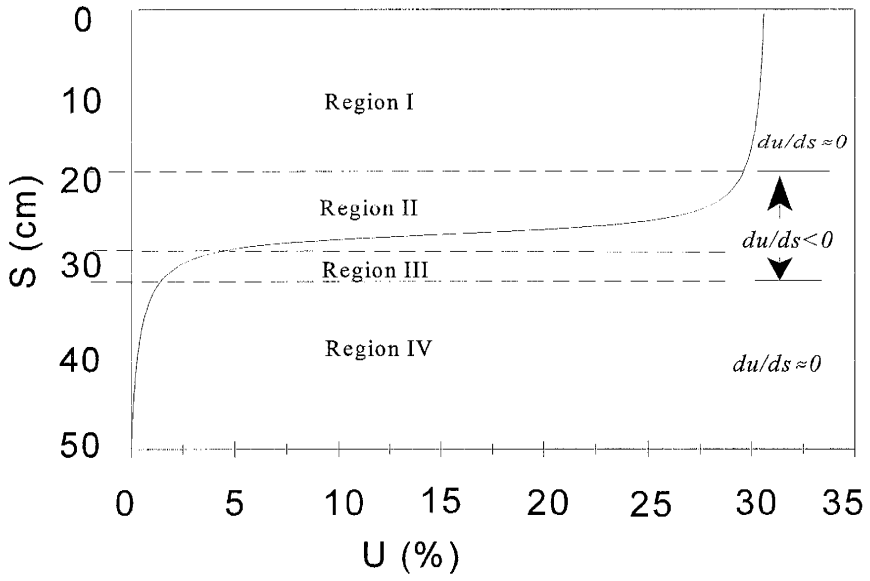

in (39). So, infinite finger diameters are obtained in regions I and IV, and each point is stable in these regions. In regions II and III *du/ds* is less than zero. The negative sign in front of the second term of (36) makes this term always positive ($du/ds<0$, $D'>0$). Thus, we can analyze the stability of regions II and III by comparing the relative magnitudes of K' and V_1. For this purpose, we consider a typical conductivity curve $K(u)$-u (Figure 6.4) where u_c is the inflection point between the convex and the concave portions of the conductivity curve. We pick a point u_1 so that the slope of the line u_1-u_0 is V_1. For any $u_1 < u_c$, we have $K'(u) > V_1$ for u near u_1, and $K'(u) < V_1$ for u near u_0, as shown in Figure 6.4. Thus, in region II the fingers rooting from the region near u_1 with $K'(u) > V_1$, will always satisfy (36) and fingers will remain ahead of the stable wetting front. For fingers rooting from region III with lower water content, $K'(u) < V_1$, equation (36) cannot hold below a certain u value and fingers will be covered by the stable wetting front. The fingers rooting from region II near u_1 exist for a long time, while the fingers rooting from the low water content region III can only exist for short time.

The discussion above demonstrates that region II which is the layer next to the distribution layer (Region I), dominates the instability of the wetting front. Permanent fingers commence from this region. This coincides with the experimental observation that fingers root from the layer next to the distribution layer [*Ritsema et al.*, 1993].

Figure 6.4. Conductivity-Water content curve, where u_c is the inflection point

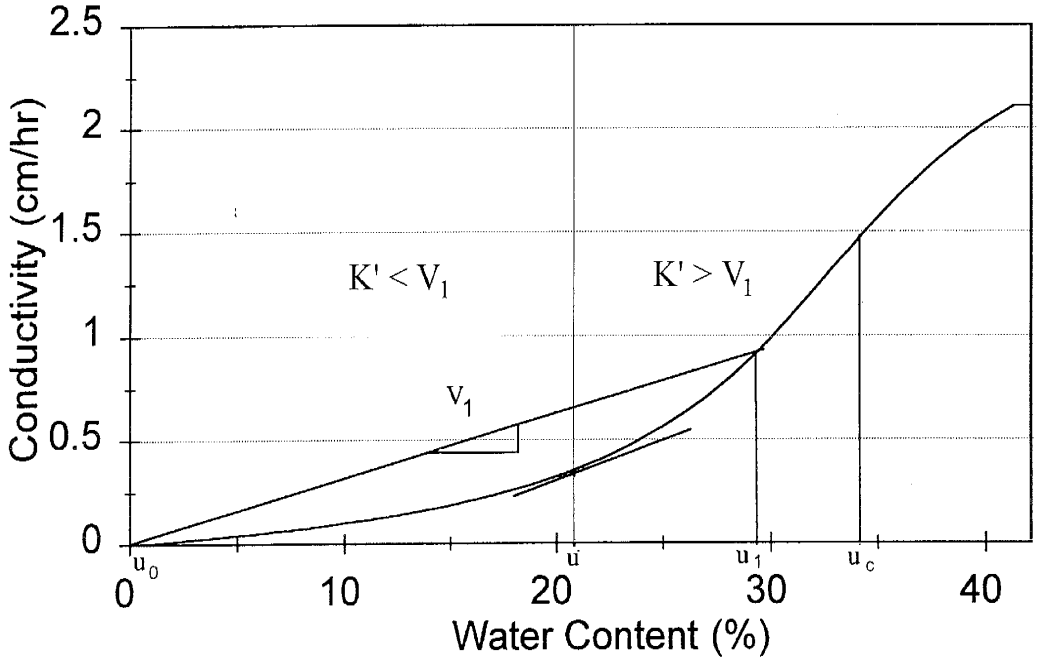

Conclusions

We have conducted a stability analysis of the unsaturated flow equation that applied to all soils, places no restriction on the values of initial soil water content, and covers all infiltration rates. Finger diameter with greatest finger velocity can be predicted at all infiltration rates using actual soil hydraulic properties together with the boundary conditions. In a companion paper [*Yao and Hendrickx*, 1998], we will verify the stability model using experimental data.

References

Chu, B.T., and J.-Y. Parlange, On the stability of laminar flame, *J. Mecan.*, *1*, 2993-312, 1962.

Diment, G.A., and K.K. Watson, Stability analysis of water movement in unsaturated porous materials: 1. Theoretical considerations, *Water Resour. Res.*, *18*, 1248-1254, 1982.

Diment, G.A., and K.K. Watson, Stability analysis of water movement in unsaturated porous materials: 2. Numerical studies, *Water Resour. Res.*, *19*, 1002-1010, 1983.

Du, X.H., T. Yao, and J.M.H. Hendrickx, An analytical solution of the Richards' equation using actual hydraulic soil properties, submitted for publication in *Soil Sci. Soc. Am. J.*, 1998.

Glass, R.J., T.S. Steenhuis, and J.-Y. Parlange, Wetting front instability: 1. Theoretical discussion and dimensional analysis, *Water Resour. Res.*, *25*, 1187-1194, 1989a.

Glass, R.J., T.S. Steenhuis, and J.-Y. Parlange, Wetting front instability: 2. Experimental determination of relationships between system parameters and two-dimensional unstable flow field behavior in initially dry porous media, *Water Resour. Res., 25*, 1195-1207, 1989b.

Glass, R. J., J. King, S. Cann, N. Bailey, J.-Y. Parlange, and T.S. Steenhuis, Wetting front instability in unsaturated porous media: A three-dimensional study, *Transp. Porous Media., 5*, 247-268, 1990.

Glass, R.J., J.-Y. Parlange., and T.S. Steenhuis, Immiscible displacement in porous media: Stability analysis of three-dimensional, axisymmetric disturbances with application to gravity-driven wetting front instability, *Water Resour. Res., 27*, 1947-1956, 1991.

Hendrickx, J.M.H., and L.W. Dekker, Experimental evidence of unstable wetting fronts in non-layered soils, 22-31, In *Proc. Natl. Symp. Preferential Flow*, Chicago, IL. 16-17 Dec. 1991, *Am. Soc. Agric. Eng.*, St. Joseph, MI., 1991.

Hendrickx, J.M.H., and L.W. Dekker., and O.H. Boersma, Unstable wetting fronts in water-repellent soils, *J. Environ. Qual., 22*, 109-118, 1993.

Hendrickx, J.M.H. and T. Yao, Prediction of wetting front stability in dry field soils using soil and precipitation data, *Geoderma, 70*, 265-280, 1996.

Liu, Y., T.S. Steenhuis, and J.-Y. Parlange, Closed-form solution for finger width in sandy soils at different water contents, *Water Resour. Res. 30*, 949-952, 1994.

Liu, Y., J.-Y., Parlange, T.S. Steenhuis, and R. Haverkamp, A soil water hysteresis model for fingered flow data, Water Resour. Res., 31, 2263-2266, 1995.

Nayfeh, A.H., Introduction to perturbation techniques, John Wiley & Sons, New York. pp.

519, 1981.

Parlange, J.-Y., and D.E. Hill, Theoretical analysis of wetting front instability in soils, *Soil Sci., 122*, 236-239, 1976.

Philip, J.R., The theory of infiltration: 4. Sorptivity and algebraic infiltration equations, *Soil Sci. 84*, 257-264, 1957.

Philip, J.R., Theory of infiltration, *Advance. Hydroscience, 5*, 215-296, 1969.

Philip, J.R., On solving the unsaturated flow equation: 1. The flux-concentration relation, *Soil Sci., 116*, 328-335, 1973.

Philip, J.R., Stability analysis of infiltration, *Soil Sci. Soc. Am. Proc., 39*, 1042-1049, 1975a.

Philip, J.R., The growth of disturbances in unstable infiltration flows, *Soil Sci. Soc. Am. Proc. 39*, 1049-1053, 1975b.

Raats, P.A.C., Unstable wetting fronts in uniform and nonuniform soils, *Soil Sci. Soc. Am. Proc. 37*, 681-685, 1973.

Ritsema, C.J., L.W. Dekker, J.M.H. Hendrickx, and W. Hamminga, Preferential flow mechanism in a water-repellent sandy soil, *Water Resour. Res., 29*, 2183-2193, 1993.

Selker, J.S., T.S. Steenhuis, and J.-Y. Parlange, Wetting front instability in homogeneous sandy soils under continuous infiltration, *Soil Sci. Soc. Am. J., 56*, 1346-1350, 1992.

Starr, J.L., H.C. DeRoo, C.R. Frink, and J.Y. Parlange, Leaching characteristics of a layered field soil, *Soil Sci. Soc. Am. J., 42*, 386-391, 1978.

Starr, J.L., J.-Y. Parlange, and C.R. Frink, Water and chloride movement through a layered field soil, *Soil Sci. Soc. Am. J., 50*, 1384-1390, 1986.

Van Dam, J.C., J.M.H., Hendrickx, H.C. van Ommen, M.H. Bannink, M.Th. van Genuchten,

and L.W. Dekker, Simulation of water and solute transport through a water repellent sand soil, *J. of Hydrology, 120*, 139-159, 1990.

Van Ommen, H.C., R. Dijksma, J.M.H. Hendrickx, L.W. Dekker, J. Hulshof, and M. van den Heuvel, Experimental assessment of preferential flow paths in a field soil, *J. of Hydrology, 105*, 253-262, 1989.

Yao, T., and J.M.H. Hendrickx, Stability of wetting fronts in homogeneous soils under low infiltration rates, *Soil Sci. Soc. Am. J., 60*, 20-28, 1996.

Yao, T., and J.M.H. Hendrickx, Stability analysis of the unsaturated water flow equation: 2. Experimental verification, submitted for publication in *Water Resour. Res.*, 1998.

7. Stability Analysis of the Unsaturated Water Flow Equation: 2. Experimental Verification

T. Yao, and J.M.H. Hendrickx

Hydrology Program, Department of Earth & Environmental Sciences,

New Mexico Tech, Socorro, NM 87801

Abstract

In this study, we verify the stability analysis of the unsaturated flow equation presented in part I. We compare finger sizes from laboratory experiments with predictions by the stability model. The model enables us to predict finger sizes from soil hydraulic properties. Using measured unsaturated hydraulic properties fitted and extrapolated over the entire water content range, we arrive at finger size predictions over the full infiltration range. The model predicts an increase of finger diameter at high and low infiltration rates for all soils. Such increases were also observed in our experiments. The model yields reliable predictions of finger diameters at high infiltration and intermediate rates but performs less at infiltration rates less than 1 cm per hour. This is caused by difficulties to precisely measure hydraulic conductivity at low infiltration rates. A sensitivity analysis for initial water content

and the shape parameter of the hydraulic conductivity curve showed that a small change of the parameters resulted in a relatively small change of finger size at high and intermediate infiltration rates but a large one of several orders of magnitude at low infiltration rates. We conclude that the instability model presented in part I of this study can be used for the assessment of wetting front instabilities in all soils over a wide range of infiltration rates.

Introduction

One-dimensional simulation of water infiltration and solute transport through unsaturated soil is frequently used to evaluate groundwater contamination risks associated with the use of agricultural chemicals or the disposal of waste materials. However, it has been found that significant pollution of the groundwater has occurred where these models predicted none. This poses doubt on the usefulness and applicability of one-dimensional water flow and solute transport models. Preferential flow channels have been found to be a common mechanism that can accelerate the transport process. They can be caused by macropores such as soil cracks or old root channels [*Bouma and Dekker*, 1978; *Beven and Germann,* 1982], funnel flow [*Kung*, 1990], water repellent soils [*Hendrickx et al.,* 1993, *Ritsema et al.*, 1993], or by unstable wetting fronts. The occurrence of such fronts is of special importance because they may cause preferential flow paths in homogeneous and layered soils which have neither macropores nor large variability of hydraulic properties. Presently, there is no practical model available that can be used to predict the instability of wetting fronts in field soils. Previous research on the prediction of unstable wetting fronts

is mainly based on delta-function soils with sharp wetting fronts [*Philip,* 1975a, b; *Parlange and Hill*, 1976; *Raats*, 1973] which is of limited practical use. Dimensional and stability analysis [*Glass et al.,* 1989a, 1991] provide an approximate prediction of finger characteristics using saturated soil hydraulic properties. This approach correctly predicts finger sizes at relatively high infiltration rates, e.g. 16-1860 cm/hr [*Glass et al.,* 1989b] and 7.6-60 cm/hr [*Selker et al.,* 1992], but fails at infiltration rates below 1 cm/hr. At these rates unstable flow with small finger sizes is predicted. Yet *Yao and Hendrickx* [1996] observed stable flow with large finger sizes in their laboratory experiments. *Parlange et al.,* [1990] suggested that the formula of *Parlange and Hill* [1976] be applied for these low infiltration rates assuming unsaturated finger tips. The drawback of this formula is that water content and conductivity inside the fingers have to be known for the prediction of finger sizes. These properties can only be obtained through a special laboratory setup. However, *Yao et al.*, [1998] demonstrated that the formula by *Parlange et al.*, [1990] can be used after approximating the water content of unsaturated fingers using data from simple infiltration experiments.

Diment and Watson [1982] conducted a theoretical stability analysis for non-sharp wetting fronts. Their model predicts stable flow for all the numerical cases they studied with 0.05 cm^3/cm^3 initial water content [*Diment and Watson*, 1983]. In contrast, their experimental results [*Diment and Watson*, 1985] showed great instability for initially dry soils with water content less than 0.001 cm^3/cm^3 and less instability for initial soil water content of 0.01-0.02 cm^3/cm^3 , but their model was unable to handle these conditions. They

concluded that a small amount of initial soil water content could significantly dampen instabilities. *Liu et al.,* [1994b] using the formula of *Parlange et al.,* [1990] with a simplified closed-form solution predicted increased finger widths from 2.5 to 6 cm when initial soil water content increased from zero to 0.05 cm^3/cm^3. They verified this prediction with two-dimensional experiments using a point source as water supply with a rate of 10 cm^3/min (133-173 cm/hr).

In order to best describe the wetting process of an initial dry soil, the initial wetting curve must be used since infiltration of water into dry soil is uniquely associated with initial wetting. *Liu et al.,* [1994b] demonstrated that an initial wetting curve is needed to study infiltration under these conditions. *Nieber* [1996] used a numerical scheme for the simulation of unstable wetting fronts using the initial wetting curve and determined finger sizes close to experimental observations. *Liu et al.,* [1994b] used the initial wetting curve to calculate finger sizes with a simplified close-form equation. *Dekker and Ritsema* [1996] observed that most soil water retention curves only describe the drying process and can, therefore, not be used to study infiltration into dry soils. In arid and semi-arid areas, this is of special importance because soils are mostly dry. They recommend that the initial wetting curve should be measured for the study of wetting front instability.

Although finger characteristics and phenomena have been widely studied with analytical and numerical models, there is still a great need for a truly predictive model that can handle gradual wetting fronts and covers a wide range of infiltration rates in all soils at

different initial water contents. In paper I of this study, we presented a perturbation analysis for non-sharp wetting fronts that can be applied to any soil and covers all infiltration rates. The objective of this paper is to compare experimental results with finger characteristics calculated with this model and to evaluate its applicability in different soils. In addition, we will use this model to investigate the influences of soil hydraulic properties and initial soil water content on finger sizes.

Materials And Methods

Experiments were conducted in the laboratory in 30 cm diameter and 1 m diameter lysimeters with heights from 50 to 75 cm. To fill the lysimeters, four different grades of perlite sand and quartz sand were used: U.S. mesh size No. 14-20 (1.41-.841mm), 20-30 (.841-.594mm), 30-40 (.594-.42mm), and 40-60 (.42-.25mm). The lysimeters were exposed to infiltration rates varying from 0.068 to 27 cm/hr; the total amounts of applied water varied from 2.5 to 8 cm. The sand was packed into the lysimeter through a randomizer to avoid structures. The soil surface was then smoothed and water was applied via a sprinkler system. After water application, the lysimeters were excavated layer by layer to visually inspect the flow pattern. For more details of our methods, we refer to *Yao and Hendrickx* [1996].

Initial Water Content

Most of our experiments have been conducted in air-dried soils. Water content in these air-dried soils has a mean of 0.003 cm^3/cm^3 of water content. The results of these experiments have been reported by *Yao and Hendrickx* [1996]. We also did experiments with higher initial water contents. For these experiments, the lysimeter was packed the same way using 20-30 sand. The lysimeter was saturated in a big drum for 10 minutes and then drained for 7 days. The top 10 cm were removed just before the start of the infiltration experiment because it had dried out more than the soil below. Water content at different depths were measured in a second reference column. Mean soil water content was 0.092 cm^3/cm^3 with standard deviation 0.02. Experiments were conducted by applying water with FD&C Blue dye at a rate of 8 cm/hr with a total application of 4 cm.

Determination of Soil Physical Characteristics

Water retention curves including initial wetting, drying, and wetting scanning curves, have been measured using the hanging water column technique on 100 cm^3 dry samples that were taken from the lysimeters. The saturated hydraulic conductivity was measured with the constant head method. The instantaneous profile method [*Watson*, 1966] was used to measure the unsaturated hydraulic conductivities in the lysimeters. The data were fitted with the RETC program of *van Genuchten et al.,* [1991] to the following soil water retention model

$$S_e = \frac{1}{(1+|\alpha h|^n)^m}$$

and unsaturated hydraulic conductivity model

$$K(S_e) = K_{sat}\, S_e^{\lambda}[1-(1-S_e^{1/m})^m)^2 \qquad (2)$$

where h is soil water pressure, K_{sat} is the saturated hydraulic conductivity, and $S_e = (\theta-\theta_r)/(\theta_s-\theta_r)$ (θ is the soil water content, θ_r is the residual water content, and θ_s is the saturated water content). Parameters α, n, m, are curve fitting parameters [*van Genuchten*, 1980] and λ is the connectivity parameter from Mualem's conductivity model (1975). The fitted model serves two purposes: 1. To simplify the input for simulation; 2. To extend the soil hydraulic properties to full water content range by extrapolation.

Implementation of Stability Analysis

The following step-by-step approach is used for the numerical implementation of the stability analysis presented in part I [*Du et al.*, 1998]. The US mesh 14-20 quartz sand is used to give an example for this approach.

Step 1. The range of relevant infiltration rates is determined by the hydraulic conductivities at the maximum and minimum water contents of interest. We divide equally the full water content range to small intervals and find their corresponding infiltration rates. In our example, we use 500 increments for the full water content range between 0.001 to 0.38

cm^3/cm^3.

Step 2. Assuming unit hydraulic gradient at the soil surface we obtain the infiltration rate i from

$$i = K(u_1) \tag{3}$$

where $K(u_1)$ is the unsaturated hydraulic conductivity at water content u_1. The hydraulic conductivity function is determined using the *van Genuchten* model. Parameters in table 7.1 were used to represent the hydraulic properties for the 14-20 quartz sand. The diffusivity function is obtained by multiplication of the conductivity function with the slope of water retention curve ($dh/d\theta$) at each water content. For example, at $u_1 = 0.3$ the conductivity and infiltration rate at unit gradient are 266 cm/hr in the 14-20 quartz sand. At this water content, the slope of water retention curve is 20.44 so the diffusivity ($D(u_1)$) becomes 5437 cm^2/hour.

Step 3. Given an initial water content u_0 and a particular water content u_1 from step 2, calculate the downward velocity of the stable wetting front V_1 as Equation 6 in *Du et al.* [1997]

$$V_1 = \frac{K(u_1) - K(u_0)}{u_1 - u_0} \tag{4}$$

where $K(u_1)$ and $K(u_0)$ are the hydraulic conductivities at water content u_1 and u_0,

Table 7.1. van Genuchten parameters of the laboratory quartz sands for the initial wetting and wetting scanning curves

Sand (US Mesh)	θr (cm^3/cm^3)	θ_s^* (cm^3/cm^3)	k_s (cm/s)	α cm^{-1}	n -	λ -	ψ_{we} cm
14-20†	.001	.38	.28	.178	3.5	1.22	3
14-20‡	.09	.38	.28	.12	5.95	-1.626	-
20-30†	.001	.42	.20	.156	2.883	.828	5
30-40†	.001	.40	.13	.09	3.46	.61	8.5
40-60†	.001	.38	.05	.0585	5.416	.1375	11

* Field saturation based on instantaneous profile experiments

† Initial wetting curve

‡ Wetting scanning curve

respectively. An initial water content of 0.001 cm^3/cm^3 results in an unsaturated conductivity of $2.1*10^{-12}$ cm/hr. For water content u_1 = 0.3 in step 2, $K(u_1)$ is 266 cm/hr and V_1 is calculated as 892 cm/hr.

$$V_f(u_p) = K'(u_p) - 2D'(u_p)\frac{du}{ds}\Big|_{s=s_p} \tag{5}$$

Step 4. The downward velocity of a finger, $V_f(u_p)$, at a point p on the wetting front with water content u_p can be calculated as Equation (35) in *Du et al.* [1998]: $K'(u_p)$ and $D'(u_p)$ functions are obtained by analytically taking derivatives of the soil hydraulic conductivity (Equation 2) and diffusivity ($D=K*dh/d\theta$) functions with respect to θ and to calculate their values numerically. The du/ds function is obtained using Equation (8) in *Du et al.* [1998].

$$\frac{du}{ds} = \frac{[K(u) - K(u_0)] - V_1(u - u_0)}{D(u)} \tag{6}$$

where $D(u)$ is the diffusivity at water content u. Finger velocities are calculated for all water contents, u_p, between u_0 and u_1. Our experience shows that water content increments of 1/5000 of the whole interval yield good results. Figure 7.1 shows the velocity distribution versus water content under the infiltration rate of 266 cm/hr. Fingers commence at the water content where the maximum finger velocity occurs as explained in the next step.

Step 5. Determine the water content u^* where $V_f(u_p) = V_f(u^*)$ is maximum. The maximum velocity $V_f(u^*)$ can be found using (5) by applying u values incrementally. For the 14-20

Figure 7.1. Finger velocity distribution at the wetting front

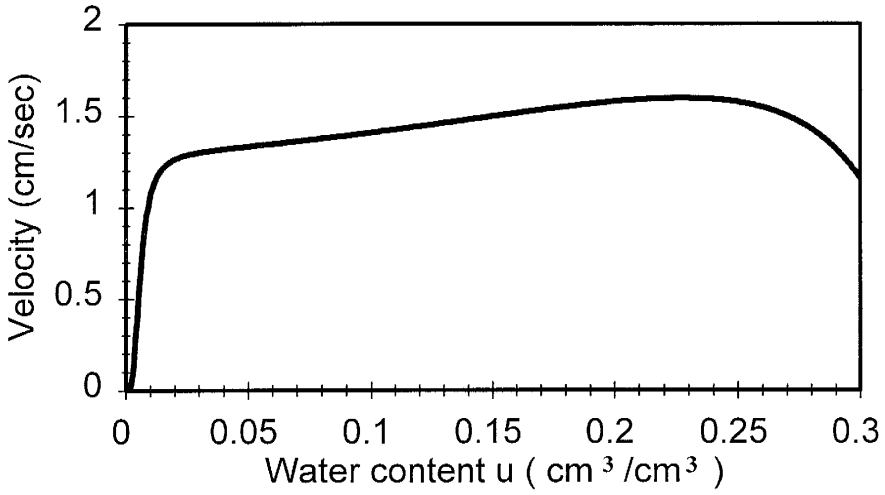

quartz sand, we find a maximum finger velocity at u* ≈ 0.227 as shown in figure 7.1.

Step 6. Compare the maximum velocity $V_f(u^*)$ found in step 5 with the stable wetting front velocity V_1 found in step 2. If $V_f(u^*)$ is greater than V_1, the wetting front is unstable and we calculate the minimum finger diameter D_c as Equation (39) in *Du et al.* [1998].

$$D_c(u^*) = \pi \cdot \sqrt{\frac{D(u^*)}{B(u^*)}} \tag{7}$$

where

$$B(u^*) = D''(u^*)\left(\frac{du}{ds}\Big|_{u=u^*}\right)^2 + D'(u^*)\frac{d^2u}{ds^2}\Big|_{u=u^*} - K''(u^*)\frac{du}{ds}\Big|_{u=u^*} \tag{8}$$

The $K''(u^*)$ and $D''(u^*)$ functions are obtained by analytically taking second derivatives of the soil hydraulic conductivity and diffusivity functions with respect to θ and to calculate their values numerically. The d^2u/ds^2 function can be obtained by taking the derivative of (6) with respect to s. For the 14-20 sand, at u*= 0.227 where the maximum velocity was observed, $K''(u^*)$, $D(u^*)$, $D'(u^*)$ and $D''(u^*)$ were calculated as 6.282 cm/sec, 0.418 cm^2/sec, 7.155 cm^2/sec and 117.5 cm^2/sec, respectively. The values of du/ds and d^2u/ds^2 at u^* were calculated as -0.083 cm^{-1} and -0.15 cm^{-2} , and finally $B(u^*)$ = 0.261 cm/sec was obtained. Using (7), $D_c(u^*)$= 4 cm was calculated. If $V_f(u^*)$ is less than V_1, the wetting front is stable

for this boundary condition and we will go to next infiltration rate, i.e. we go back to step 2.

Step 7. Go to the next value of the infiltration rate *i*, repeat steps 2 to 6. After completing the full range of infiltration rates, obtain the relationship between the infiltration rates and the minimum finger diameters from the fingers with the highest downward velocity. Figure 7.2 shows the results for 14-20 sand.

Finger Size Predictions Using Actual Soil Hydraulic Properties

Hydraulic properties of the laboratory quartz sands (Table 7.1) were used to implement the stability analysis. We did not include the hydraulic properties from perlite sands in this study because measurements by *Yao and Hendrickx* [1996] have shown that the hydraulic properties of perlite and quartz sands are similar. We examined in which manner wetting front stability and finger sizes are influenced by the grain size of the porous media, initial water content, unsaturated hydraulic conductivities, and water retention properties.

To test for the effect of grain size, we used the four different laboratory sands at an initial water content of 0.003 cm^3/cm^3. To test the influence of initial water content, we used the 14-20 sand with initial water contents of 0.001, 0.05, and 0.1 cm^3/cm^3. For the case with 0.1 cm^3/cm^3 of initial water content, the wetting scanning curve was used (Table 7.1). We also tested the sensitivity of parameter λ in the hydraulic conductivity model [*Mualem,* 1976; *van Genuchten*, 1980] presented in equation (2) on finger sizes. For the 14-20 sand,

Figure 7.2. Finger sizes from prediction and experiment for initial dry sand (water content 0.003 cm^3/cm^3)

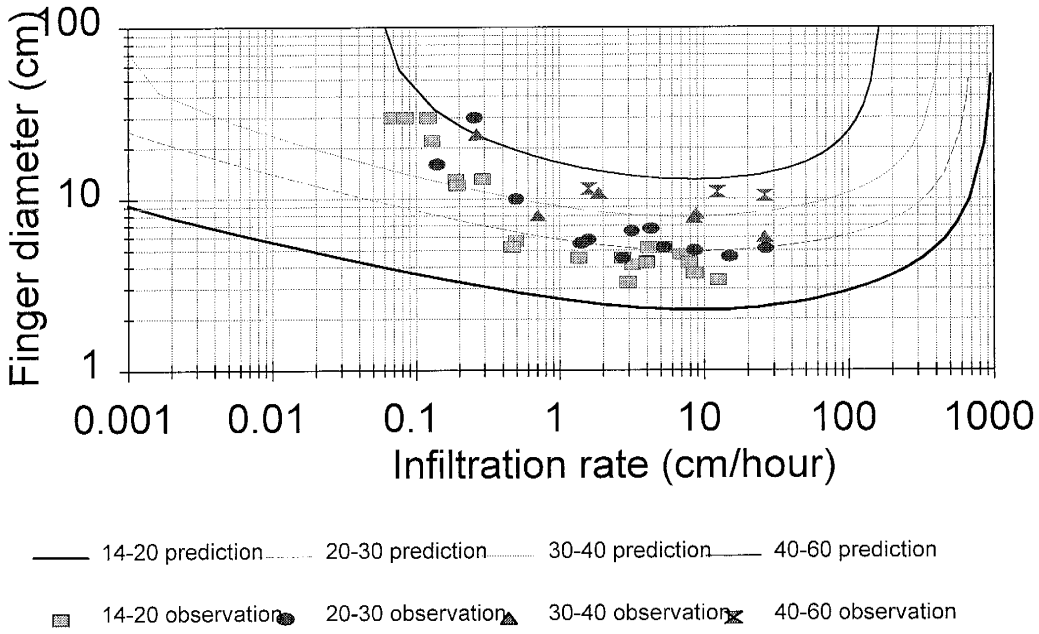

different λ values were used for the simulation. Finally, we compare the results simulated by the stability model of this study to the predictions from previous models by *Liu et al.,* [1994b].

Results and Discussion

Effect of Grain Size on Instability

Figure 7.2 shows the predicted and observed relationships between infiltration rate and finger diameter in our four laboratory soils with an initial soil water content of 0.003 cm^3/cm^3. The experimental data have been previously discussed by *Yao and Hendrickx* [1996] and *Hendrickx and Yao* [1996]. They demonstrated that finger diameters become larger and wetting fronts become more stable when the soil texture becomes finer and the infiltration rate becomes smaller. Other researchers [e. g. *Glass et al.*, 1989a,b] have found that wetting fronts also become stable at infiltration rates approaching the saturated hydraulic conductivity of the soil. The stability model by *Du et al.*, [1998] captures these experimentally observed features very well. When the infiltration rate falls below approximately 0.5 cm/hr or when the infiltration rate approaches the saturated hydraulic conductivity of the soil, finger diameters become larger. They also increase when soil texture becomes finer. For the three coarsest soils, the model predicts reasonably well below what infiltration rate wetting front commence to stabilize. The model predicts stabilization to start at rates less than about 1 to 2 cm/hr and the experimental data confirm this in the 14-20, 20-

30, and 30-40 sands. The model also yields good predictions of the smallest finger sizes that have been observed in the experiments. In the 14-20 sand the model predicts 2.2 cm while the mean observed finger diameter during an experiment using an infiltration rate of 3 cm/hr was 3 cm. The other three sands also have an almost perfect match between smallest predicted and observed mean finger diameters. In 20-30 sand, 5 cm predicted minimum finger diameter matches a mean observed finger diameter of 5 cm; in 30-40 sand, it is 8 cm predicted versus 7.8 cm observed; in 40-60 sand, it is 12 cm predicted versus 11 cm observed. We also compared the observations of *Glass et al.* [1990] and *Selker et al.* [1992] with our predictions. *Glass et al.* [1990] observed finger diameters of 1.9 cm with water applied at the rate of 29.7 cm/hr. Our prediction is 2.2 cm. *Selker et al.* [1992] observed finger diameters of 1.8 cm with water applied at 7.6 cm/hr cm while our prediction is 1.9 cm. All predicted minimum diameters are close to the observed mean finger diameters measured in our and other experiments. The only feature that the model does not predict correctly is the rate at which wetting fronts become stable at low infiltration rates. The experimental data in our sand soils show wetting fronts to be stable at infiltration rates of 0.1 cm/hr while the model predicts total stability at rates that are two orders of magnitude smaller. This issue will be explored in the next two sections.

Effect of Initial Water Content

Figures 7.3 and 7.4 show that the initial water content plays an important role for the instability of wetting fronts. Only a slight change of the initial soil wetness will change the

Figure 7.3. Predicted finger sizes for 14-20 sand with series of initial water contents

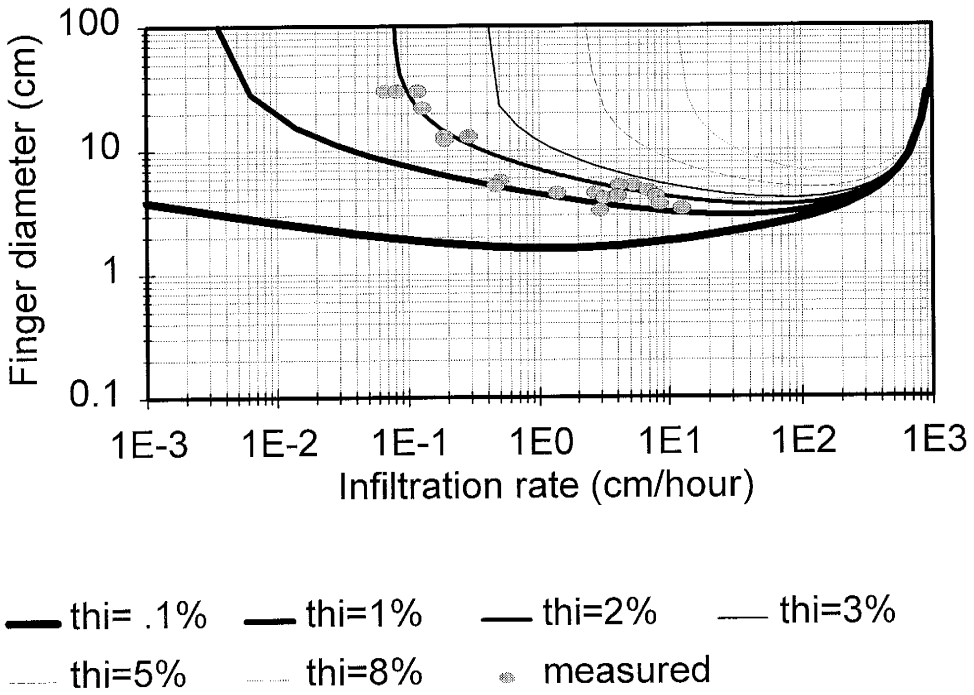

finger size greatly at the same infiltration rates, especially at the drier range. In the 14-20 sand, model predictions with an initial water content of 0.02 cm^3/cm^3 yield an almost perfect match with the data. Figure 7.4 shows that an soil water content increase from 0.001 to 0.05 cm^3/cm^3 cause the finger size to increase from 1.9 to 25 cm at an infiltration rate at 3 cm/hr. We conducted laboratory experiments with an initial soil water content of approximately 0.092 cm^3/cm^3 at a water application rate of 8 cm/hr and found stable wetting for the 14-20 sand in our 30 cm diameter lysimeter. We simulate this experiment using the wetting scanning curve (Table 7.1) and 0.1 cm^3/cm^3 of initial water content. The prediction (Figure 7.4) shows that the smallest finger size is greater than 250 cm at a abnormal high infiltration rate of 500 cm/hr. For all practical purposes this means that the wetting front is stable.

Liu et al., [1994a] observed increases of finger diameter from a dry topsoil to a wet subsoil. Their sand has similar properties as our 14-20 sand. Figure 7.4 shows that our model predicts a 3 cm finger size with a water application rate of 122 cm/hr for initial dry soil and a finger size of 6.5 cm for a water application rate of 20 cm/hr with an initial soil water content at 0.05 cm^3/cm^3. *Liu et al.,* [1994a] observed finger sizes of 2.5 and 6 cm for the same infiltration rates and initial water content. Clearly, our model predicts quite well the effect of initial water content on finger size.

Figure 7.4. Predicted finger sizes for 20-30 sand with 0.001 , 0.05, and 0.1 cm^3/cm^3 of initial water contents.

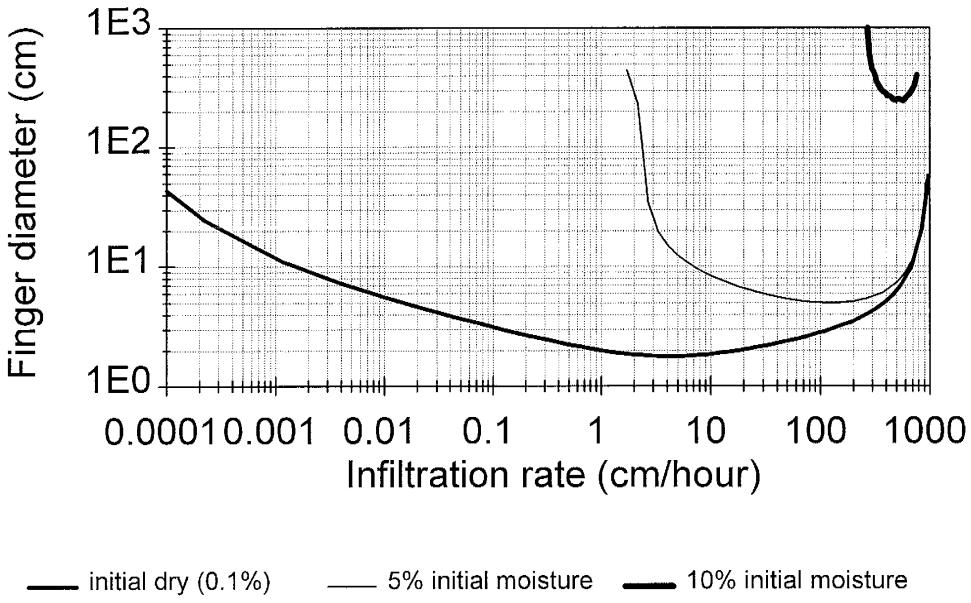

Effect of Unsaturated Hydraulic Conductivity

Figure 7.2 shows the inconsistency of predicted finger sizes with the observed data after the point where stabilization commences under low infiltration regimes. One possible cause for the mismatch may be errors during the determination of initial water content as has been discussed in the previous section. Another one may be errors in the determination of the unsaturated hydraulic conductivity curve at low water contents. In this study, conductivities measured in a relatively wet soil have been used for extrapolation to drier conditions using van Genuchten functions with the Mualem conductivity model. The 14-20 sand is used to discuss the effect of this procedure on the finger sizes calculated with our model. Figure 7.5 shows that the selected conductivity model cannot completely fit the experimental data. Most λ values from 0 to 1.97 fit the data reasonably well from 0.38 to 0.15 cm^3/cm^3 of water content, but quite poorly at lower water contents. Because we preferred to use repeatable procedures for our model testing, the hydraulic parameters resulting from the original curve fitting with the RETC program (Table 7.1) have been used for finger predictions in Figures 7.2, 7.3, and 7.4. The λ parameter valued 1.22. However, the hydraulic properties at low water contents can not be obtained with our instantaneous profile method. To improve the fit of the conductivity curve at the drier range, λ values of the coarse sand were adjusted. Figure 7.6 demonstrates the sensitivity of finger size prediction to λ. A decrease in λ from 1.22 to 0.2-0.3 results in a better prediction of finger sizes at low infiltration rates. Prediction of dry range hydraulic conductivity from wet range data was studied by Khaleel et al. [1995]. They observed an overestimation of unsaturated

hydraulic conductivities by an order of 1 to 2 at low water content range for the coarse sands they studied. From figure 7.5, we can observe that an increase of 1 or 2 orders of magnitude in hydraulic conductivity for water contents below 0.1 cm^3/cm^3 is achieved by changing the λ value from 1.22 to 0.2-0.3. This change, however, will influence the unsaturated hydraulic conductivities at the wet range less than in the dry range (Figure 7.5). This is the reason why the value of parameter λ causes such a significant change of instability in the dry range (low infiltration rate) but not in the wet range.

Since finger size predictions at low infiltration rates are so sensitive for both initial water content and the connectivity parameter λ, we used trial-and-error to find which values of these parameters would result in a perfect fit for the 14-20 sand. Figure 7.7 shows that different combinations of reasonable values result in "perfect fits". This is evidence that the mismatch between predicted and observed finger sizes in figure 7.2 is due to uncertainties of the hydraulic properties at low water contents and not to a flaw of our model.

Figure 7.5. 14-20 sand unsaturated hydraulic conductivity curve with various connectivity parameters (λ).

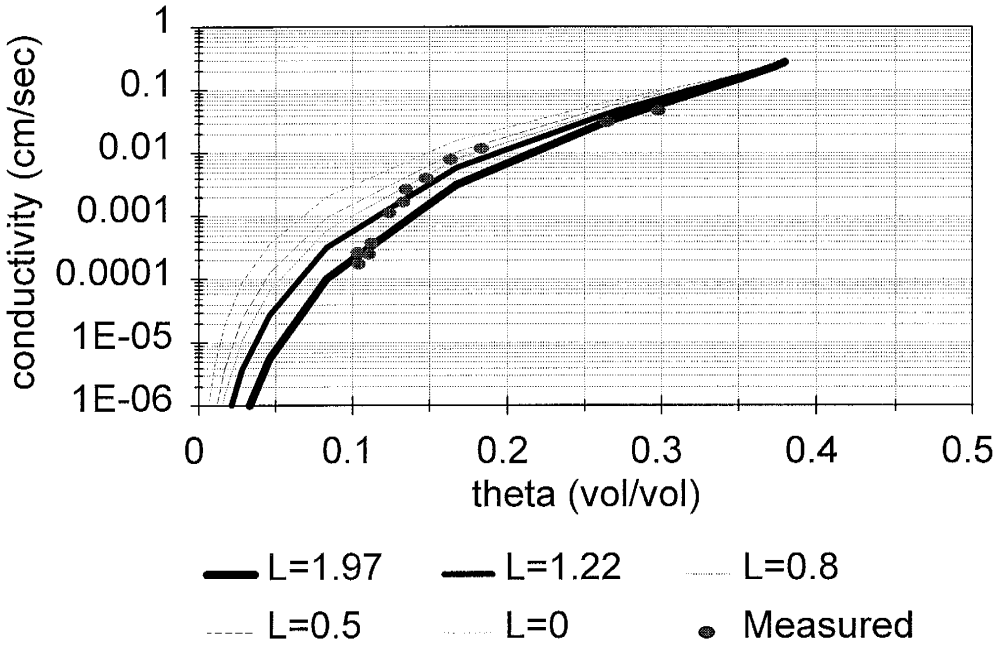

Figure 7.6. Predicted finger sizes for 14-20 sand with series of connectivity parameters (λ). Initial water content is 0.003 cm^3/cm^3 for all simulations

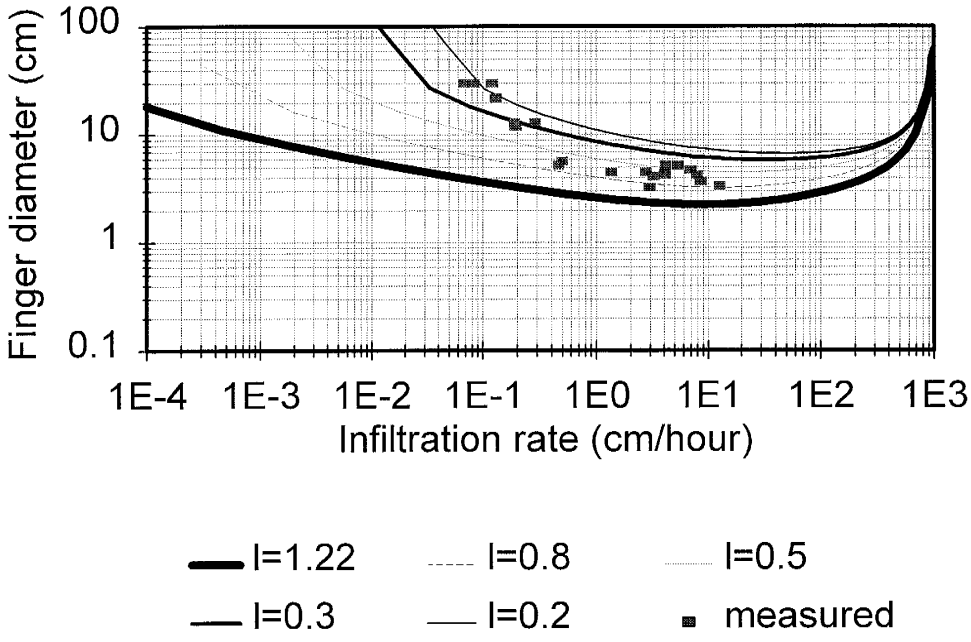

Figure 7.7. Best fits of experimental data with predictions of 14-20 sand

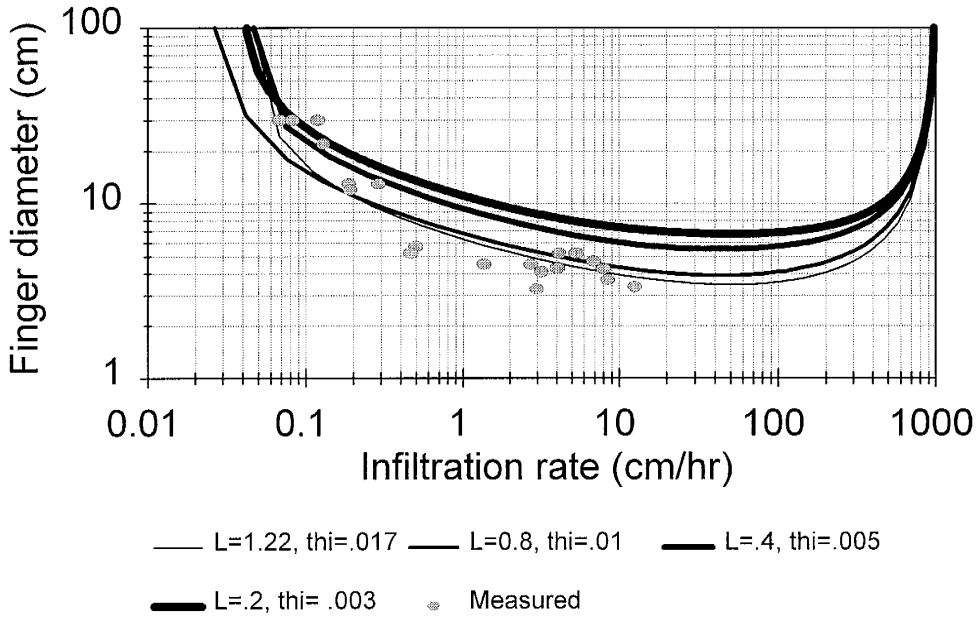

Conclusions

In this paper we have conducted an experimental verification of the wetting front stability model presented in Part I of this study by *Du et al.,* [1998] using experimental data of *Yao and Hendrickx* [1996]. The model performs well in a qualitative and quantitative fashion. Using measured soil hydraulic properties, the model correctly predicts the behavior of unstable wetting fronts under a wide range of infiltration rates and initial water contents. The model yields predictions of minimum finger diameters in sand soils that match observed ones. A sensitivity analysis demonstrated that the behavior of unstable fronts at infiltration rates below 1 cm/hr is quite sensitive for small changes in initial soil water content and the shape of the unsaturated hydraulic conductivity at low water contents (0.001-0.1 cm^3/cm^3). Our experimental verification has demonstrated that the model by *Du et al.,* [1998] is a powerful tool for the assessment of wetting front instability in homogeneous soils under a wide range of infiltration rates and initial water contents.

References

Diment, G.A., and K.K. Watson, Stability analysis of water movement in unsaturated porous materials: 2. Numerical studies, Water Resour. Res., 19, 1002-1010, 1983.

Diment, G.A., and K.K. Watson, Stability analysis of water movement in unsaturated porous materials: 3. Experimental studies, Water Resour. Res., 21, 979-984, 1985.

Diment, G.A., K.K. Watson, and P. J. Blennerhassett, Stability analysis of water movement in unsaturated porous materials: 1. Theoretical considerations, Water Resour. Res., 18, 1248-1254, 1982.

Du, X.H., T. Yao, W.D., Stone, and J.M.H., Hendrickx, An analytical solution of the Richards' equation using actual hydraulic soil properties, Submitted for publication in Soil Sci. Soc. Am. J., 1997.

Du, X.H., T. Yao, W.D., Stone, and J.M.H., Hendrickx, Stability analysis of the unsaturated water flow equation: 1. Mathematical derivation, Submitted for publication in Water Resour. Res., 1998.

Glass, R.J., J. King, S. Cann, N. Bailey, J.-Y. Parlange, and T.S. Steenhuis, Wetting front instability in unsaturated porous media: A three-dimensional study, Transp. Porous Media., 5, 247-268, 1990.

Glass, R.J., J.-Y. Parlange., and T.S. Steenhuis, Immiscible displacement in porous media: Stability analysis of three-dimensional, axisymmetric disturbances with application to gravity-driven wetting front instability, Water Resour. Res., 27, 1947-1956, 1991.

Glass, R.J., T.S. Steenhuis, and J.-Y. Parlange, Wetting front instability: 1. Theoretical discussion and dimensional analysis, Water Resour. Res., 25, 1187-1194, 1989a.

Glass, R.J., T.S. Steenhuis, and J.-Y. Parlange, Wetting front instability: 2. Experimental determination of relationships between system parameters and two-dimensional unstable flow field behavior in initially dry porous media, Water Resour. Res., 25, 1195-1207, 1989b.

Hendrickx, J.M.H. and T. Yao, Prediction of wetting front stability in dry field soils using soil and precipitation data, Geoderma, 70, 265-280, 1996.

Hendrickx, J.M.H., L.W. Dekker, and O.H. Boersma, Unstable wetting fronts in water repellent field soils, J. of Environmental Quality, 22, 109-118, 1993.

Hill, S., Channeling in packed columns, Chem. Eng. Sci., 1, 247-253, 1952.

Khaleel, R; J.F., Relyea, and J.L., Conca, Evaluation of van Genuchten-Mualem relationships to estimate unsaturated hydraulic conductivity at low water contents, Water Resour. Res., 31, 2659-2668, 1995.

Liu, Y., T.S. Steenhuis, and J.-Y. Parlange, Formation and persistence of fingered flow fields in coarse grained soils under different moisture contents, J. Hydrology, 159, 187-195, 1994a.

Liu, Y., T.S. Steenhuis, and J.-Y. Parlange, Closed-form solution for finger width in sandy soils at different water contents, Water Resour. Res., 30, 949-952, 1994b.

Nieber, J.L., Modeling finger development and persistence in initially dry porous media, Geoderma, 70, 207-229, 1996.

Parlange, J.-Y., and D.E. Hill, Theoretical analysis of wetting front instability in soils, Soil

Sci., 122, 236-239, 1976.

Philip, J.R., Stability analysis of infiltration, Soil Sci. Soc. Am. Proc, 39, 1042-1049, 1975a.

Philip, J.R., The growth of disturbances in unstable infiltration flows, Soil Sci. Soc. Am. Proc., 39, 1049-1053, 1975b.

Raats, P.A.C., Unstable wetting fronts in uniform and nonuniform soils, Soil Sci. Soc. Am. Proc., 37, 681-685, 1973.

Ritsema, C.J., L.W., Dekker, J.M.H., Hendrickx, and W., Haminga, Preferential flow mechanism in a water repellent sandy soils, Water Resour. Res., 29, 2183-2193, 1993.

Selker, J.S., T.S. Steenhuis, and J.-Y. Parlange, Wetting front instability in homogeneous sandy soils under continuous infiltration, Soil Sci. Soc. Am. J., 56, 1346-1350, 1992.

Van Genuchten, M.Th., A closed-form equation for predicting the hydraulic conductivity of unsaturated soils, Soil Sci. Soc. Am. J., 44, 892-898, 1980.

Van Genuchten, M.Th., F.J. Leij, and S.R. Yates, The RETC code for quantifying the hydraulic functions of unsaturated soils, U.S. Salinity Laboratory, U. S. Department of Agriculture, Agricultural Research Service, Riverside, CA, 1991.

Watson, K.K., An instantaneous profile method for determining the hydraulic conductivity of unsaturated porous materials, Water. Resour. Res., 2, 709-715, 1966.

Yao, T., J.M.H., Hendrickx, Stability of wetting fronts in homogeneous soils under low infiltration rates, Soil Sci. Soc. Am. J., 60, 20-28, 1996.

8. Prediction of Wetting Front Stability in Dune Sands of New Mexico and The Netherlands Using Mathematical and Empirical Approaches

Tzung-mow Yao, and Jan M.H. Hendrickx

Hydrology Program, Department of Earth and Environmental Sciences,

New Mexico Tech, Socorro, NM, 87801

Abstract

Wetting front stability in field soils is an important factor in assessment of the vulnerability of ground water aquifers for contamination. In this study we predict wetting front instability in two field soils using mathematical and empirical models. We used two natural dune sands as our experimental material, one from New Mexico and the other one from Netherlands. The mathematical model predicts small fingers in the Dutch dune sand but large ones in the New Mexico dune sand. The empirical model predicts that instabilities frequently occur in the Dutch dune sand but not in New Mexico. In contrast, previous theories predicted small fingers to occur for both cases under natural precipitation rates. Field

observations and laboratory experiments support the predictions from our mathematical and empirical models. Fingers frequently have been found in the Dutch dune sands but rarely in New Mexico dune sands.

Introduction

The assessment of the vulnerability of ground water aquifers for contamination using one-dimensional simulation has great uncertainty because of preferential flow. Contaminants have been detected unexpectedly in various groundwater aquifers where one-dimensional models predict none. The deviation between model predictions and the observations can at least partly be attributed to the existence of preferential flow paths. Preferential flow can occur under various conditions; it can be caused by macropores such as soil cracks or old root channels (Bouma and Dekker 1978; Beven and Germann, 1982), funnel flow (Kung, 1990), water repellency of soils (Hendrickx et al., 1993), air pressure increases at the wetting front (White et al., 1976), layered soils with fine texture overlaying coarse texture (Hill and Parlange, 1972, Hillel and Baker, 1988). Even in homogeneous soils wetting front instability can occur under unsaturated fluxes (Selker et al., 1992c; Yao and Hendrickx, 1996). The occurrence of unstable fronts is of special importance because they may cause preferential flow paths in homogeneous and layered soils which have neither macropores nor large variability of hydraulic properties. Since contaminant movement is to a large extent determined by the flow mechanism of water, consideration of the stability of wetting fronts should become standard for all infiltration studies. Hillel (1987) reviews unstable flow in

layered soils and states that "Wetting front instability can invalidate our best-laid theories of vertical infiltration and groundwater recharge... At the very last, the loss of our predictive power means that we cannot manage our system with the necessary degree of security".

Although many studies provide insight into the mechanism of unstable flow (e.g. Glass et al. 1989a,b,c, 1991; Liu et al. 1994a,b; Parlange and Hill 1976; Philip 1957a,b; Raats 1973; Selker et al. 1992a,b,c), few provide guidelines for the prediction of unstable wetting in field soils. In this paper, we will discuss a mathematical approach (Du et al., 1998a) and an empirical one (Hendrickx and Yao, 1996) for wetting front stability prediction. The mathematical approach was developed through an instability analysis of the Richards' equation and predicts the stability of the wetting front using soil hydraulic properties and infiltration rate. The empirical approach uses a time criterion to determine when gravity forces become dominant over the capillary forces. Instability may occur when gravity is the dominating force. This simple criterion helps to explain many field observations and enables to assess the risk for occurrence of unstable wetting. The purpose of this paper is to compare the predictions from the mathematical approach and empirical approach with field observations and experimental results in dune sands from New Mexico and the Netherlands.

Theory

Three infiltration rates are distinguished in analyzing the effect of flow rate on the stability of wetting fronts, namely: high, intermediate, and low. High infiltration rates exceed or are similar to the saturated hydraulic conductivity of the soil while intermediate rates are between the saturated hydraulic conductivity and the rate of a gentle rainstorm. At low infiltration rates capillary forces dominate over gravity forces during the infiltration process and the wetting front remains stable (Yao and Hendrickx 1996). At high infiltration rates wetting fronts also are stable (Glass et al. 1989b; Rice et al. 1991). At intermediate infiltration rates unstable wetting is frequently observed in sandy soils (Dekker and Ritsema 1994; Glass et al. 1989b; Hendrickx and Dekker 1991; Hendrickx et al. 1988a, b, 1993; Selker et al. 1992; Yao and Hendrickx 1996).

Mathematical Approach

Du et al. (1998a) presented a one-dimensional analytical solution of the Richards' equation and used this solution to derive a general stability analysis of the Richards' equation (Du et al., 1998b) and a new expression for calculation of the finger diameter. For a particular infiltration rate, the finger diameter for the fastest moving finger can be calculated as:

$$d = \pi \sqrt{\frac{D(\theta_1^*)}{B(\theta_1^*)}} \qquad (1)$$

where $D(\theta)$ is the diffusivity, θ_1^* is a water content where finger has the greatest velocity, and $B(\theta)$ *is* a function with the property $B(\theta) \to 0$ as $\theta \to \theta_o$ or $\theta \to \theta_s$, where θ_o is the initial water content and θ_s is the saturated water content. The function $B(\theta_1^*)$ and parameter θ_1^* are determined by Du et al., (1998b). At high and low infiltration rates, $B(\theta_1^*)$ approaches to zero. Consequently, Eq. [1] predicts that d becomes very large, i.e. the wetting front becomes stable. Input data for the instability model are: unsaturated hydraulic properties of the soil, initial water content and the infiltration rate. The model output is the relationship between finger diameter and infiltration rates for a given set of input data. Small finger diameters indicate unstable wetting while large ones indicate stable wetting.

Empirical Approach

Hendrickx and Yao (1996) present an empirical approach for the prediction of wetting front stability in dry field soils. They consider that in the early stages of infiltration capillary forces dominate, whereas at later times gravity becomes the dominant driving force for flow. Because unstable wetting is a gravity-driven phenomenon (Raats 1973; Parlange & Hill 1976; Philip 1975a, b) , it was hypothesized that no instabilities will occur during the initial stages of the infiltration process when capillary forces are dominant. For the determination of the time during which capillarity controls the infiltration process, Hendrickx

and Yao (1996) used the gravitational characteristic time, t_{grav}, introduced by Philip (1969):

$$t_{grav} = \left(\frac{S(h)}{K_i(h) - K_o(h_o)} \right)^2 \qquad \textbf{(2)}$$

where $S(h)$ is the sorptivity of the soil at supply water pressure h, $K_i(h)$ is the hydraulic conductivity at the supply soil water pressure h, and K_o is the hydraulic conductivity at the initial soil water pressure (h_0) of the soil. Yao and Hendrickx (1996) and Hendrickx and Yao (1996) show that at low infiltration rates t_{grav} quickly becomes much larger than the duration of the infiltration event and consequently the opportunity for gravity-driven unstable wetting fronts will disappear (Hendrickx and Yao 1996). Experimental data from well-sorted laboratory sands show that wetting fronts are stable when $t_{infil} < 0.002\ t_{grav}$; t_{infil} is the duration of the infiltration event and t_{grav} is the gravitational time that indicates when gravity and capillarity each contribute equally to the process of infiltration (Philip 1969). One other important criterion is the minimum amount of water that is needed for the initiation of unstable wetting. Hendrickx and Yao (1996) show that wetting fronts remain stable as long as the total amount of water applied to the soil is smaller than the amount of water needed to wet a distribution layer near the surface. The thickness of the distribution layer often is approximately equal to the finger diameter (Hendrickx and Yao 1996). Using this relationship they derived the minimum thickness for the distribution before finger start to develop, this relationship states:

$$W < 4.8 \frac{\theta_d}{\theta_s} \frac{S_W^2}{K_s} \qquad (3)$$

where θ_d is the volumetric water content of the distribution layer, S_w is the sorptivity of the soil at water entry value, θ_s is the saturated water content, W is the minimum amount of water that needs to infiltrate before unstable wetting fronts can form.

Material And Methods

Soil Hydraulic Properties and Simulations

Two similar field soils were used as our experimental material. An eolian dune sand from inland dunes near Kootwijk in the Netherlands and an inland eolian sand from the Sevilleta at approximately 30 km north of Socorro, New Mexico, U.S.A. The particle size distributions of both sands are shown in Figure 8.1. Water retention curves (Figure 8.2) including initial wetting, drying, and wetting scanning curves, have been measured for both sands using the hanging water column technique on 100 cm^3 dry samples that were taken from the lysimeters. The data were fitted with the RETC program of *van Genuchten et al.,* [1991]. For Sevilleta sand, the saturated hydraulic conductivity was measured with the constant head method. The instantaneous profile method (Watson, 1966) was applied in the laboratory to measure the unsaturated hydraulic conductivities. For the Kootwijk sand, only the saturated hydraulic conductivity was measured. The unsaturated hydraulic conductivity

Figure 8.1. Grain size distribution of Dutch and Sevilleta Dune Sands

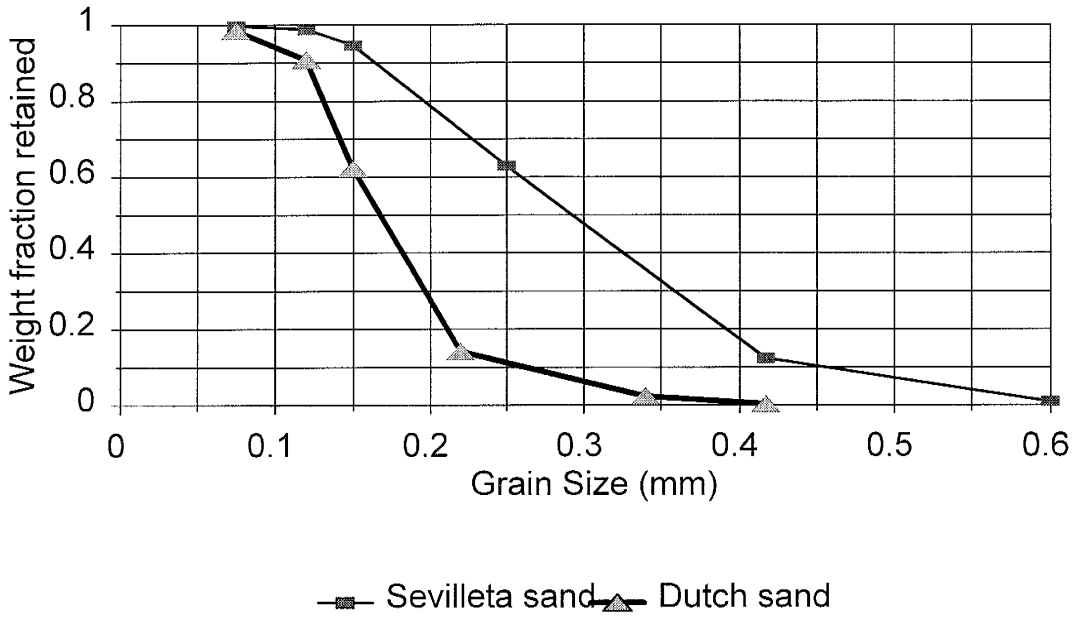

Figure 8.2. Water retention curves of Dutch and Sevilleta dune sands

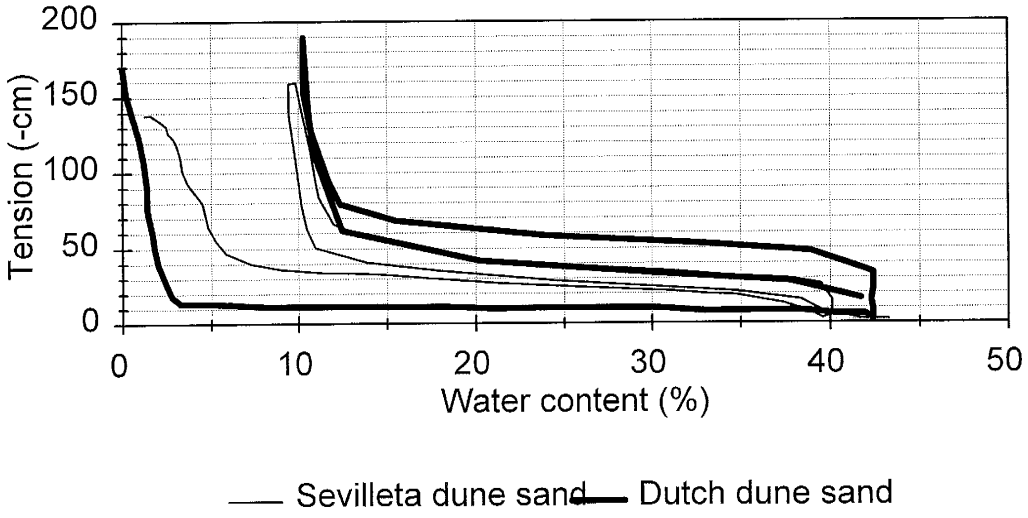

was obtained by assuming the connectivity parameter equal to 0.5 (van Genuchten, 1980). Soil hydraulic property parameters for both sands are shown in Table 1. These parameters are used to determine relationship between finger size and infiltration rate in the two soils with two different initial soil water content condition, 0.001 and 0.03 cm^3/cm^3 , using the model by Du et al. (1998b).

Laboratory Experiments

Field sands were taken to the laboratory to conduct lysimeter experiments. Experiments were conducted in small lysimeters (diameter 30 cm, height 50 cm) for both sands and a large one (diameter 100 cm, height 75 cm) for the Sevilleta dune sand. Sands were packed into the lysimeters using the same method as Yao and Hendrickx (1996). Four centimeters of water were applied by a sprinkler system at rates of 4 cm/hr for Sevilleta sand, 3.5 and 0.0625 cm/hr for Dutch dune sand. After water application, the lysimeters were sliced layer by layer to study the wetting patterns.

Lysimeter and Field Experiments

For Dutch dune sand, outdoor lysimeter (height 1.2 m, widths 1.2 x 1.4 m) experiments were conducted by Hendrickx and Dekker (1991). A lysimeter with an initial soil water content of 0.005 cm^3/cm^3 received a total precipitation of 40.3 cm for a four months period. Wetting patterns were studied by excavating layer by layer with 10 cm

Table 8.1. van Genuchten parameters of the dune sands for the initial wetting curve

Sand	θ_r	$\theta_s^{\dagger}$	k_s	α	n	λ
(US Mesh)	(cm^3/cm^3)	(cm^3/cm^3)	(cm/s)	cm^{-1}	-	-
Sevilleta	0	0.40	0.013	.04	3.85	0.295
Dutch	0	0.35	0.0086	.097	8.95	0.5

†. Field saturation based on instantaneous profile experiments

interval down to 1 m depth.

For the sand dune of New Mexico field experiments were conducted. We used a rain simulator of one by one meter. Water was applied with regimes similar to the New Mexico rains. Experiments with different infiltration rates were conducted. Wetting patterns were studied by excavating sand layer by layer every 15 cm down to the depth of 90 cm.

Results And Discussion

Effect of Infiltration Rate

Figure 8.3 presents the results of the mathematical model for Sevilleta and Dutch dune sands. It demonstrates that for Sevilleta sand the smallest finger diameter is approximately 22 cm at infiltration rates between 1 and 2 cm/hr; for Dutch dune sand the smallest finger is approximately 2.2 cm at infiltration rates between 0.5 and 1 cm/hr. For both sands, at lower rates the finger diameter increases rapidly, i.e. the wetting front stabilizes. For higher infiltration rates close to saturated hydraulic conductivity, the wetting front also becomes stable. Comparison of predictions with laboratory and field observations will be performed in the next section because the initial water content of each experiment also has to be considered.

Figure 8.3. Finger sizes vs. infiltration rates for Sevilleta and Dutch dune sand at different initial water content calculated with the mathematical model.

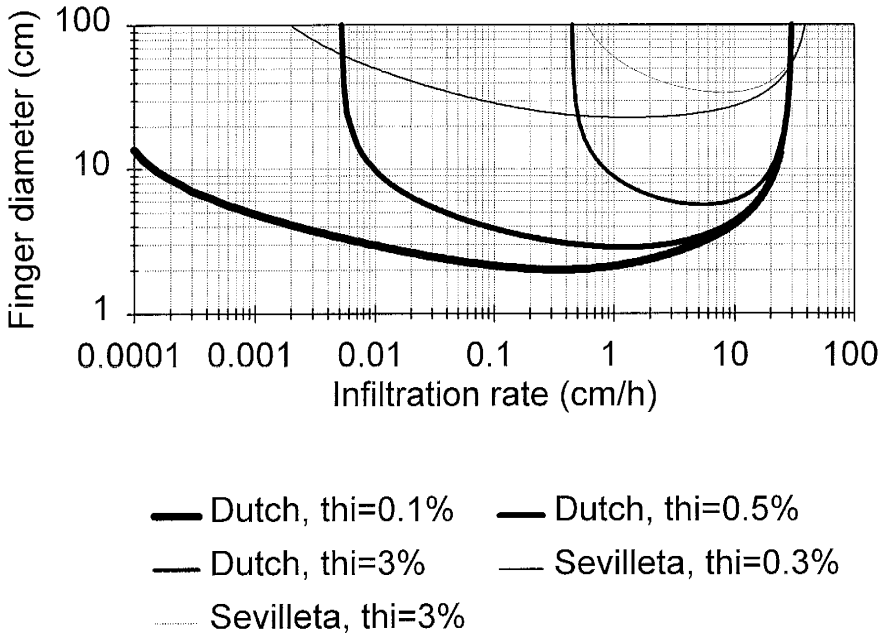

Effect of Initial Water Content

Sevilleta dune sand

Figure 8.3 shows that the stabilizing effect at low infiltration rates greatly changes due to a small increase in initial water content from 0.003 to 0.03 cm^3/cm^3. At an infiltration rate of 1 cm/hr the finger diameter increases from approximately 22 to 60 cm. In addition, we observe that an increase in initial water content results in stable wetting fronts at higher infiltration rates. At initial water content 0.003 cm^3/cm^3 unstable wetting can occur between rates 30 to 0.01 cm/hr, at 0.03 cm^3/cm^3 only between rates 30 to 2 cm/hr. Liu et al. (1994a) also observed an increase in finger diameter from approximately 2 to 7 cm when initial water content was increased from 0 to 0.05 cm^3/cm^3. The finger diameters of 22 cm in dry Sevilleta sand that are predicted by the model are rather close to the approximately 30 cm diameters observed during laboratory experiments at 0.003 cm^3/cm^3 initial water content (Figure 8.4a and 8.4b). Several experiments conducted during the summers of 1992 and 1995 in the Sevilleta dunes in order to create unstable wetting in field soils with an initial water content between 0.02 and 0.03 cm^3/cm^3 have not been successful. Stable wetting fronts were observed for these 1-meter scale experiments (Figure 8.5). The model results (Figure 8.2) indicate that this was due to the stabilizing effect of the initial water content in combination with the decreasing infiltration rate range in which instabilities can develop. Thus, even a minor increase in initial water content can have a great stabilizing effect on the wetting fronts in the Sevilleta dunes.

Figure 8.4. Wetting patterns observed in the 1 m diameter lysimeter in Sevilleta dune sand after application of 8 cm water at rate of 0.9 cm/hr (a) wetting pattern at depth 52 cm (b) wetting pattern at depth 60 cm.

Fig. 4 (A)

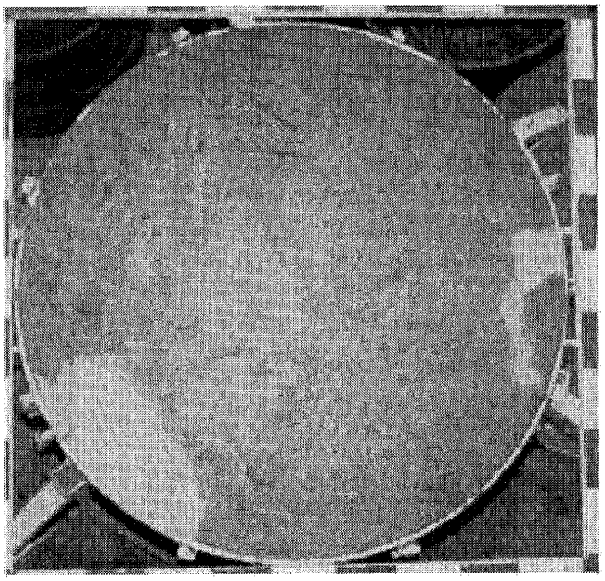

4 (B)

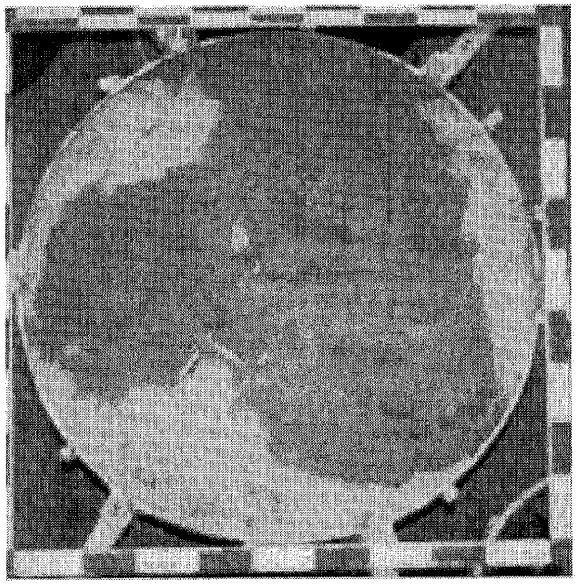

Figure 8.5. Field experiment in Sevilleta sand dune, wetting front was stable for 7 cm of water applied at 8.3 cm/hr.

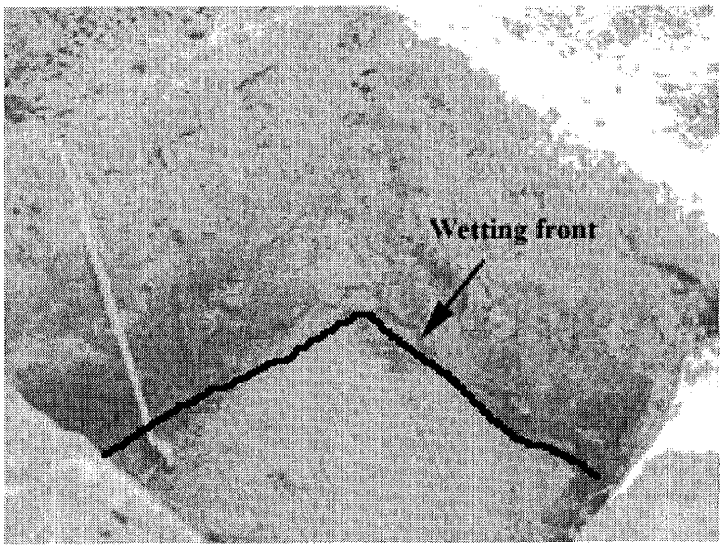

Dutch dune sand

Figure 8.3 also presents results of the mathematical model for the dune sand in the Netherlands using the initial wetting curves for three initial soil water contents (0.001, 0.005, and 0.03 cm^3/cm^3). The smallest finger diameters are predicted to be 2 cm and found close to the smallest finger size observed (2.5-15 cm) in the outdoor lysimeter at the 40 cm depth with 0.005 cm^3/cm^3 initial water content (Figure 8.6). Initial water content appears to play a minor role in this soil at high and intermediate rates. For example, at an infiltration rate of 1 cm/hr the finger size increases from 2 cm to 9 cm for an initial water content increase from 0.001 to 0.03 cm^3/cm^3. Figure 8.7a shows the experimental results from a lysimeter experiment after application of 4 cm of water at rate of 3.5 cm/hr. The unstable pattern starts at only 1 cm depth. Small and persistent fingers can be observed in figures 8.7b and 8.7c at the depth of 5 and 10 cm. Finger sizes range from 1 to 5 cm. From figure 8.3 at the infiltration rate of 3.5 cm/hr, with initial water content at 0.001 cm^3/cm^3 the finger size is predicted to be 1.7 cm. We also conducted a low infiltration rate experiment and found that under an infiltration rate of 0.06 cm/hr after 4 cm of water applied, the wetting front is stable in a 30 cm diameter lysimeter. Figures 8.8a, 8.8b, and 8.8c show the stable wetting patterns at depths of 1, 5, and 10 cm. Note that an edge effect was prevented in these experiments by partly covering the edge. Water was uniformly applied at the central 22 cm diameter area of the lysimeter. We compared these results with finger size predictions in figure 8.3 and found that the finger diameter has been grossly under-estimated. This most likely is a result of the uncertainty in hydraulic properties when we extrapolate wet experimental data toward the

Figure 8.6. Wetting pattern at 40 cm depth, fingers were observed in the lysimeter experiment of Hendrickx and Dekker (1991)

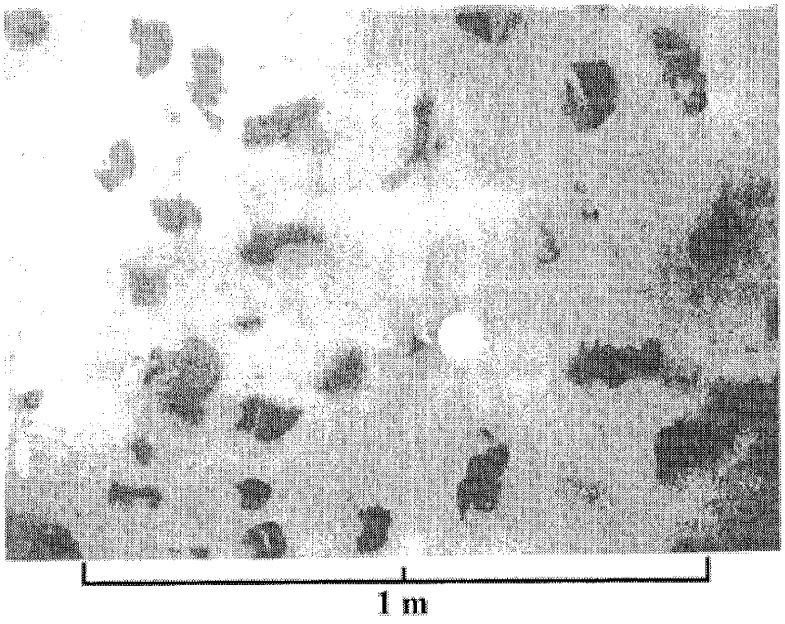

Figure 8.7. **Wetting patterns observed in the 30 cm diameter lysimeter in Dutch dune sand after application of 4 cm water at rate of 3.5 cm/hr (a) wetting pattern at depth 1 cm (b) wetting pattern at depth 5 cm (c) wetting pattern at depth 10 cm**

(a)

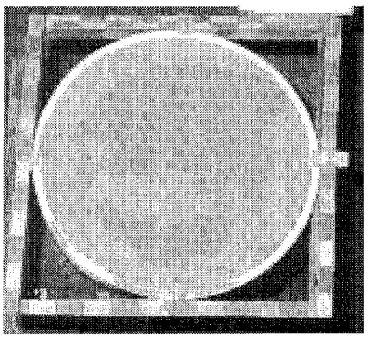

(b)

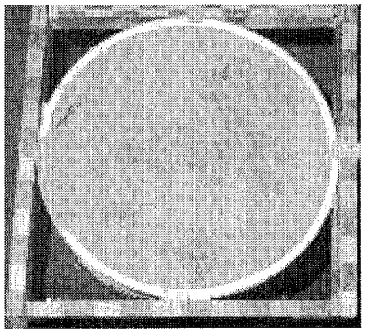

(c)

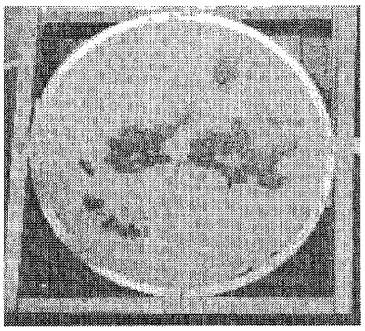

Figure 8.8. Wetting patterns observed in the 30 cm diameter lysimeter in Dutch dune sand after application of 4 cm water at rate of 0.06 cm/hr (a) wetting pattern at depth 1 cm (b) wetting pattern at depth 5 cm (c) wetting pattern at depth 10 cm

(a)

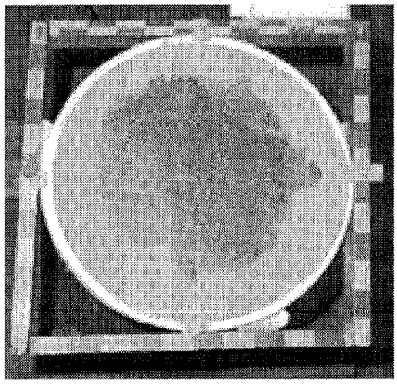

(b)

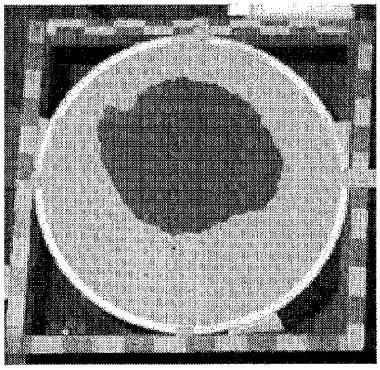

(c)

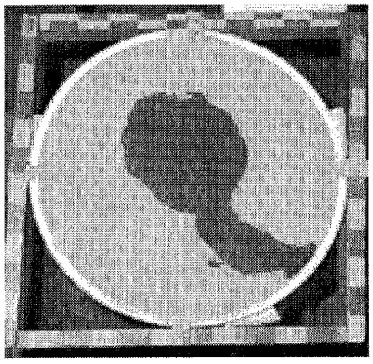

very dry range. This phenomenon has been discussed by Yao and Hendrickx (1998, chapter 7 of this thesis).

Empirical Approach

Before fingers start in an infiltration process, a distribution layer is formed. Hendrickx and Yao (1996) found a 1:1 linear relationship between the finger sizes and the thickness of the distribution layer. It was determined with equation (3) that Sevilleta dune sand needs a minimum amount of 44 mm water to trigger instabilities while Dutch dune sand only needs 7 to 13 mm. This indicates that a small amount of precipitation may be sufficient to trigger unstable wetting fronts in the Dutch dune sand but a major rainstorm is necessary for the Sevilleta dune sand. These numbers were calculated using very dry soils where instability has an optimal opportunity to occur.

Using a local rate-duration-frequency curve, Hendrickx and Yao [1996] analyzed precipitation events for return periods of 2, 10, and 100 years. They found that only few precipitation events with a 100 years return period may supply the 44 mm of rainfall needed to start unstable wetting fronts in Sevilleta dune sand under initial dry conditions. This explains why fingering phenomena have not been observed in Sevilleta dune sand while they are so often encountered in the Dutch dune sand.

Conclusion

The mathematical model predicted minimum finger sizes to be 2 cm for Dutch dune sand, while minimum finger sizes of 22 cm were predicted for New Mexico dune sand. These predictions are comparable with our experimental observations. The mathematical approach yield reasonable estimates for finger diameters. The empirical model predicts that instability will often occur in Dutch dune sands after only a small amount of precipitation. However, a large rainstorm with a long return period is needed to cause instability in New Mexico dune sand. These results explain why unstable wetting phenomena have been reported frequently in dunes of the Netherlands while they are so rare in the inland dunes of New Mexico. The examples of New Mexico and the Netherlands demonstrate that combining the mathematical and empirical methods yields valuable information about the occurrence of unstable wetting fronts in field soils.

References

Beven, K., and P. Germann, Macropores and water flow in soils, *Water Resour. Res.*, 18(5), 1311-1325, 1982.

Bouma, J., and L.W. Dekker, A case study on infiltration into dry clay. I. Morphological observations, *Geoderma*, 20, 27-40, 1978.

Dekker, L.W. and C.J. Ritsema, Fingered flow: the creator of sand columns in dune and beach sands. *Earth surface processes and landforms*, 19, 153-164, 1994.

Du, X.H., T. Yao, W.D., Stone, and J.M.H., Hendrickx, Stability analysis of the unsaturated water flow equation: 1. Mathematical derivation, submitted for publication in *Water Resour. Res.*, 1998a.

Du, X.H., T. Yao, W.D., Stone, and J.M.H., Hendrickx, An analytical solution of the Richards' equation using actual hydraulic soil properties, submitted for publication in *Soil Sci. Soc. Am. J.*, 1998b.

Glass, R.J., T.S. Steenhuis, and J.-Y. Parlange, Wetting front instability: 1. Theoretical discussion and dimensional analysis, *Water Resour. Res., 25*, 1187-1194, 1989a.

Glass, R.J., T.S. Steenhuis, and J.-Y. Parlange, Wetting front instability: 2. Experimental determination of relationships between system parameters and two-dimensional unstable flow field behavior in initially dry porous media, *Water Resour. Res., 25*, 1195-1207, 1989b.

Glass, R.J., T.S. Steenhuis, and J.-Y. Parlange, Mechanism for finger persistence in homogeneous, unsaturated, porous media: theory and verification, *Soil Sci.,* 148, 60-70, 1989c.

Glass, R.J., J.-Y. Parlange., and T.S. Steenhuis, Immiscible displacement in porous media: Stability analysis of three-dimensional, axisymmetric disturbances with application to gravity-driven wetting front instability, *Water Resour. Res., 27*, 1947-1956, 1991.

Hendrickx, J.M.H., L.W. Dekker, and P.A.C. Raats, Formation of sand columns caused by unstable wetting fronts, *Grondboor en Hamer,* 6, 173-175, (in Dutch), 1988a.

Hendrickx, J.M.H., L.W. Dekker, E.J. Van Zuilen, and O.H. Boersma, Water and Solute movement through a water-repellent sand soil with grasscover, 131-146, In:

Wierenga, P.J. and D. Bachelet, 1988, Validation of flow and transport models for the unsaturated zone: *Conference Proceedings*; May 23-26, 1988 Ruidoso, New Mexico. Research Report 88-SS-04 Dept. of Agronomy and Horticulture, New Mexico State University, Las Cruces, N.M., 545 p, 1988b

Hendrickx, J.M.H., and L.W. Dekker, Experimental evidence of unstable wetting fronts in non-layered soils, 22-31, In *Proc. Natl. Symp. Preferential Flow*, Chicago, IL. 16-17 Dec. 1991, *Am. Soc. Agric. Eng.*, St. Joseph, MI., 1991.

Hendrickx, J.M.H., and L.W. Dekker., and O.H. Boersma, Unstable wetting fronts in water-repellent soils, *J. Environ. Qual., 22*, 109-118, 1993.

Hendrickx, J.M.H. and T. Yao, Prediction of wetting front stability in dry field soils using soil and precipitation data, *Geoderma, 70*, 265-280, 1996.

Hillel, D., Unstable flow in layered soils: A review, *Hydrol. Processes*, 1, 143-147, 1987.

Kung, K.-J. S, Preferential flow in a sandy vadose zone: 1. Field observation, *Geoderma*, 46, 51-58, 1990.

Liu, Y., T.S. Steenhuis, and J.-Y. Parlange, Closed-form solution for finger width in sandy soils at different water contents, *Water Resour. Res. 30*, 949-952, 1994a.

Liu, Y., T.S. Steenhuis, and J.-Y. Parlange, Formation and persistence of fingered flow in coarse grained soils under different moisture contents, *J. Hydrol.*, 159, 187-195, 1994b.

Parlange, J.-Y., and D.E. Hill, Theoretical analysis of wetting front instability in soils, *Soil Sci., 122*, 236-239, 1976.

Philip, J.R., Theory of infiltration, *Advance. Hydroscience, 5*, 215-296, 1969.

Philip, J.R., Stability analysis of infiltration, *Soil Sci. Soc. Am. Proc., 39*, 1042-1049, 1975a.

Philip, J.R., The growth of disturbances in unstable infiltration flows, *Soil Sci. Soc. Am. Proc. 39*, 1049-1053, 1975b.

Raats, P.A.C., Unstable wetting fronts in uniform and nonuniform soils, *Soil Sci. Soc. Am. Proc. 37*, 681-685, 1973.

Rice, R.C., D.B. Jaynes, and R.S. Bowman, Preferential flow of solutes and herbicides under irrigated fields, *Transactions of the ASAE*, 34, 914-918, 1991.

Selker, J.S., T.S. Steenhuis, and J.-Y. Parlange, Wetting front instability in homogeneous sandy soils under continuous infiltration, *Soil Sci. Soc. Am. J.*, 56, 1346-1350, 1992a..

Selker, J.S., P. Leclerq, J.-Y. Parlange, and T.S. Steenhuis, Fingered flow in two dimensions. 1. Measurement of matric potential, *Water Resour. Res.,* 28, 2513-2521, 1992b..

Selker, J.S., J.-Y. Parlange, and T.S. Steenhuis, Fingered flow in two dimensions. 2. Predicting finger moisture profile, *Water Resour. Res.*, 28, 2523-2528, 1992c.

Van Genuchten, M.Th., A closed-form equation for predicting the hydraulic conductivity of unsaturated soils, *Soil Sci. Soc. Am. J.*, 44, 892-898, 1980.

Van Genuchten, M.Th., F. J. Leij, and S. R. Yates, The RETC code for quantifying the hydraulic functions of unsaturated soils, U.S. Salinity Laboratory, U. S. Department of Agriculture, Agricultural Research Service, Riverside, CA, 1991.

Watson, K.K., An instantaneous profile method for determining the hydraulic conductivity of unsaturated porous materials, *Water. Resour. Res.*, 2, 709-715, 1966.

Yao, T., and J.M.H., Hendrickx, Stability of wetting fronts in homogeneous soils

under low infiltration rates, *Soil Sci. Soc. Am. J., 60*, 20-28, 1996.

Yao, T., and J.M.H., Hendrickx, Stability analysis of the unsaturated water flow equation: 2. Experimental verification, submitted for publication in *Water Resour. Res.*, 1998.

9. General Conclusions

The existence of unstable wetting fronts was clearly reconfirmed in this study since fingers were observed under field and laboratory conditions. In this thesis I explored the prediction of wetting front instability. My first step was to set up a systematic measurement program to identify the controlling factors (chapter 2). At rates that are representative of natural precipitation intensities, the experimental results in the coarse sand showed that, for infiltration rates varying between 0.3 and 12 cm/hr, finger diameters remain more or less constant. This observation agrees with existing theories. However, at infiltration rates lower than 0.12 cm/hr, the coarse sand experiments show that the wetting fronts became stable. For rates between 0.3 and 0.12 cm/hr, the wetting is semi-stable; that is, there is incomplete wetting without distinct development of fingers. This phenomenon has not been observed in previous experimental studies and is not predicted by current wetting front instability theories. Our experimental results also demonstrated that coarser soils will enhance instability and initially wet soils will dampen instability.

Using these data, an existing model for prediction of instability was improved (chapter 3). It was demonstrated that equation derived from stability analysis for the prediction of finger sizes can be applied over the full range of infiltration rates. To apply this equation over the full range of infiltration rates, we differentiated two conditions: saturated and unsaturated fingers. For infiltration rates exceeding approximately 1 cm/hr, the finger

tip is assumed to be saturated and the equation uses easily determined hydraulic properties close to saturation and at water entry value. Under these conditions it yields a range of finger size predictions which were found to bound the experimentally observed finger sizes. Under lower infiltration rates, the finger tip is no longer saturated and the hydraulic parameters for finger size prediction are more difficult to obtain. We described an approximate scheme to obtain these parameters from infiltration experiments. The equation was proved to correctly predict finger sizes at infiltration rates less than 1 cm/hr if the proper hydraulic parameters are used. We also presented a step-by-step approach for practical finger size estimation in field soils.

In chapter 4, a simple approach for the evaluation of wetting front stability in dry soils was developed empirically. We showed that the stability of wetting fronts in the top layer of a soil depends both on the soil texture and the intensity of the precipitation. Our approach distinguishes stability criteria for wetting events that are different for a high, intermediate, and low infiltration rate. At *high infiltration rates*, wetting fronts are stable if the infiltration rate exceeds or equals the saturated hydraulic conductivity of the soil. The stability criterion for *low infiltration rates* (less than approximately 0.2 cm/hr for sand soils) is based on two characteristics times: a gravitational time t_{grav} and an infiltration time t_{infil}. Experimental and literature data show that in well-sorted laboratory sands, wetting fronts are stable when $t_{infil}<0.002\ t_{grav}$. For *intermediate infiltration rates,* wetting fronts remain stable as long as rainfall amount is smaller than the amount of water needed to wet a distribution layer near the surface. The application of the stability criteria was demonstrated with a case

study from the Sevilleta dunes near Socorro, NM. This model is aimed at use by practitioners and a practical flow chart was supplied to help to evaluate the instability.

Although the empirical model improved our capability for the prediction of instabilities under specific circumstances, no existing theory can be used for the prediction of instability in all field soils under a wide range of infiltration rates. It is necessary to conduct a stability analysis using perturbation analysis on a gradual wetting front solution to derive analytical solutions for finger characteristics. Before we conducted this stability analysis, we had to derive an analytical solution that can represent wetting fronts at all times. In chapter 5, we developed a method to solve the one-dimensional Richards' equation under the conditions of constant soil water content at the top boundary and uniform initial soil water content deeper in the profile. The hydraulic conductivity and diffusivity can be any differentiable functions of water content. We used the large time traveling wave solution as our base solution and added two extra functions of time, $\alpha(t)$ and $\beta(t)$, which can describe the downward propagation of the wetting front from early to large times. The function $\alpha(t)$ describes the change of the wetting front shape with time while $\beta(t)$ represents the wetting front travel distance from the surface. The functions $\alpha(t)$ and $\beta(t)$ are determined by two parameters, V_0 and V_2, which are calculated using the soil water content profile at large times. Compared to other methods reported in the literature, our method requires relatively simple calculations and can be applied at all times. The applicability of our method was verified by comparing its results to analytical solutions and numerical simulations of infiltration into a clay and sand soil.

In chapter 6, we used this solution as the basic flow on which three-dimensional perturbations are introduced. By locally linearizing the three-dimensional Richards' equation, a linear partial differential equation was obtained which governs the perturbation variables. The stability of each point at the wetting front was considered in the local coordinate system. The analysis of this perturbation equation at these points of the wetting front provides not only the relationship between the finger sizes and the infiltration rates at the top surface, but also the traveling speeds of the fingers rooted from these points. The stability of the wetting front is determined by two factors: finger sizes and downward velocities of fingers. If the size of the finger rooting from some point is large, then this point is considered to be stable whatever the downward velocity is; if the size of the finger is not large, but the downward velocity of the finger is smaller than that of the stable wetting front, then the finger will be covered eventually by the distribution layer and this point remains stable. Instability will occur only when the finger size is small and the downward velocity of the finger is larger than that of the stable wetting front. Under these conditions, the finger will remain ahead of the stable wetting front at all times. For any homogeneous soil profile with uniform initial water content, this model can predict instability and finger characteristics over the full range of infiltration rates.

This analytical model was verified by comparing predictions for sand soils and results from laboratory experiments (chapter 7). We compared finger sizes from laboratory experiments with predictions by the stability model. The model enables us to predict finger sizes from soil hydraulic properties. Using measured unsaturated hydraulic properties fitted

and extrapolated over the entire water content range, we arrive at finger size predictions over the full infiltration range. The model predicts an increase of finger diameter at high and low infiltration rates for all soils. Such increases were also observed in our experiments. The model yields reliable predictions of finger diameters at high infiltration and intermediate rates but performs less at infiltration rates less than 1 cm/hr. This is caused by difficulties to precisely measure hydraulic conductivity at low infiltration rates. A sensitivity analysis demonstrated that the behavior of unstable fronts at infiltration rates below 1 cm/hr is quite sensitive for small changes in initial soil water content and the shape of the unsaturated hydraulic conductivity of low water contents (0.001-0.1 cm^3/cm^3). Our experimental verification demonstrated that the model presented in chapter 6 is a powerful tool for the assessment of wetting front instability in homogeneous real soils under a wide range of infiltration rates and initial water contents.

Finally, in chapter 8 we predicted wetting front instability in two field soils using mathematical and empirical models, respectively, from chapters 4 and 6. We used two natural dune sands as our experimental material, one from New Mexico and the other one from Netherlands. The mathematical model predicted the minimum finger size to be 2 cm in Dutch dune sand under dry conditions, while 22 cm was predicted for New Mexico dune sand. These predictions are comparable with our experimental findings. The mathematical approach proved to yield reasonable estimates for the prediction of finger diameters. The empirical model predicts that instability can easily occur in the Dutch dune sand after a small amount of precipitation while a large rainstorm is needed for the New Mexico dune

sand. These results explain why unstable wetting phenomena have been reported frequently in dunes of the Netherlands while they appear to be rare in the inland dunes of New Mexico. The examples of New Mexico and the Netherlands demonstrate that combining the mathematical and empirical methods yields valuable information about the occurrence of unstable wetting fronts in field soils.

The mathematical and empirical models developed during the course of this study allow us to forecast if and when fingers are likely to occur in the field soils. It also enables us to estimate finger characteristics. Both the occurrence of fingers and their characteristics are important to assess water and contaminant flow through the vadose zone. Simulation of water movement in the vadose zone without considering fingers or flow instability can result in serious mistakes. The developed theory will lead to better risk assessments for groundwater contamination, allow improved construction of landfills and storage ponds, and help design more efficient groundwater recharge systems.

APPENDIX A. Geometry and surface properties of experimental sands

Two methods were used to study the grain geometry and surface properties of the experimental sands.

Thin sections:

The petrographic microscope was used to examine thin sections for grain size distribution, shape, and roundness. The experimental sands, including perlite, quartz, Sevilleta dune, and Dutch dune sands were impregnated using polyester resin. The impregnated sand blocks were used to make thin sections for the microscope study. Power's grain roundness chart (Powers, 1953) was used to estimate the roundness of sedimentary particles, under the 20X objective lens. Figure A-1 shows that the 20-30 mesh perlite sand has a particle roundness ranging from angular to sub-angular. Figure A-2 shows that the 14-20 quartz sand has a particle roundness ranging from sub-rounded to sub-angular. Figures A-3 and A-4 shows that Sevilleta dune sand has a wider grain size distribution and slightly greater grain size than Dutch dune sand. Both sands are sub-rounded to sub-angular.

Figure A-1 also shows some small surface structure on the edge of these grains and small lens inside the grains. The reason for these fracture-like edges is associated with the crushing and grinding processes of the perlite sand. The small lenses were

proved to be small vesicles (see SEM study in the next section).

Scanning Electron Microscopy (SEM)

SEM was used to analyze the surface micro structure. The 20-30 perlite and 14-20 quartz sand grains were mounted on the sample holder and a thin carbon layer was coated on the surface to avoid deflection of the incident beam and voltage drop problems. Figure A-5 shows the grain shape and surface structure of perlite sand. There are some scattered vesicles on the perlite surface (Figure A-6). However, most of the areas between these vesicles are relatively flat (Figure A-7). The vesicles do not appear to be connected to each other.

The quartz sand has a flatter surface without vesicles (Figure A-8). Most of the surface on the quartz grains is flat (Figure A-9). However, the quartz sand we used has a small portion of feldspar grains which can be observed in Figure A-8 with a complicated dissolution surface. Figure A-10 shows the highly complicated relief on a feldspar grain surface.

By comparing the shape of perlite (Figure A-5) and quartz (Figure A-8) sands, similar observations were obtained as in the thin section studies. The perlite sand has particles with angular to sub-angular shapes whereas the quartz sand has sub-rounded to sub-angular shapes.

There is a slight difference in shape between perlite and quartz sands. Quartz sand has a relatively flat surface whereas perlite has some vesicles on the surface. However, the vesicles on the perlite surface likely do not play a major role because the surface area in between these scattered vesicles is flat and similar to the surface of quartz grains. It was proved in chapter 2 that the infiltration experiments in quartz and perlite sands yield identical results which demonstrates that the minor difference of surface roughness between perlite and quartz sands do not cause different surface-water interaction properties.

References

Powers, M.C., 1953, A new roundness scale for sedimentary particles, J. Sed. Petrology, v.23, Fig. 1, p. 118.

Figure A-1. 20-30 perlite sand (20X)

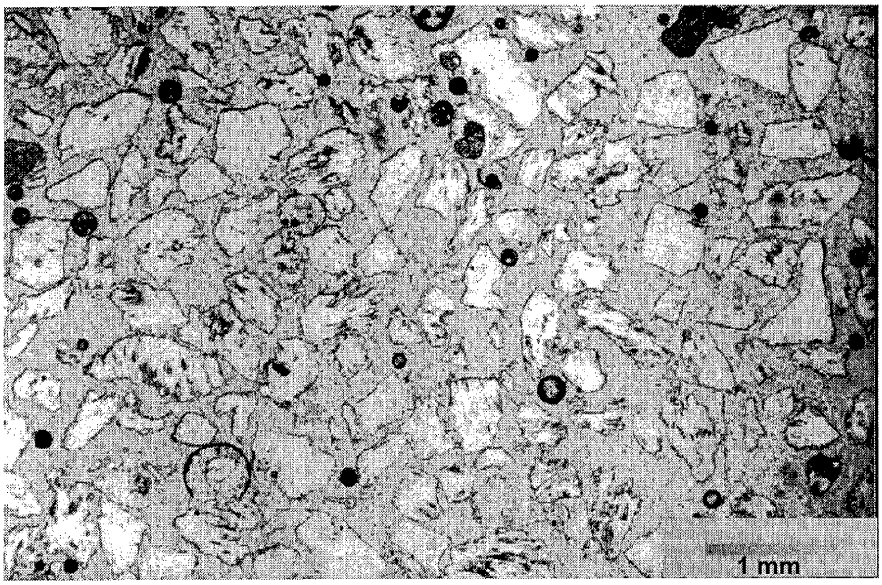

Figure A-2. 14-20 quartz sand (20X)

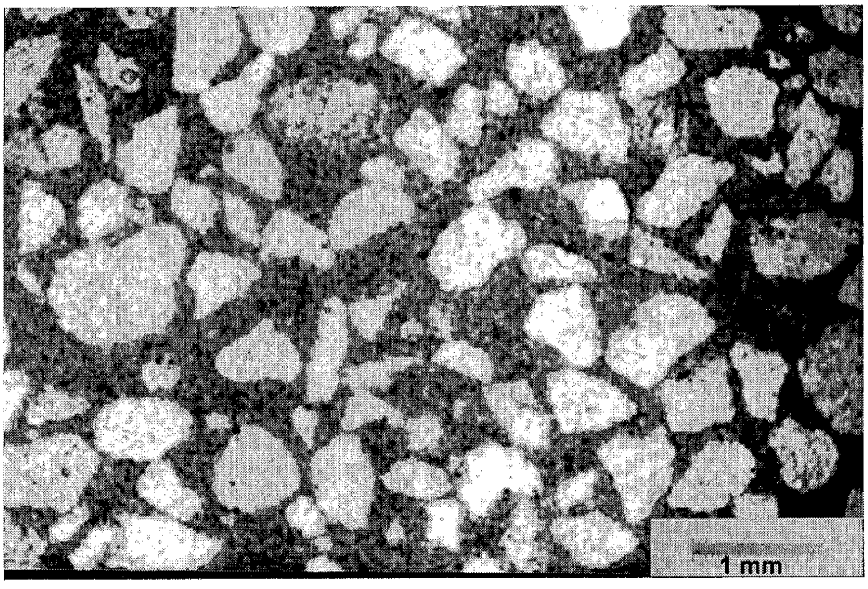

Figure A-3. Sevilleta dune sand (20X)

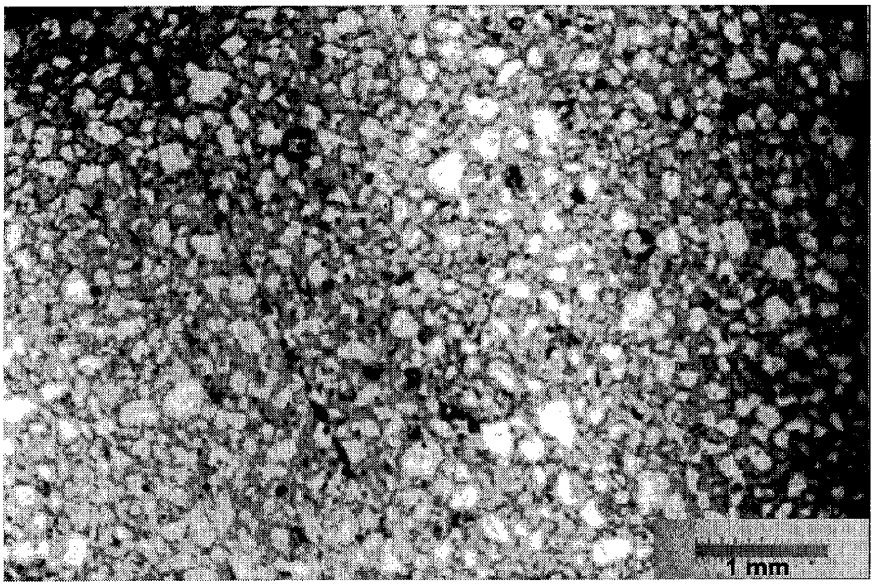

Figure A-4. Dutch dune sand (20X)

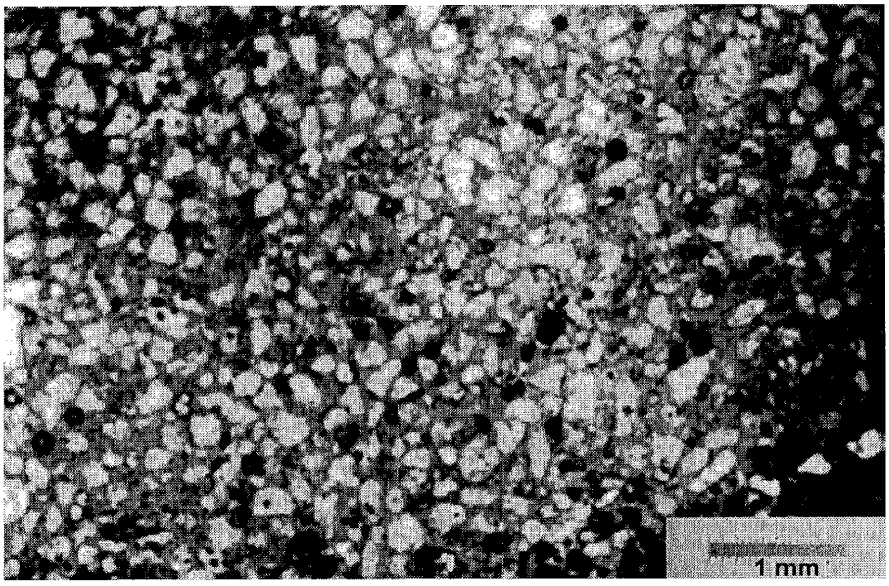

Figure A-5. Surface structure of perlite sand from SEM (~45X)

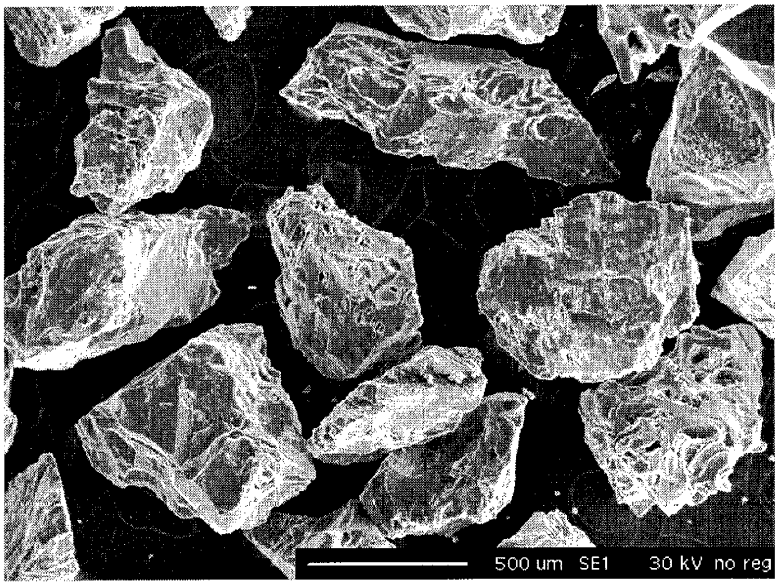

Figure A-6. Vesicles on the surface of perlite sand from SEM (~350 X)

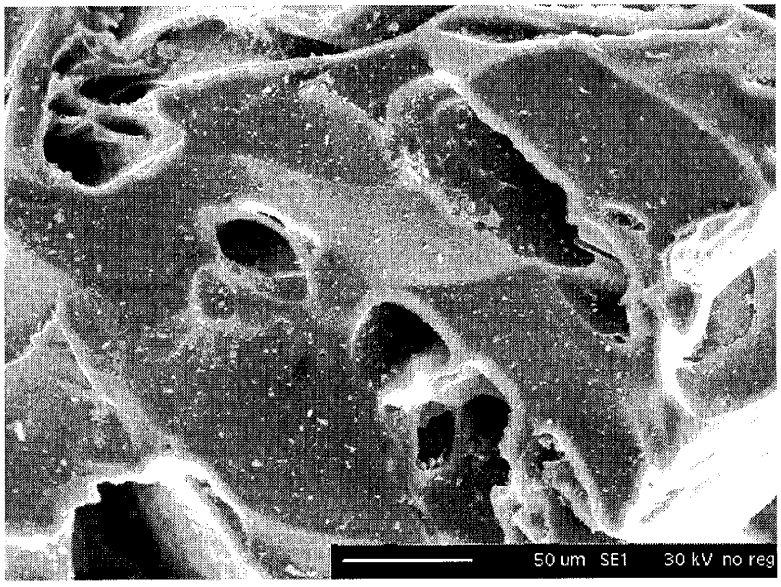

Figure A-7. Flat surface of perlite sand from SEM (~2700X)

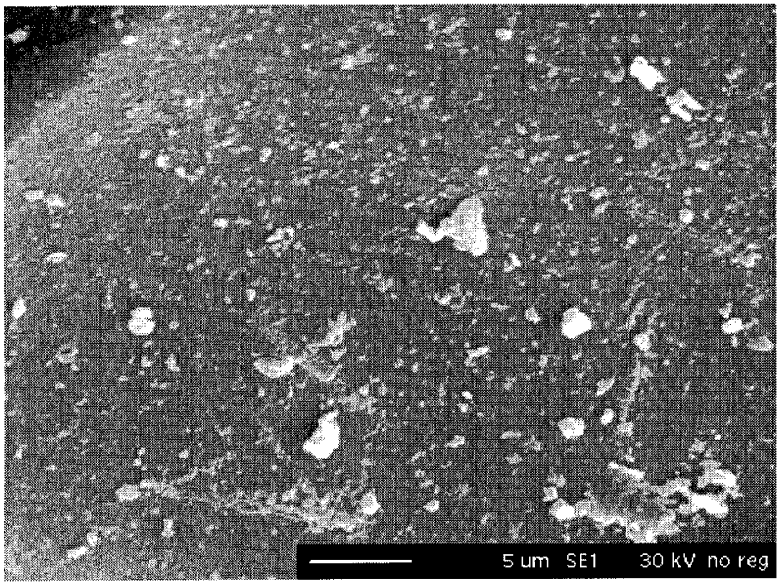

Figure A-8. Surface structure of quartz sand from SEM (~45X)

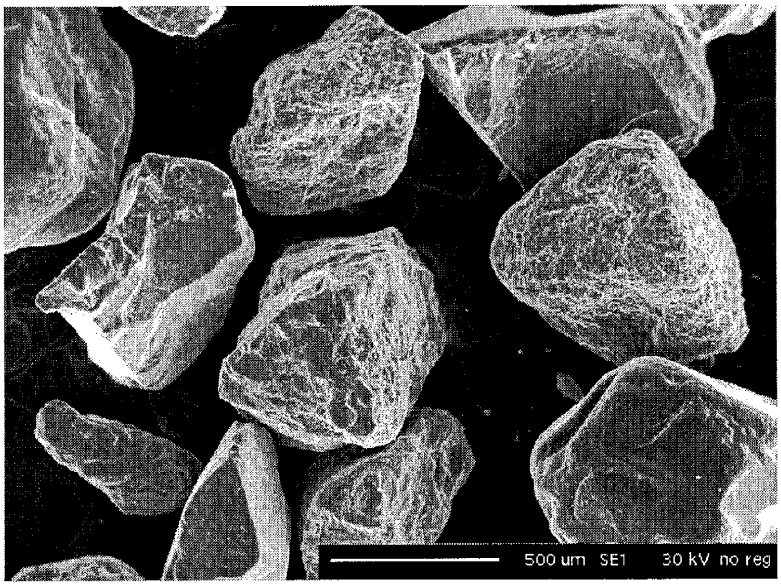

Figure A-9. Flat surface of quartz sand from SEM (~1400X)

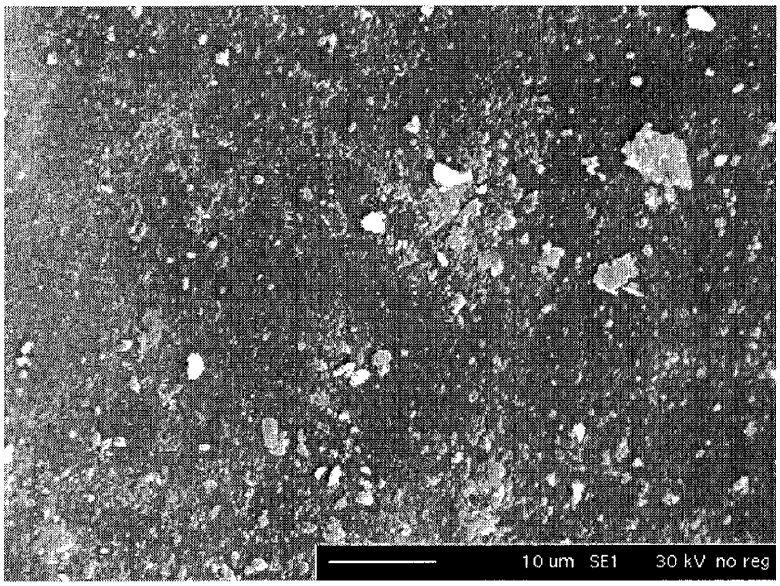

Figure A-10. Complicated surface structure of feldspar grain in quartz sand from SEM (~675X)

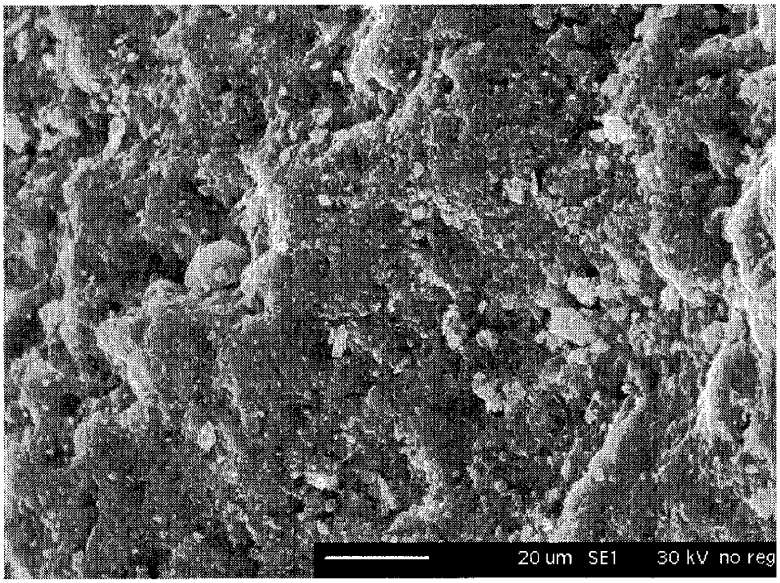

Appendix B. Future research directions from the dimensional analysis

Dimensional analysis has the potential to resolve the relative contributions of different forces to the instability problem and to help direct future research directions. To study wetting front instability, Glass (1989a) showed explicitly the effect of mean grain size, fluid surface tension, viscosity, and density on finger width for a family of similar porous media. Nondimensionalizing the flow equation yields scaled forms of K_S (saturated conductivity), S (sorptivity), R_F (flux-conductivity ratio; effectively a viscous force-gravity ratio), N (a gravity force-capillarity ratio), and finger diameter d:

$$K_S = \frac{\rho g m^2}{\mu} K_{S*} \tag{1}$$

$$R_F = \frac{\mu}{\rho g m^2} \frac{q_F}{K_{s*}} \tag{2}$$

$$S^2 = \frac{\sigma m}{\mu} S_*^2 \tag{3}$$

$$N = \frac{m \rho g}{\sigma} \frac{d\ K_{S*}(\theta_S - \theta_i)}{S_*^2} \tag{4}$$

and

$$d = \frac{\sigma}{\rho g m} \frac{\pi S_*^2}{K_{S*}(\theta_s - \theta_i)} \left[\frac{1}{1 - R_F}\right] \quad \textbf{(5)}$$

where ρ is the density, g is the gravitational constant, m is the mean grain size, μ is the viscosity, σ is the surface tension, θ_s is the saturated water content, θ_i is the initial water content, and q_F is the flux inside fingers. K_{s*} and S_* are dimensionless forms of the saturated conductivity and sorptivity, respectively.

The dimensionless finger diameter d_* can be represented as

$$d_* = \frac{\rho g m}{\sigma} d \quad \textbf{(6)}$$

Glass et al., (1989a) defined the system flux-conductivity ratio $R_s = q_s / K_s$, and found $R_S = R_F^2$ if R_S is not too small (Glass et al., 1989b). The plot of finger diameter vs. infiltration rate (Figure B-1) can be plotted dimensionlessly using d_* and $R_S^{1/2}$ as shown in Figure B-2. In Figure B-2, using the formula by Glass et al., (1989a) all predictive curves (Figure 2-5) collapse to one if $R_S^{1/2} > 0.082$ ($R_S > 0.007$). Glass et al., (1996) demonstrated that these relationships were developed within a specific range of R_F ($0.1 < R_F < 0.9$) and R_S ($0.007 < R_S < 0.82$).

Experimental results from four different grades of sand merge together within the R_S range of 0.007 to 0.82 but not below 0.007 ($R_S^{1/2} = 0.082$).

Figure B-1. Finger diameter versus infiltration rate

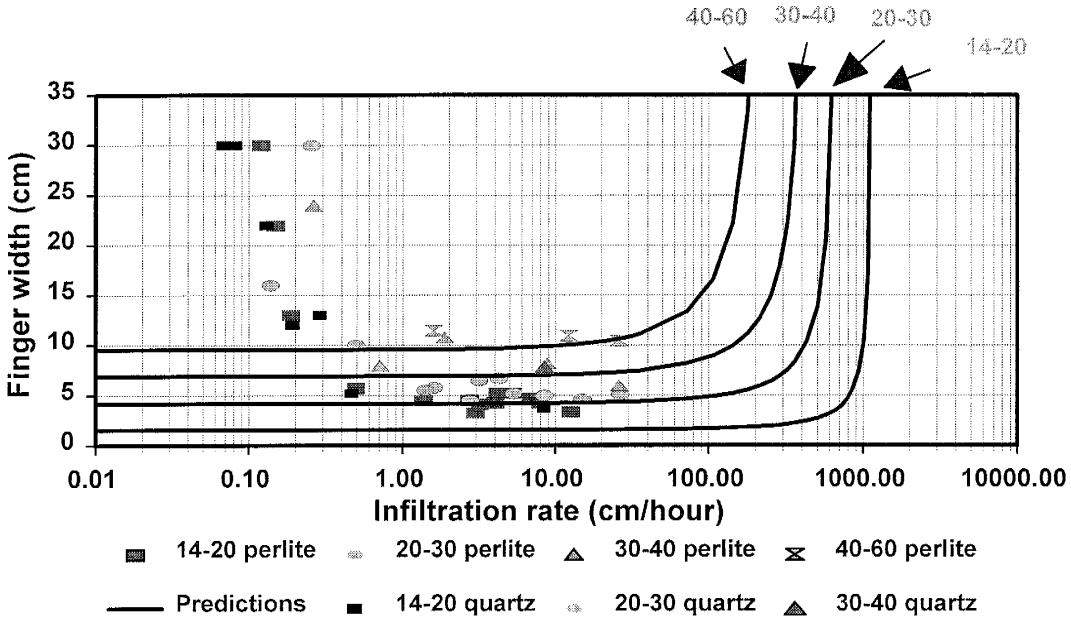

Figure B-2. Dimensionless finger diameter d_* versus $R_S^{1/2}$

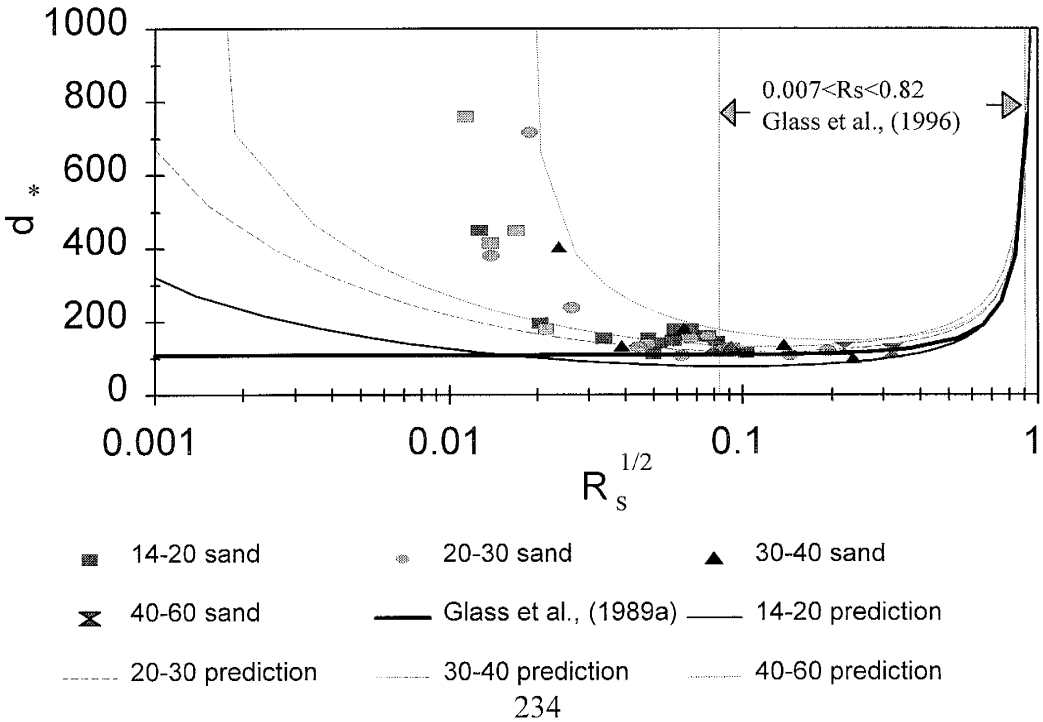

Predictions from Du et al., (1998) converge to the Glass model and the data within this R_S range ($0.007 < R_S < 0.82$). For R_S below 0.007, Du et al., (1998) predict larger finger sizes, strongly dependent on soil properties. The reasons that the predictions deviate from the experimental results were explained in Chapter 7. It is apparent that the model by Du et al., (1998) provides a better representation of the data at low infiltration rates than the model derived from current dimensional analysis. This points out the need for a more general dimensional analysis to cover the full range of infiltration rates or an analysis that will account for the mechanism at low infiltration rates.

Since R_F is the flux-conductivity ratio which represents the ratio of viscous to gravity forces and N is the gravity-capillarity ratio which represents the ratio of gravity to capillary forces, plotting $1/N$ versus R_F using Equation (7) can show us the dominant forces in different regions of the plot. By substituting Equations (1) and (3) into (4), N can be expressed as

$$N = \pi \left[\frac{1}{1-R_F}\right] \tag{7}$$

Figure B-3 shows the plot of $1/N$ versus R_F.

Figure B-3. Plot of 1/N versus R_F

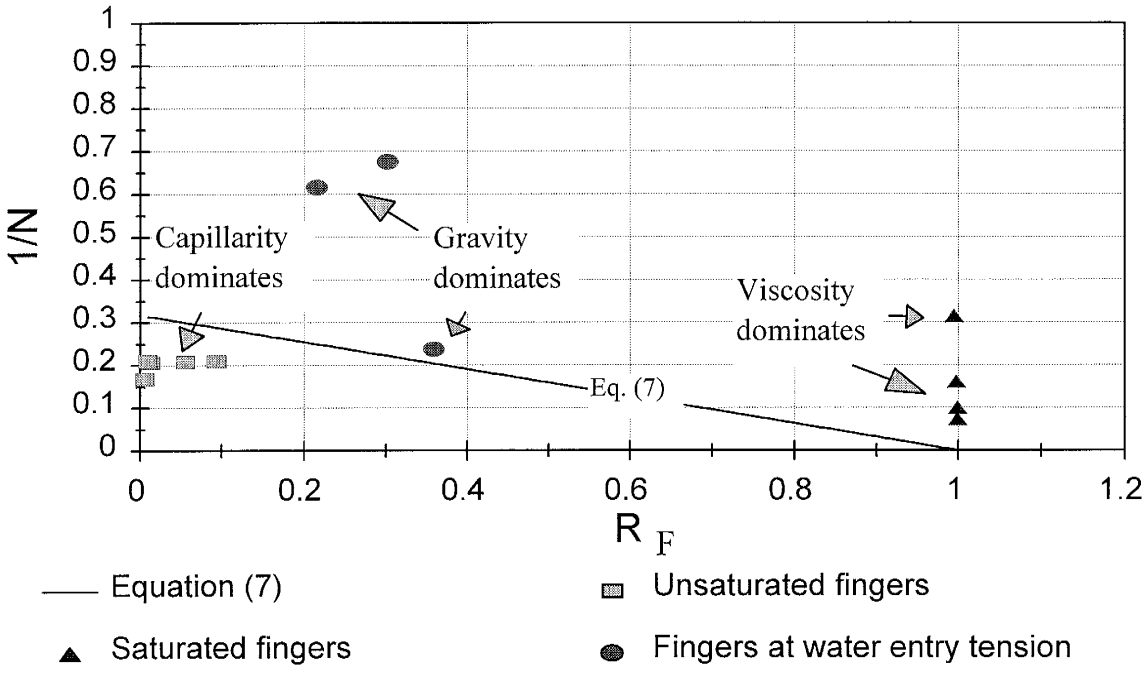

To verify Equation (7), N can be calculated through the following equation (Glass et al., 1989a) which also considers the unsaturated fingers.

$$N = \frac{d\ K_F(\theta_F - \theta_i)}{S_F^2} \tag{8}$$

In Figure B-3, experimental data from different infiltration schemes are plotted. Since fingers are not saturated at low rates, data from Table 3-2 are used to calculate N using Equation (8). For intermediate infiltration rates, soil hydraulic properties at the water entry values from Table 2-2 are used. For high infiltration rates, saturated soil hydraulic properties from Table 2-2 are used. These data points do not converge to the curve calculated using Equation (7), possibly because the finger properties are not measured in our experiments. Approximated and calculated properties are used instead.

These preliminary findings suggest that dimensional analysis can be usefully employed to analyze the competing forces that determine the stability of a wetting front. However, it appears that we need additional dimensional analysis to cover capillary dominated conditions at low infiltration rates.

References

Du, X.H., T. Yao, W.D. Stone, and J.M.H. Hendrickx. 1998. Stability analysis of the unsaturated water flow equation: 1. Mathematical derivation. Submitted for publication in *Water Resour. Res.*

Glass, R.J., T.S. Steenhuis, and J.-Y. Parlange. 1989a. Wetting front instability: 1. Theoretical discussion and dimensional analysis. *Water Resour. Res.* 25:1187-1194.

Glass, R.J., T.S. Steenhuis, and J.-Y. Parlange. 1989b. Wetting front instability: 2. Experimental determination of relationships between system parameters and two-dimensional unstable flow field behavior in initially dry porous media. *Water Resour. Res.* 25:1195-1207.

Glass, R.J., and M.J. Nicholl. 1996. Physics of gravity fingering of immiscible fluids within porous media: An overview of current understanding and selected complicating factors. *Geoderma*, 70:133-163.